Wissenschaftszentrum Weihenstephan für Ernährung, Landnutzung und Umwelt
Forschungsdepartment Ökologie und Ökosystemmanagement, Lehrstuhl für Aquatische Systembiologie

Methods for multitemporal mapping of submerged aquatic macrophytes using multi- and hyperspectral remote sensing

Sebastian Rößler

Vollständiger Abdruck der von der Fakultät Wissenschaftszentrum Weihenstephan für Ernährung, Landnutzung und Umwelt der Technischen Universität München zur Erlangung des akademischen Grades eines

Doktors der Naturwissenschaften

genehmigten Dissertation.

Vorsitzender: Univ.-Prof. Dr. Thomas Knoke

Prüfer der Dissertation:

1. Univ.-Prof. Dr. Arnulf Melzer
2. Univ.-Prof. Dr.-Ing. Uwe Stilla

Die Dissertation wurde am 02.01.2014 bei der Technischen Universität München eingereicht und durch die Fakultät Wissenschaftszentrum Weihenstephan für Ernährung, Landnutzung und Umwelt am 16.07.2014 angenommen.

“Physical concepts are free creations of the human mind, and are not, however it may seem, uniquely determined by the external world.”

Albert Einstein & Leopold Infeld (1938)
The evolution of physics

ABSTRACT

In the freshwater lakes of Bavaria (southern Germany) an increased spread of the two invasive submerged aquatic macrophytes, *Elodea nuttallii* and *Najas marina,* is observed. Since these species are suspected to benefit from recent climate warming, their identification can help to detect changes in the ecosystem at an early stage. Up to now, the mapping of vegetation coverage of shallow water regions is carried out by scientific diving – a time- and cost consuming method when mapping whole lakeshores. In the EU Water Framework Directive regular mapping for littoral areas of lakes exceeding a certain area is scheduled every three years. Multiseasonal (within one year) and multitemporal (over several years) remote sensing data now offer the possibility to capture large areas by means of regular image data acquisition.

In earlier studies, hyperspectral imagers (e.g. HyMap) were successfully used to map the distribution of high- and low-growing macrophytes and to detect species. However, the use of airborne sensors is often limited by a short recording period, it is cost intensive and has an environmental impact due to the flight-related emission of greenhouse gases. A fully automated processing is restricted to satellite-borne sensors since multispectral systems like RapidEye offer the required temporal (revisit time) and spatial resolution needed for frequent observations of the expansion behaviour of invasive aquatic plants.

The main problem of shallow water remote sensing is the exponentially decreasing light intensity with increasing depth due to the attenuation of the water column (with its absorbing and scattering constituents). In this thesis two different methods for correcting this characteristic of the water column are presented. The first method is semi-empirical, using band ratios transformed by *in situ* measured attenuation coefficients. The second method uses a bio-optical model which incorporates an estimation of depth, water constituent retrieval and linear bottom unmixing for predetermined bottom coverages (with provided reflectance). A precise atmospheric correction is required as prerequisite. Since the result of bio-optical model inversion strongly depends on the accuracy of the provided bottom albedo, artificial surfaces with known reflectance behaviour were used as reference targets during hyperspectral flight campaigns.

This cumulative thesis shows how the information content of hyperspectral imagery can be compensated by the use of multiseasonal multispectral remote sensors. These are cost-intensive and – due to short operation periods (limited availability, appropriate flight conditions) – unsuitable for regular monitoring efforts. Modern multispectral sensors have a high temporal resolution (daily coverage) and the phenological development of aquatic plants allows predicting the occurrence of different species. Multiseasonal reflectance databases increases classification accuracy due to the use of trustworthy reflections of the lake bottom. A reliable differentiation between sediment and vegetation is possible using both methods. This allows monitoring vegetation development throughout the year.

KURZFASSUNG

In bayerischen Seen wird eine Zunahme der invasiven Wasserpflanzen *Elodea nuttallii* und *Najas marina* beobachtet. Da diese Arten vom Klimawandel zu profitieren scheinen, kann deren Identifizierung dabei helfen, Veränderungen im Ökosystem frühzeitig zu erkennen. Bisher wird die Kartierung der Ufervegetation von Tauchern durchgeführt – eine sehr kosten- und zeitintensive Methode. Die Europäische Wasserrahmenrichtlinie schreibt für alle Seen ab einer gewissen Größe Kartierungen alle drei Jahre vor. Die multisaisonale (innerhalb eines Jahres) und multitemporale (mehrere Jahre) Fernerkundung bietet nun die Möglichkeit, große Gebiete mithilfe regelmäßiger Aufnahmen zu erfassen.

In früheren Studien wurden hyperspektrale bildgebende Sensoren (z. B. HyMap) genutzt um die Verbreitung hoch- und niedrigwüchsiger Makrophyten zu erfassen und Arten zu unterscheiden. Dennoch ist die Nutzung von flugzeugbasierten Sensoren begrenzt durch ein schmales zeitliches Aufnahmefenster, hohe Kosten und den umweltschädigenden Einfluss durch den Ausstoß klimawirksamer Treibhausgase. Eine vollständig automatisierte Prozessierung ist daher begrenzt auf satellitengetragene Sensoren da multispektrale Systeme wie RapidEye die benötigte zeitliche und räumliche Auflösung bieten, die für regelmäßige Beobachtungen des Ausbreitungsverhaltens invasiver Wasserpflanzen benötigt wird.

Das Hauptproblem der Flachwasserfernerkundung ist die mit zunehmender Tiefe exponentiell abnehmende Strahlung durch die Attenuation der Wassersäule (mit ihren absorbierenden und streuenden Bestandteilen). In dieser Dissertation werden zwei Methoden präsentiert um diese Eigenschaft der Wassersäule zu korrigieren. Die erste, halb-empirische Methode nutzt die *in situ* gemessene Attenuation, um logarithmisch transformierte Steigungen zwischen spektralen Bändern zu berechnen. Die zweite Methode nutzt ein bio-optisches Modell zur Bestimmung der Tiefe, der Wasserinhaltsstoffe und der linearen spektralen Entmischung vorher festzulegender Endglieder (mit bereitzustellenden Reflexionsspektren). Eine präzise Atmosphärenkorrektur ist hierbei Voraussetzung. Da das Ergebnis der Modellinvertierung stark von der Genauigkeit der Bodenreflexion abhängt, wurden während der hyperspektralen Flugkampagnen künstliche Referenzflächen mit bekannten Reflexionsverhalten ausgebracht.

Diese kumulative Arbeit zeigt, inwieweit der Informationsgehalt hyperspektraler Fernerkundungssysteme durch multisaisonale Aufnahmen multispektraler Systeme kompensiert werden kann. Diese sind teuer und – durch kurze Betriebszeiten (begrenzte Verfügbarkeit, geeignete Flugbedingungen) – ungeeignet für eine regelmäßige Überwachung. Neuere multispektrale Sensoren erlauben eine sehr hohe zeitliche Auflösung (tägliche Abdeckung) und durch die phänologische Entwicklung der Wasserpflanzen sind auch hier Aussagen über das Vorkommen bestimmter Arten möglich. Es wurde festgestellt, dass multisaisonale Reflexionsdatenbanken die Identifikationsgenauigkeit erhöhen, da verlässliche Reflexionen des Seebodens genutzt werden können. Eine sichere Unterscheidung zwischen Sediment und Vegetation ist bei beiden vorgestellten Methoden gegeben. Das erlaubt die Beobachtung der Vegetationsentwicklung über das ganze Jahr.

TABLE OF CONTENTS

LIST OF FIGURES

LIST OF TABLES

1. INTRODUCTION

1.1 Scientific background

Lakes can be regarded as mirrors of the surrounding catchment area. They receive all land discharges which can be the results of erosion, groundwater and sewage input and inflow of rivers. In the euphotic littoral zones of lakes, aquatic plants can occur emergent, submergent or floating (Silva et al. 2008). They are summarized as macrophytes and play an important role in primary production, in providing a habitat for fishes and aquatic invertebrates (Herold et al. 2007), in producing oxygen and acting as food for animals. Macrophytes are used to determine the trophic state of lakes which can give further information about the management and health of the catchment area (Onaindia et al. 1996). In the Water Framework Directive (Directive 2000/60/EC of the European Parliament and of the Council of 23 October 2000 establishing a framework for Community action in the field of water policy) it is stated that all member states of the European Union will achieve a good qualitative and quantitative status of all water bodies by 2015. This requires a regular monitoring of the current state of lakes and rivers. Since certain macrophytes have only a narrow phenotypic plasticity they can act as an indicator for ecologic conditions and changing environment (Lacoul and Freedman 2006). Their presence or absence is used as an indicator for nutrient conditions (Melzer 1976, 1999) and the mapping of species composition has become part of the regular littoral bottom coverage mapping by divers as one of the tasks in the context of the European Water Framework Directive.

The mapping of submerged aquatic vegetation (SAV) by diving is time consuming, expensive and often limited to favourable environmental conditions like low swell and good weather conditions (Vahtmäe and Kutser 2007), a short phenological cycle (Kutser et al. 2006; Pinnel 2007) and good accessibility of the littoral zone (Vis et al. 2003). These limiting factors lead to the application of remote sensing on this task, since the 1960s studies have been discussing the differentiation of SAVs using remote sensing methods (Anderson 1969). The reliable differentiation of benthic bottom coverage and thus also of submerged aquatic vegetation is a major task in remote sensing applications on coastal zone and shallow inland water bodies (Silva et al. 2008).

The development of water remote sensors was driven by a global approach towards water constituent retrieval on a large spatial scale and a short revisit time. Typical sensors that are used for “Ocean Colour” activities are SeaWiFS (Ciotti and Bricaud 2006; Gordon and Wang 1994), MERIS (Kallio et al. 2005; Koponen et al. 2002; Minghelli-Roman and Dupouy 2013) and MODIS (Carder et al. 2004; Kallio et al. 2005). Due to very low reflectance of optically deep water and the desired large areal coverage, their spatial resolutions are very coarse (SeaWiFS: 1100 m; MERIS: 300 m; MODIS: 500 m). From the Water Framework Directive new fields of application emerged for water remote sensing of inland water bodies, but also show the limitations of these sensors.

The main limitation for these sensors is the spatial heterogeneity especially of shallow water areas and small lakes. Thus, only few studies used them for bathymetric applications of shallow littoral areas (Feng et al. 2011; Hu 2008; Minghelli-Roman et al. 2009; Zhang et al. 2011). The heterogeneity at small spatial scales requires sensors with a high spatial resolution rather than a high spectral resolution. This was confirmed by Vahtmäe and

Kutser (2007) who compared QuickBird (2.4 m spatial resolution) images with hyperspectral spaceborne Hyperion data (30 m spatial resolution).

Most studies were performed on multispectral imagery like QuickBird (Botha et al. 2013; Ceyhun and Yalçın 2010; Dogan et al. 2009; Minghelli-Roman et al. 2009; Mishra et al. 2006; Phinn et al. 2008; Sawaya et al. 2003; Vahtmäe and Kutser 2007; Wolter et al. 2005; Yuan and Zhang 2007), IKONOS (Andréfouët et al. 2003; Bejarano et al. 2010; Herold et al. 2007; Knudby et al. 2010; Knudby and Nordlund 2011; Mishra et al. 2005; Mishra et al. 2007; O'Neill and Costa 2013; Sagawa et al. 2008; Sawaya et al. 2003; Stumpf et al. 2003), ETM+ (Arias-González et al. 2012; Carvalho Júnior et al. 2010; Cho 2007; Doxaran et al. 2006; Gullström et al. 2006; Kallio et al. 2005; Vanderstraete et al. 2006) and SPOT (de Vel and Bour 1990; Doxaran et al. 2006; Huen and Zhang 2011; Kao et al. 2009; Lafon et al. 2004; Lafon et al. 2000; Lafon et al. 2002; Maritorena 1996; Mumby et al. 1997; Spitzer and Dirks 1987; Topliss et al. 1990). Besides bathymetric applications, multispectral data were used for three major tasks: The mapping of coral reefs (Andréfouët et al. 2003; Arias-González et al. 2012; Bejarano et al. 2010; Botha et al. 2013; Knudby et al. 2010; Mishra et al. 2006; Vanderstraete et al. 2006), the mapping of seagrass (Gullström et al. 2006; Knudby and Nordlund 2011; O'Neill and Costa 2013; Phinn et al. 2008; Sagawa et al. 2008; Vahtmäe and Kutser 2007) and the mapping of freshwater macrophytes (Ackleson and Klemas 1987; Dogan et al. 2009; Sawaya et al. 2003; Wolter et al. 2005).

However, the wavelength dependent absorption and scattering of water constituents and the water itself, as well as narrow spectral features of littoral bottom coverage like macrophytes in lakes again leads to the wish for a higher spectral resolution. As already mentioned, the use of the only spaceborne hyperspectral sensors Hyperion and CHRIS/Proba is precluded due to its coarse spatial resolutions. As an alternative, airborne sensors (e.g. AISA, APEX, CASI, HyMap and ROSIS) offering the also desired spatial resolution were used for macrophyte identification (Dierssen et al. 2003; Giardino et al. 2012; Giardino and Zilioli 2001; Heege et al. 2003; Hestir et al. 2008; O'Neill and Costa 2013; Pinnel 2007; Ustin et al. 2002; Williams et al. 2003).

For an accurate differentiation of SAV, spectral libraries have to be built taking into account the strong seasonality due to phenology (Kutser et al. 2006; Pinnel 2007). Besides this, the spectral signal (reflectance) of SAV is always influenced by the overlaying water column with its apparent and inherent optical properties (Mobley 1994) which reduces the signal strength of SAV exponentially with increasing depth. This is accounted for by either using SAV reflectances measured *in situ* above the surface (i.e. including the water column) for classification (Louchard et al. 2003; Vahtmäe and Kutser 2007) or by correcting the disturbing influence of the water column using empirical methods (Lyzenga 1978, 1981, 1985; Maritorena 1996; Sagawa et al. 2010; Tassan 1996) or physically based models (Gege 2004; Gege and Pinnel 2011; Giardino et al. 2012; Heege et al. 2003; Pinnel 2007). The latter have to be preferred since they allow application at a much larger types of water bodies from case 1 to case 2 waters (Morel 1980).

In the lakes of Bavaria (southern Germany), an increased spread of indigenous species like *Najas marina* and invasive alien species like *Elodea nuttallii* has been observed. It is assumed that these species benefit from climate warming, as was observed for other species

(Rahel and Olden 2008). Until now, only few studies explicitly treat the monitoring of the expansion behaviour of invasive submergent aquatic plants (Theriault et al. 2006).

The phenology leads to changing reflectance of macrophytes (Peñuelas et al. 1993). This temporal aspect leads to the use of multiseasonal datasets for classification approaches (Louchard et al. 2003). However, the water body itself show also variations which have to be considered.

The bottom coverage composition may alter (Vanderstraete et al. 2006), the water constituent composition may vary seasonally (Thiemann and Kaufmann 2002) and the water depth can also change (Van Hengel and Spitzer 1991). The latter may be regarded as an effect mainly restricted to tidal areas and rivers, but increasing flooding also affects inland lakes and causes other problems like reed decline (Melzer et al. 1993).

In summary, it can be stated that shallow water remote sensing for monitoring/identification of selected macrophytes comprises several problems which are still challenging. Thus, the main purpose behind this thesis was to find ways being best suited to minimize the problems using different methodological approaches.

1.2 Aims and Objectives

The aim of this thesis was to study the occurrence and the expansion behaviour of selected invasive aquatic macrophytes in freshwater lakes of southern Germany using different optical remote sensing data (airborne hyperspectral and spaceborne multispectral) and simultaneously collecting *in situ* data. Multitemporal reflectance measurements of the invasive species *Elodea nuttallii* and *Najas marina* and other common submerged aquatic macrophytes were made with and without the overlaying water column. Transfer functions had to be developed to compensate the information loss of coarser spectral (spectral transfer function) and geometric resolution (geometric transfer function). The specific objectives can be derived from the workflow shown in **Figure 1-1**.

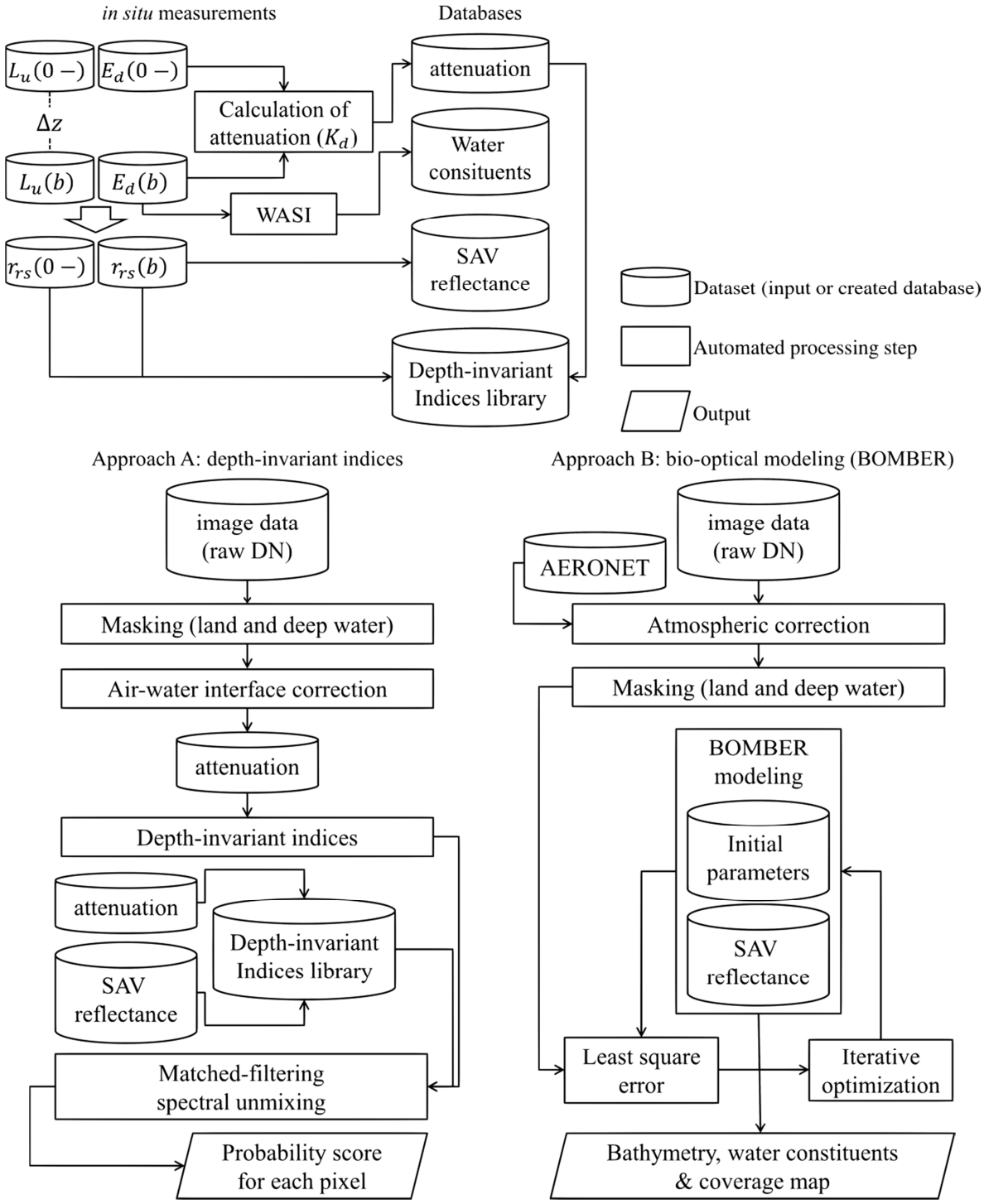

Figure 1-1: workflow of the thesis

Figure 1-1 summarizes the activities of this thesis which are presented in the attached original publications. Starting from the *in situ* data collection, the workflow proceeds to the creation of databases which are necessary for further image processing. The two different approaches for water column correction and bottom classification using the *in situ* derived data are shown. The following objectives were defined:

- Classify multi- and hyperspectral remote sensing data by using multiseasonal *in situ* data of invasive (*Elodea nuttallii* and *Najas marina*) and other common macrophytes (*Chara* spec. and *Potamogeton perfoliatus*) (**Chapters 3 and 4**).

- Study the potentials of geometric high resolution multispectral imagery for littoral bottom mapping using transformed band ratio techniques and pixel-based endmember unmixing (**Chapter 3**).
- Evaluate classification results of high resolution multispectral imagery using physically based bio-optical models. Show the advantages and the necessity of using multiseasonal data acquisitions (**Chapter 4**).
- Enhance water constituent retrieval during hyperspectral airborne flight campaigns using artificial submersed surfaces with known reflectance behaviour (**Chapter 5**).

1.3 Embedded original publications

The thesis is composed of six chapters: the introduction is followed by a methodological chapter, three chapters containing original publications and finally a synthesis. The publications are peer-reviewed original research papers (Roessler et al. 2013; Rößler et al. 2013a; Rößler et al. 2013b) that have been published in international publication organs (Table 1-1).

Table 1-1: Overview of publications presented within this thesis

Publication	Chapter
Roessler, S., Wolf, P., Schneider, T., & Melzer, A. (2013). Multispectral Remote Sensing of Invasive Aquatic Plants Using RapidEye. In J.M. Krisp, L. Meng, R. Pail, & U. Stilla (Eds.), *Earth Observation of Global Changes (EOGC)* (pp. 109-123): Springer Berlin Heidelberg	3
Rößler, S., Wolf, P., Schneider, T., & Melzer, A. (2013). Littoral bottom mapping in lakes using multitemporal RapidEye data. In E. Borg, H. Daedelow, & R. Johnson (Eds.), *RapidEye Science Archiven (RESA) - From the Basics to the Service* (pp. 107-127). Berlin: GITO Verlag	4
Rößler, S., Wolf, P., Schneider, T., Zimmermann, S., & Melzer, A. (2013). Water constituent retrieval and littoral bottom mapping using hyperspectral APEX imagery and submersed artificial surfaces. *EARSeL eProceedings, 12*, 44-57	5

1.4 Author's contributions

Chapter 3: The study idea was developed by S. Rößler, P. Wolf, T. Schneider and A. Melzer. S. Rößler and P. Wolf performed the *in situ* data acquisition and the subsequent analysis and data interpretation. Literature review and remote sensing data processing was done by S. Rößler. The procurement of RapidEye data (within the RESA project no. 455) was carried out by S. Rößler and T. Schneider. The preparation of the manuscript and the revision was mainly performed by S. Rößler with the assistance of P. Wolf, T. Schneider and A. Melzer. The figures were created by S. Rößler and P. Wolf.

Chapter 4: The study idea was developed by S. Rößler, P. Wolf, T. Schneider and A. Melzer. *In situ* data were acquired by S. Rößler and P. Wolf. Data analysis was done by S. Rößler. Literature review and remote sensing data processing was done by S. Rößler. The procurement of RapidEye data was carried out by S. Rößler and T. Schneider. The

preparation of the manuscript and the revision was mainly performed by S. Rößler with the assistance of P. Wolf, T. Schneider and A. Melzer. The figures were created by S. Rößler.

Chapter 5: The study design was developed by S. Rößler, P. Wolf, T. Schneider and A. Melzer. The experimental setup – including purchasing of silo foils and diving operations planning – was done by S. Zimmermann. *In situ* data were acquired by S. Rößler, P. Wolf and T. Schneider. Data analysis was done by S. Rößler. Literature review and remote sensing data processing was done by S. Rößler. The procurement of APEX data was carried out by S. Rößler, T. Schneider and A. Melzer. The preparation of the manuscript, and the revision was mainly performed by S. Rößler with the assistance of P. Wolf, T. Schneider and A. Melzer. The figures were created by S. Rößler.

1.5 Summary of original publications

1.5.1 Paper I

The publication 'Multispectral Remote Sensing of Invasive Aquatic Plants using RapidEye' (**Chapter 3**) describes the combination of *in situ* collected data and multispectral and multitemporal remote sensing data of the RapidEye satellites for benthic bottom coverage mapping. A semi-empirical ratio method was used to correct the attenuating water column with respect to its seasonal variability.

The study focused especially on the detection of the two submerged macrophytes *Elodea nuttallii* and *Najas marina* which are suspected to become invasive due to climate warming. Therefore, extensive measurements of the reflectance behaviour were made using a set of submersible hyperspectral spectroradiometers (RAMSES). The data were used to create a reflectance database of the two plants and to calculate the seasonal changing attenuation coefficients from measurements of the in-water downwelling irradiance in different depths. The attenuation curves were resampled to the spectral resolution of RapidEye and used for the calculation of depth-invariant indices based on transformed reflectance values (subtraction of deep-water reflectance and logarithmic transformation). The same transformation was applied to the *in situ* measured reflectances (also spectrally resampled) and used for subsequent pixel-based spectral unmixing of the image data. To prevent a forced assignment of unsuitable endmember, a matched filtering method was used instead of linear spectral unmixing. As a result the authors obtained probability scores for a possible contribution to the pixel.

One task was to assess the separability between the plants under observation and between those and other common macrophytes. The Jeffries-Matusita Index calculated from the transformed band ratios indicates in general a bad separability for multispectral remote sensors. However, the authors found that the multitemporal aspect offers new possibilities for data interpretation. Especially the transformed band ratio between the Red and the Red Edge spectral channel offers a new and robust possibility to separate between bare sediment and overgrown littoral areas. Multitemporal images can be used to monitor the vegetation development in shallow water regions. This gives new interpretation possibilities since low growing macrophytes like *Characea* forms dense meadows from the beginning of the growing season, whereas *Najas marina* forms dense stands only in September. The advantages and disadvantages of this simple water column correction method are presented as well.

1.5.2 Paper II

In the publication ‘Littoral bottom mapping in lakes using multitemporal RapidEye data’ (**Chapter 4**) the named data is used to monitor the expansion behaviour of submerged macrophytes. In contrast to the previous paper, another water column correction method is used, which– except for bottom reflectance – needs no auxiliary data for image data processing.

A bio-optical model named BOMBER is used to derive benthic bottom properties (depth and coverage) as well as water constituent concentrations (phytoplankton, suspended particulate matter and coloured dissolved organic matter) from atmospherically corrected RapidEye imagery. The model has been developed based on the results of radiative transfer modelling in shallow waters and is intended primarily for the application on hyperspectral remote sensing data (see Paper III). In this study the authors tried to find out whether this model inversion procedure is suitable for low spectral resolution sensors like RapidEye.

Since a precise correction of the atmosphere is essential for reasonable results, a robust atmospheric correction for inland water bodies was sought. The authors used a simple atmospheric correction with uniform aerosol properties and achieved good results for all processed images.

In the application of BOMBER three questions were raised: (1) Are the concentrations of optically active water constituents accurately determined; (2) Is the temporal evolution visible and (3) are different macrophytes distinguishable. The first point was validated using the interpolated inversion results of the downwelling irradiance with the program WASI – an accurate method for the determination of water constituents. There was a considerable development visible but the derived concentrations showed large deviations. As to the second point a clear seasonal development was visible from non-vegetated areas to fully overgrown patches. The separability was estimated by calculating M-statistics from the reflectance database. An increasing separability was observed with the progressing vegetation period.

1.5.3 Paper III

The publication ‘water constituent retrieval and littoral bottom mapping using hyperspectral APEX imagery and submersed artificial surfaces’ (**Chapter 5**) presents an experimental approach using spatial and spectral high resolution APEX data in combination with bio-optical modelling and artificial reference surfaces placed under water.

The apparent reflectance in shallow water is always a function of bottom reflectivity, water depth and the composition and concentration of optically relevant water constituents. For a reliable estimation of the latter two, a valid bottom albedo must be provided or is derived by spectral unmixing. Natural surfaces have a variability of reflectance in shape and intensity resulting in inaccuracies of water depth and constituent retrieval.

In this approach white and black plastic foils (10 metres wide and 50 metres long) were spread out on the littoral bottom of Lake Starnberg to provide areas large enough to be captured by airborne remote sensors (APEX in case of this paper). Image data was inverted to estimate water inherent optical properties and depth using the bio-optical model BOMBER. Reflectance spectra of the foils are known from laboratory measurements. The

sensor APEX was chosen due to the highest spectral resolution of all acquired hyperspectral data. In contrast to the initial assumption the white foil was not best suited to estimate depth and water constituent concentrations.

Best results were obtained above the black foil. The water depth and the concentrations of water constituents were determined accurately compared to WASI inversion results of *in situ* downwelling irradiance measurements. A subsequent inversion of the whole image (only shallow water regions) lead to similar water depth and water constituent concentrations as the inversion result from *in situ* measured RAMSES spectra above the black foil. For the spectral unmixing, reflectance spectra of *Najas marina*, *Chara* spec. and uncovered sediment were used. This allowed estimating the occurrence of the invasive macrophytes *Najas marina* for the image acquisition date.

2. METHODS

2.1 Study area

The main study area is Lake Starnberg (47°55'N, 11°19'E) situated 25 km southwest of Munich. With an area of 56 km² it is Germany's fifth largest lake and was glacially created (Fesq-Martin et al. 2008). The maximum depth is 128 m, and the areal extent with depths greater than 8 m (the maximum depth where macrophytes occur in Lake Starnberg) accounts for 87.5% (**Figure 2-1**). The test sites were selected according to the occurrence of extended littoral areas and high abundances of common macrophytes. In **Figure 2-1** the locations of the test sites are shown: regular *in situ* measurements were carried out at "Starnberg" (1) and "Bernried" (2). Additional test sites are the small bay "Karpfenwinkel" (3) known for large areas covered by *Najas marina* (mapped by diving) and the shallow area surrounding the island "Roseninsel" (4) with large *Chara* spec. patches on sandy bottom.

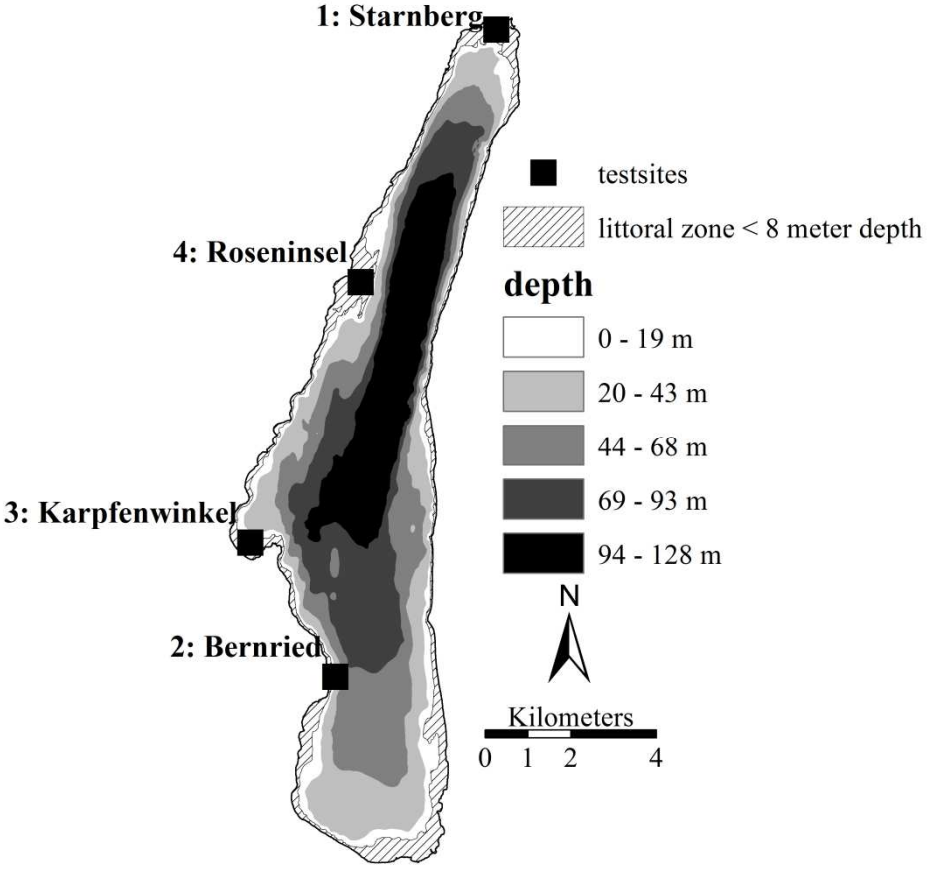

Figure 2-1: depth model of Lake Starnberg showing the colonization area (depth < 8 metre) for macrophytes and the location of the test sites

2.2 Passive optical remote sensing

2.2.1 Radiative transfer in water

The interpretation of remote sensing data always requires knowledge of the different radiation contributors which results in the top-of-atmosphere (TOA) radiance received by the sensor (Lillesand et al. 2008). An overview of the four different radiation sources is given in **Figure 2-2**.

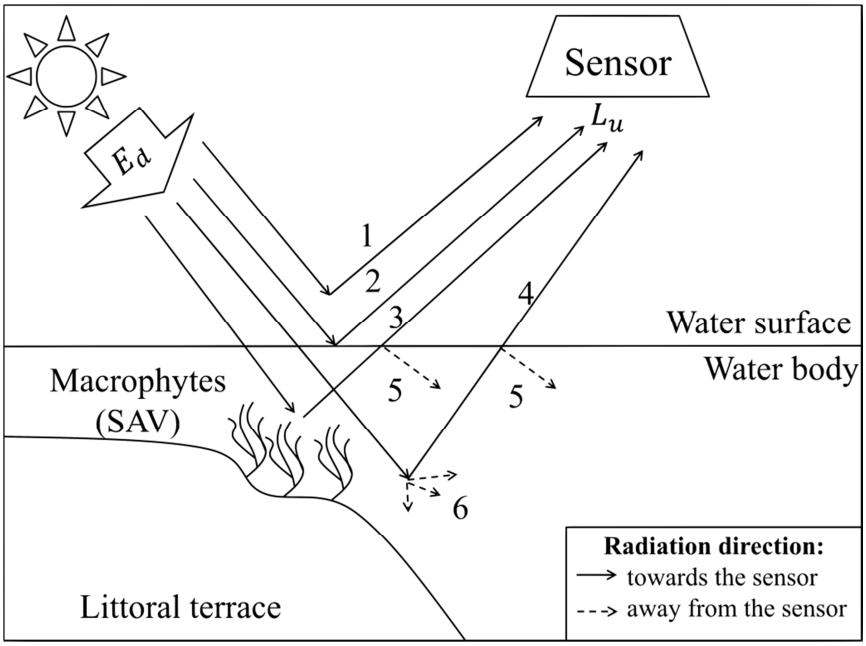

Figure 2-2: Schematic overview of radiative transfer in water and the different radiation sources reaching the sensor: light backscattered in the atmosphere (1), specular reflected light at the water surface (2), reflectance of submerged macrophytes (3) and volume backscattering of the water body. Additionally, the amounts of refracted and backscattered upwelling radiance at the water surface (5) and the diffuse scattering (not backscattering) in the water column (6) are indicated.

Water bodies with no influence of the bottom (i.e. optically deep water) usually have a very low reflectance, only 2 – 6% of the downwelling irradiance (E_d) is reflected (Dekker et al. 2001). From the remaining 94 – 98% a small fraction is backscattered from the atmosphere (source 1 in **Figure 2-2**) or is absorbed by it, the main fraction penetrates the water. Since the fraction backscattered by the atmosphere is comparatively high in the short-wave spectral region, a precise atmospheric correction is essential. The commonly practiced method ATCOR (Richter 1996) uses regionalized look-up-tables for atmospheric correction calculated with the radiative transfer code MODTRAN. The main contributors to the total scattering of the atmosphere is aerosol and the molecular Rayleigh scattering (Gordon and Wang 1994). Rayleigh scattering can be computed using the atmospheric pressure and the viewing and solar geometry (Doerffer 1992; Hansen and Travis 1974; Mishra et al. 2005). Aerosol estimation from images is more challenging, as an approximation a simple ratio technique has been developed by Mishra et al. (2005), from sensors with at least two spectral bands in the near-infrared (NIR) (e.g. SeaWiFS and WorldView-2), the Aerosol optical thickness (AOT) can be estimated from the image data (Gordon and Wang 1994).

From the remaining irradiance reaching the water surface, 2% are reflected according to the Fresnel reflection of unpolarised light (Jerlov 1976). In the case of optically deep water, the additional reflections (up to 4%) are mainly caused by the backscattering of suspended particulate matter (SPM). The Fresnel reflection represents the ideal case for a flat water surface. In fact, waves and unfavourable sun-target-sensor constellations may cause specular reflectance of the sunlight (sun glint) which contains no information from the water column or from the bottom (Hochberg et al. 2003).

The last two remaining radiation sources (3 and 4) contain information on the water column (4) and the plant coverage (3) in shallow water areas. In water, light underlies an exponential decrease which is explained by the Beer-Lambert law (Beer 1852). This attenuation affects the incident light, the light reflected by macrophytes and the light backscattered by water constituents.

2.2.2 Remote sensors for littoral bottom mapping

Remote sensors are either carried by satellites (spaceborne) or by planes (airborne). The entrance optic (lens) of the sensor defines the Field Of View (FOV) which determines the ground swath captured (depending on flight altitude and ground elevation). Remote sensing instruments are characterized mainly by four specific properties: the geometric resolution, the spectral resolution, the radiometric resolution and the temporal resolution. An overview of important sensor-specific terms concerning the image acquisition is given in **Figure 2-3**.

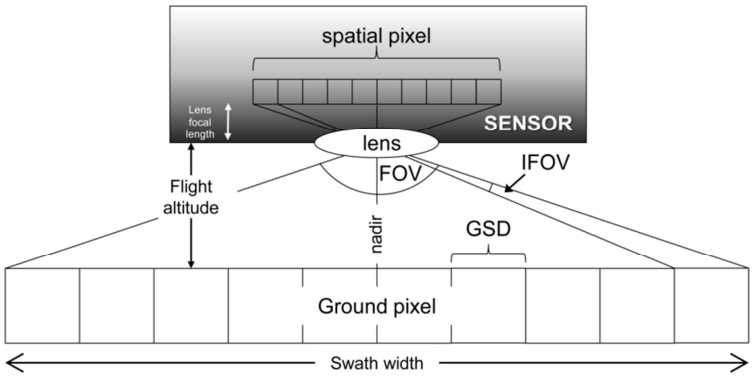

Figure 2-3: Schematic draft of image acquisition by satellites or planes (for CCD-array sensor with 10 spatial pixels): The lens (with its lens focal length) defines the Field Of View (FOV) of the sensor; the Instantaneous Field Of View (IFOV) describes the angular aperture of every pixel. The Ground Sampling Distance (GSD) depends on the flight altitude, and the length of all ground pixels corresponding to the spatial pixels of the sensor defines the Swath width. The perpendicular direction of view is called nadir.

The geometric resolution describes the equivalent of the pixel size on the ground (Ground sampling distance – GSD). The pixel size increases from the nadir-viewing to the edges. Technically it is strongly connected to the spectral resolution which describes the number of spectral bands. Narrow bands of hyperspectral imaging spectrometer receive much less energy reflected by the ground than broadband multispectral sensors. Therefore, hyperspectral satellite sensors like Hyperion need higher geometric resolutions to receive sufficient energy. Hyperion has a geometric resolution of 30 metres; the same is envisaged for the new German hyperspectral satellite EnMap (www.enmap.org). Thus, spatially high-resolution hyperspectral image acquisition can only be conducted by airplanes flying at low altitudes

The radiometric resolution (dynamic range) of a system refers to the number of grey levels in an image to distinguish differences of intensity (Lillesand et al. 2008). It describes the sensor's sensitivity and is specified as bits or as digital numbers (DN). Older sensors like ETM+ (Landsat 7) have a dynamic range of 8-bit (256 DN), WorldView-2 has 11-bit (2 048 DN) RapidEye and the hyperspectral sensor AISA 12-bit (4 096 DN) and the hyperspectral imager APEX even 14-bit (16 384 DN) in the visible spectral region (VIS).

Mapping of submerged aquatic vegetation has a strong temporal aspect due to rapid seasonal developments from bare to vegetated littoral bottom. This has to be considered when planning image acquisition with hyperspectral airborne sensors (which are only limited by the appropriate flight conditions and the availability of a sensor). The temporal resolution (revisit time) of spaceborne sensors depend on their swath width, on flight altitude and on orbit orientation. RapidEye consists of five identical platforms allowing daily revisits since the platforms can be turned across the track (± 25 degrees off-nadir pointing capability). WorldView-2 has a comparable revisit time (1.1 days) with a pointing capability of ± 30 degrees across-track. These off-nadir image acquisitions lead to problems like sun glint which depends on the sun-target-geometry (Wolf et al. 2013b).

Within this project, three different hyperspectral airborne sensors (HyMap, AISA, and APEX) and two multispectral spaceborne sensors (RapidEye, WorldView-2) were used. To compare their different spectral resolutions, the specific spectral response curves can be compared (**Figure 2-4**).

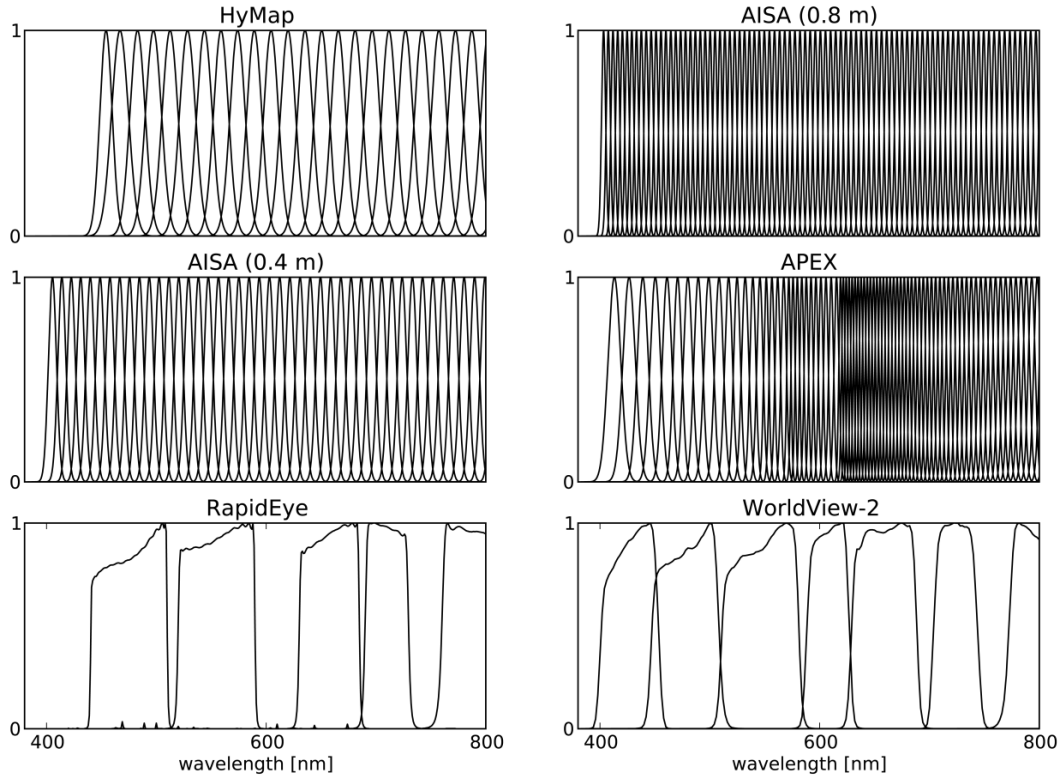

Figure 2-4: relative spectral response of all used hyperspectral and multispectral sensors (limited to the spectral range used for water applications: 380 – 800 nm). The AISA sensor was used with different settings for two flight altitudes and varying spectral resolutions.

2.2.3 Comparison of hyper- and multispectral systems

Hyperspectral image acquisition took place in 2010 and 2011 using three systems with different specifications. The sensor HyMap, which has been used in previous studies of lake littoral mapping (Heege et al. 2003; Pinnel 2007), offers 22 channels in the VIS to NIR suitable for water remote sensing (up to 800 nm). The sensor AISA, also used for water remote sensing (Kallio et al. 2001; Koponen et al. 2002; Mishra et al. 2007; O'Neill and Costa 2013), was operated in two modes enabling a spectral resolution of up to 87 channels in the VIS to NIR. APEX has a comparably high resolution of 80 channels in this

spectral range but many more variable bands concerning the spectral sampling and the individual band-widths (expressed as Full-Width-Half-Maximum – FWHM).

With a FOV of 45° and a flight altitude of 2500 m, HyMap covered a swath width of 2048 m and achieved a GSD of 4 m. The lens of AISA has a FOV of 37.7° and has been operated from two flight altitudes of 1200 and 600 m; swath widths of 820 and 410 m were achieved with a GSD of 0.8 and 0.4 m, respectively. With a FOV of only 28° but a much higher flight altitude (4900 m), APEX had the largest areal coverage (swath width of 2443 m) and a GSD of 4 m. **Figure 2-5** shows the coverage of the western shore of Lake Starnberg during these campaigns.

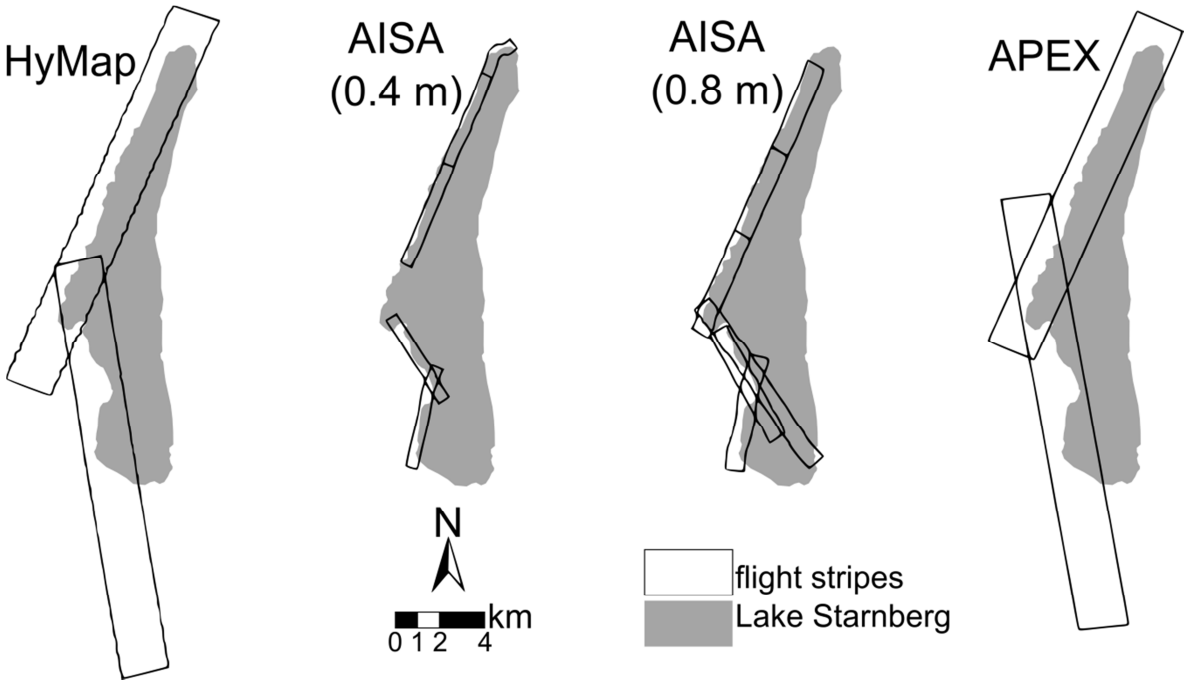

Figure 2-5: location and strip coverage of the hyperspectral airborne sensors HyMap (22/08/2010), AISA (two flight altitudes; 17/08/2011) and APEX (10/09/2011)

In contrast to the airborne hyperspectral imagers, the sensors carried by RapidEye and WorldView-2 cover much larger areas. RapidEye has a FOV of 7° and a flight altitude (orbit height) of 630 km. The resulting swath width is 77 km and a GSD of 6.5 m (resampled to 5 m in level 3A processing). WorldView-2 has a narrower FOV (1.3°) and an orbit height of 770 km. The swath width is only 17.5 km and the spatial resolution is 1.85 m (resampled to 2 m).

Regarding the areal coverage of the hyperspectral airborne campaigns (**Figure 2-5**), a major disadvantage becomes obvious: To cover large areas, numerous overflights are necessary. A subgoal of this thesis (compensation of a coarser spectral resolution, see **Chapter 1.2**) can be explained best by the scaling approach.

In this thesis, the term “scale” is used in a wider sense and not only for the spatial scale (local, regional and global). According to the sensor specifications, the different resolutions are treated as scales (the technically restricted radiometric resolution was omitted). The used sensors are drawn in **Figure 2-6** to compare their different scales.

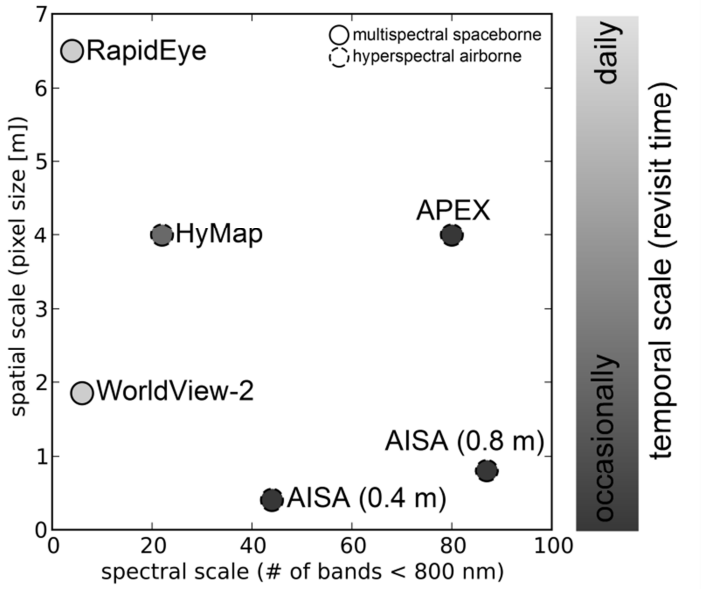

Figure 2-6: comparison of the different scales of the used remote sensors

With a larger number of spectral bands, hyperspectral sensors are on one edge of the spectral scale (the other edge would be represented by panchromatic systems). In general, this is an advantage as it increases the retrieval of information due to the possible use of small spectral features. The sensitivity of multispectral sensors is between the hyperspectral and panchromatic systems. For shallow water remote sensing (the field of application for macrophyte detection), multispectral systems with various rather narrow channels in the visible range (e.g. WorldView-2) are most suitable.

Regarding the spatial scale, there is almost no difference between the used space- and airborne sensors. In contrast to the spectral scale (where hyperspectral airborne systems are clearly better suited), the multispectral spaceborne sensors are better suited regarding the temporal scale (theoretically, RapidEye can acquire images every day). Besides technical and operational restrictions, also economic aspects have to be considered. Regular monitoring is only feasible to reasonable prices and a good cost-value ratio regarding the information content. RapidEye charges 0.95 €/km² and for on-demand tasking the minimum order size is 3500 km², this is much less than the cheapest hyperspectral dataset of this project (APEX: 11000 €).

To find out which limitations are given for multispectral imagery compared to hyperspectral data, a subsequent upscaling was performed from hyperspectral *in situ* measurements made in-water directly above the macrophytes to records including the overlaying water column using RAMSES spectroradiometers. Image data were achieved and processed from different hyper- and multispectral sensors to compare results in terms of water column correction and bottom coverage identification. Due to the potential daily revisit and availability of RapidEye data provided within the RESA project, these datasets were used to test processing routines. Within this cumulative thesis also APEX imagery is presented, results from other hyperspectral sensors were published in non-peer-reviewed publications (see appendix).

2.3 *In situ* measurements

The reflectance R is defined as the ratio of the upwelling irradiance E_u to the downwelling irradiance E_d. The directional remote sensing reflectance R_{rs} is the ratio of the upwelling radiance L_u to E_d (Mobley 1994). *In situ* measurements of the underwater light field above different substrate types (macrophytes and bare sediments) were carried out 2010 and 2011 at Lake Starnberg (47°54'N, 11°18'E). Three submersible RAMSES spectroradiometers (TriOS) were used to collect L_u, E_d and E_u simultaneously. L_u was measured using a RAMSES ARC VIS (SN: 810E). E_d was recorded with a RAMSES ACC VIS (SN: 8109) with integrated tilt- and pressure sensor. And E_u was determined a similar RAMSES ACC VIS device (SN: 8110). All sensors have a spectral range of 320 – 900 nm, the sampling interval was set to 3.3 nm and the spectral resolution (FWHM) was 10 nm.

In 2010, the entrance optics were aligned at the same depth level (**Figure 2-7**, left), so that the derivatives R_{rs}, R and the anisotropy of the underwater light field $Q = E_u/L_u$ could be calculated directly. In 2011, a new measurement cube was employed containing a stereo-camera system in addition to the RAMSES sensors. To avoid self-shadowing of the instruments, the entrance optics were no longer aligned at the same depth (**Figure 2-7**, right). As a consequence of the new setup, derivatives like reflection could not be calculated directly anymore because the water column between the sensor levels had to be taken into account. However, an increasing stability was achieved accompanied by an undisturbed field of view for the irradiance sensors and the possibility of attaching a stereo camera system.

Figure 2-7: Measurement setup 2010 (left) and 2011 (right)

Measurements were made either from a jetty in Starnberg over patches of *Chara* spp., *Elodea nuttallii* and *Potamogeton perfoliatus* (setup "Starnberg" in **Figure 2-8**) or from a boat in Bernried (setup "Bernried" in **Figure 2-8**). Iterations were made during solar noon (± two hours) to include diurnal variations in the reflection. The measurements were performed in 2 m depth at "Starnberg" and in 2 m and 4 m depths at "Bernried". At both sites they were made directly above the vegetation patch (r_{rs}^{b}) as well as just below the water surface (r_{rs}^{0-}). A detailed description is given in Wolf et al. (2013a).

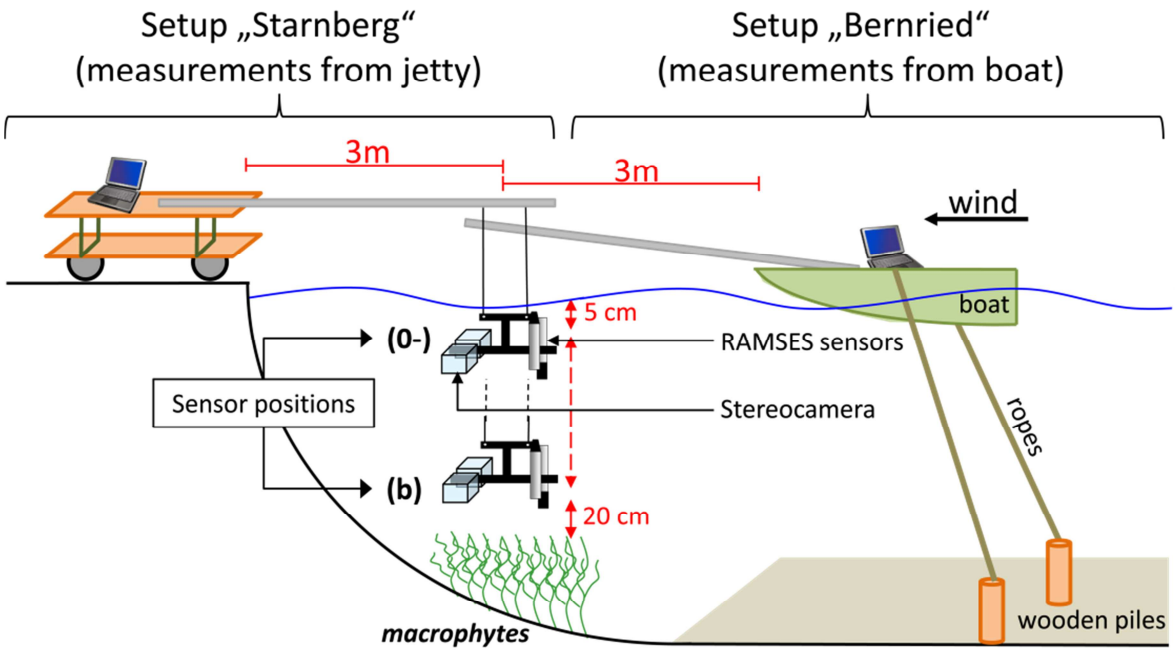

Figure 2-8: *in situ* measurement setup for the test site “Starnberg” (where measurements were made from a boat jetty) and “Bernried” (measurements from a boat) changed after Wolf et al. (2013a)

At each site, measurements were made every three weeks during the growing season (depending on the weather). **Table 2-1** shows the dates and locations of the field measurements 2010 and 2011.

Table 2-1: overview of *in situ* measurements performed 2010 and 2011

2010		2011	
Starnberg*	**Bernried****	**Starnberg***	**Bernried****
16.07.2010	10.08.2010	13.05.2011	19.05.2011
21.08.2010	26.08.2010	15.06.2011	28.06.2011
06.09.2010	22.09.2010	27.06.2011	27.07.2011
20.09.2010	22.10.2010	26.07.2011	12.08.2011
11.10.2010		10.08.2011	03.09.2011
29.10.2010		06.09.2011	21.09.2011
		28.09.2011	18.10.2011
		15.10.2011	

* *Chara* spec., *Elodea nuttallii*, *Potamogeton perfoliatus*
** *Najas marina*

Besides spectral measurements of the four macrophytes mentioned in **Table 2-1**, a sediment reflectance database was created. Sediment samples were collected by divers at 13 locations on the western shore of Lake Starnberg in four different depths zones (0 – 1 m, 1 – 2 m, 2 – 4 m and greater 4 metres) using a PVC-core. The first 2 cm of the samples were measured in the laboratory using an ASD FieldSpec FR device (Analytical Spectral Devices) and the resulting spectra were used for spectral unmixing.

The large variability of the reflectance shown in the uppermost plot of **Figure 2-9** (for the wavelength range 400 – 2500 nm) can be explained by the brightness of the sediment, which varied from grey sand to black-brownish silt. The spectral range used for water

applications (400 – 800 nm) shown in the middle plot also presents absorption features. These can be examined by plotting the curves continuum removed (i.e. by setting all local maximums to 1). In the lower plot of **Figure 2-9**, the absorption maxima of different chlorophyll types are indicated. These small absorption features shows the need of a proper spectra selection for subsequent spectral unmixing.

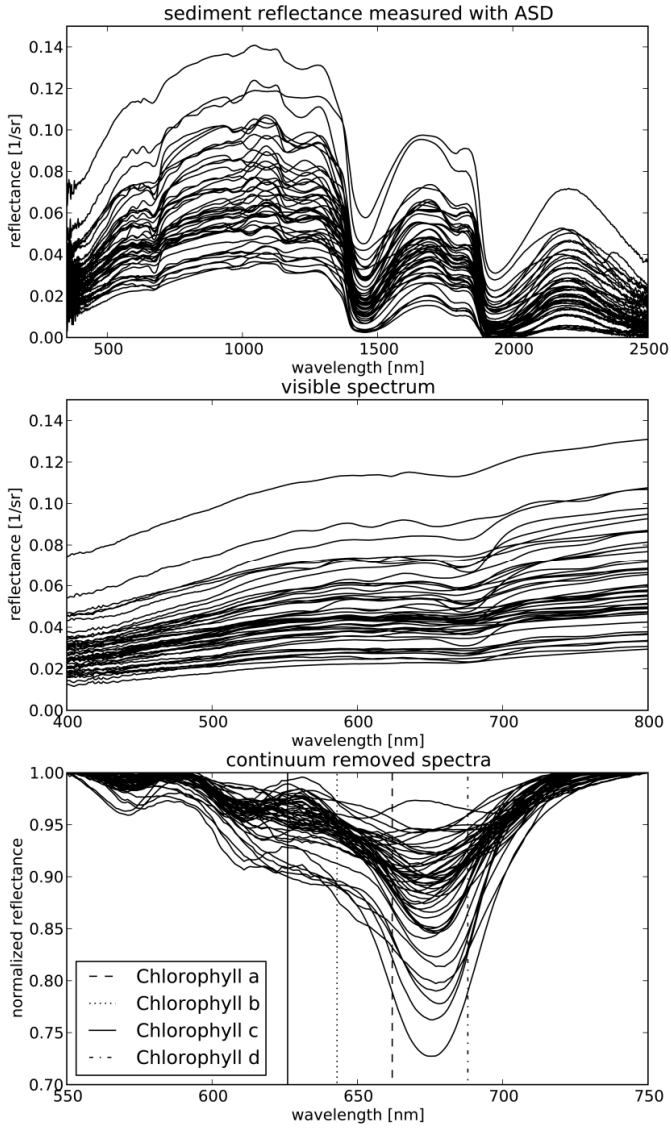

Figure 2-9: Reflectance database of collected sediment samples from Lake Starnberg. Above: reflectance of the full spectral resolution of the ASD-FieldSpec (350 – 2500 nm); middle: reflectance spectra of sediments for the wavelength region relevant for shallow water applications (400 – 800 nm); below: continuum-removed reflectance spectra for the absorption regions of different chlorophyll types.

2.4 Modelling

2.4.1 The bio-optical model BOMBER

The ENVI add-on BOMBER (Bio-Optical Model Based tool for Estimating water quality and bottom properties from Remote sensing images) of Giardino et al. (2012) relies on the radiative transfer modelling of Lee et al. (1998, 1999) which has been developed based on Hydrolight simulations. It is designed for image based water constituent retrieval in deep water as well as water constituent retrieval, bottom unmixing and depth

determination in shallow water. According to Lee (1998, 1999) the deep water contribution r_{rs}^{∞} is related to the total absorption a and total backscattering b_b according to Eq. 2.1:

$$r_{rs}^{\infty} = \left[g_0 + g_1 \left(\frac{b_b}{a + b_b} \right)^{g_2} \right] \frac{b_b}{a + b_b} \tag{2.1}$$

The factors g_0, g_1 and g_2 have been empirically defined by Lee et al. (1999). The inherent optical properties (IOPs) total absorption a and the total backscattering b_b are the sum of individual absorption and backscattering values of water, phytoplankton (CHL), colored dissolved organic matter (cDOM) and suspended particulate matter (SPM). In BOMBER, the absorption and backscattering spectra needed for the calculation are taken from literature; details are given in Giardino et al. (2012). The shallow water mode needs three possible bottom reflectances (r_{rs}^{b}) for spectral unmixing as auxiliary input data. The reflectance just below the water surface $r_{rs}(0-, H)$ for a water depth H is modeled using Eq. 2.2 (Lee et al. 1998, 1999):

$$\begin{aligned} r_{rs}(0-, H) = r_{rs}^{\infty}\{1 - A_0 \exp[-(K_d + K_{uw})H]\} \\ + A_1 r_{rs}^{b} \exp[-(K_d + K_{ub})H] \end{aligned} \tag{2.2}$$

Where A_0 and A_1 are weighting factors for the bottom and the water contribution to the overall signal received at the sensor, values were defined by Lee et al. (1998, 1999) and Albert and Mobley (2003). The attenuation coefficients for the upwelling radiance of the bottom (K_{ub}) and the water column (K_{uw}) are parameterizations of Lee et al. (1999). The model performs a least-squared optimization to minimize the error which is calculated from modelled (R_{rs}^{*}) and image derived reflectance (R_{rs}) for all wavelengths λ according to Eq. 2.3 (Giardino et al. 2012):

$$error = \sqrt{\sum_{\lambda_{min}}^{\lambda_{max}} \left(R_{rs}(\lambda) - R_{rs}^{*}(\lambda) \right)^2} \tag{2.3}$$

2.4.2 Calculation of AOPs from in situ measurements

The *in situ* measured spectra of E_d, E_u and L_u offer various possibilities of calculating the Apparent Optical Properties (AOPs) of the (deep) water column even in shallow areas. The pressure sensor attached to the E_d-device (SN: 8109) delivers the depth with a very high accuracy (± 1 cm) and thus can be taken as reference depth for the entrance optics. Since the sensors were not aligned at the same depth, the 2011 dataset needs to be corrected for the depth difference between the entrance optics of E_d and L_u 0.455 metre before r_{rs} can be calculated. First, the vertical diffuse attenuation of downwelling irradiance K_d is calculated using the mean of E_d measurements in different sensor depths ($z_1 < z_2$) according to Eq. 2.4 (see **Chapter 3**):

$$K_d = \frac{1}{(z_2 - z_1)} \ln \frac{E_d(z_1)}{E_d(z_2)} \tag{2.4}$$

The derived calculated K_d is then used to calculate r_{rs} and r (Eq. 2.5):

$$r_{rs} = \frac{L_u}{E_d \exp(-K_d \cdot 0.455)}$$
$$r = \frac{E_u}{E_d \exp(-K_d \cdot 0.455)} \quad (2.5)$$

The taken measurements above the bottom and directly below the water surface additionally allow the estimation of the corresponding deep water reflectance r_{rs}^{∞} if the simple model for radiative transfer in shallow water is used (Maritorena et al. 1994) (Eq. 2.6):

$$r_{rs}(0-,H) = r_{rs}^{\infty} + (r_{rs}^{b} - r_{rs}^{\infty}) \exp(-2KH) \quad (2.6)$$

$r_{rs}(0-,H)$ is the remote sensing reflectance just below the water surface for shallow water with the water depth H, r_{rs}^{∞} the deep water reflectance, r_{rs}^{b} the reflectance of the bottom and K the attenuation coefficient. Assuming that K_d is a good approximation for K (Maritorena et al. 1994) and solving for r_{rs}^{∞} leads to Eq. 2.7 (see **Chapter 4**):

$$r_{rs}^{\infty} = \frac{r_{rs}(0-,H) - r_{rs}^{b} \exp(-2K_d H)}{1 - \exp(-2K_d H)} \quad (2.7)$$

The resulting r_{rs}^{∞} can be used for the retrieval of water constituents using inversion methods of physically based models. It is related to the IOPs total absorption a and total backscattering b_b through Eq. 2.8 where the factor f is either set constant (Gordon et al. 1975) or as a function of the underwater sun zenith angle (Albert and Mobley 2003; Kirk 1984; Morel and Gentili 1993; Sathyendranath and Platt 1997):

$$r_{rs}^{\infty} = f \frac{b_b}{a + b_b} \quad (2.8)$$

2.4.3 Calculation of spectral separability

The *in situ* collected reflectance just above the vegetation patches r_{rs}^{b} were used to estimate the spectral separability between different bottom types without the overlaying water column (**Chapter 4**). After resampling to the desired multispectral resolution (by using the channel specific spectral response functions), the M-statistic (Kaufman and Remer 1994) was calculated for every spectral band λ by using the mean value (μ) and the standard deviation (σ) of two bottom types (1 and 2) that are compared (Eq. 2.9):

$$M(\lambda) = \frac{|\mu_1(\lambda) - \mu_2(\lambda)|}{|\sigma_1(\lambda) - \sigma_2(\lambda)|} \quad (2.9)$$

The equation of Kaufman and Remer (1994) was changed to achieve positive values only (i.e. by calculating with absolute values). This index has already been used successfully for benthic substrate mapping using *in situ* collected reference data (O'Neill et al. 2011) A value below 1 indicates bad separability, higher values indicate good separability.

2.4.4 Creation of endmember using a semi-empirical method

The estimated deep water reflectance r_{rs}^{∞}, the bottom reflectance r_{rs}^{b} and the vertical diffuse attenuation K_d are used to calculate deep-invariant indices according to Lyzenga (1978, 1981) which are used for subpixel spectral unmixing (**Chapter 3**). **Figure 2-10** shows the reflectance of *Najas marina* and uncovered sediment in five water depths (1 to 5 metres). These simulated spectra were first resampled from hyperspectral RAMSES resolution (A) to the multispectral resolution of RapidEye (B) using the channel specific spectral response functions.

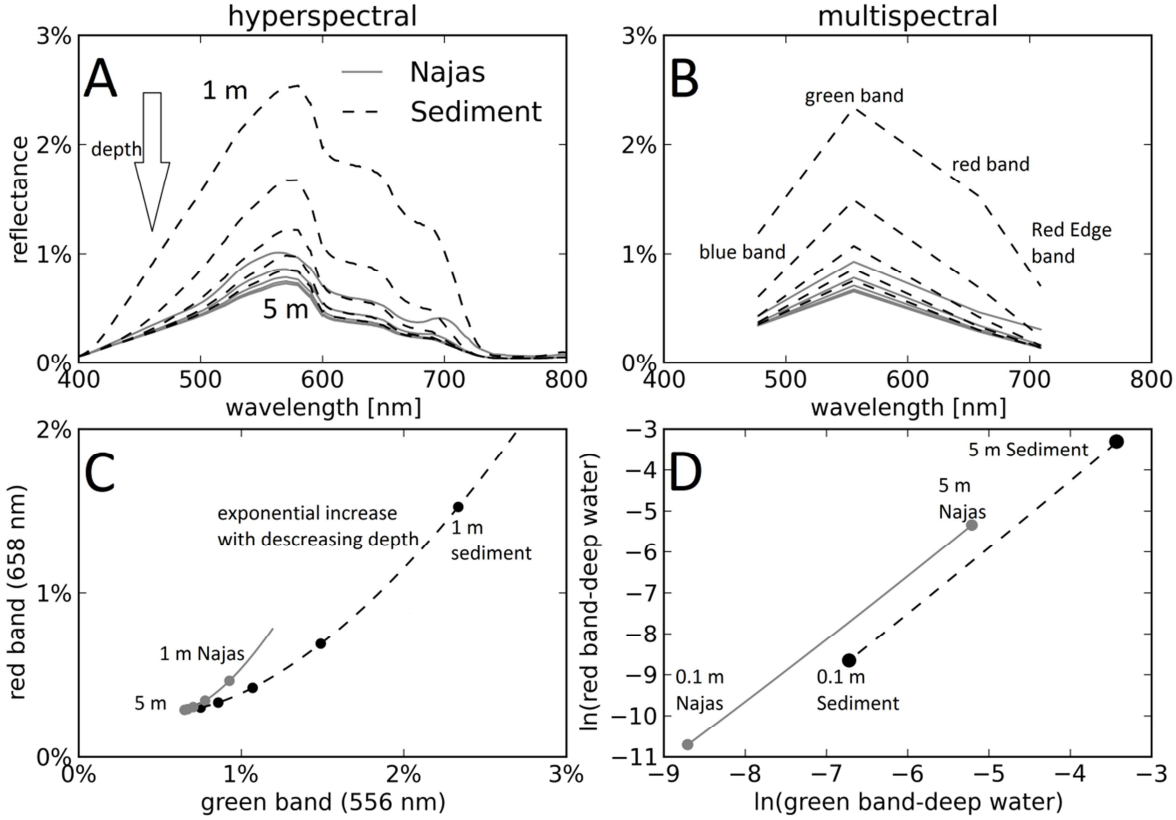

Figure 2-10: (A) simulated hyperspectral reflectance spectra of *Najas marina* and uncovered sediment at five water depths (1 – 5 m), (B) spectra resampled to the spectral resolution of RapidEye, (C) scatterplot of the reflectance values of the Red and the Green spectral band, (D) *ln*-transformed reflectance spectra of the Green and the Red spectral band.

The exponential depth dependency can be visualized by plotting the specific reflectance values of two spectral bands as a scatterplot (C). To correct for depth-depending intensity loss of the signal, a linearization of each spectral band λ is performed using the natural logarithm after subtracting the corresponding deep water reflectance in this band (Lyzenga 1978) using Eq. 2.10:

$$X_\lambda = \ln[r_{rs}(\lambda) - r_{rs}^{\infty}(\lambda)] \tag{2.10}$$

X_λ is the linearized form of r_{rs} in the RapidEye band λ. If the ln-transformed values of two bands are plotted against each other (D), the transformed "distances" in the scatterplot between the bottom types remain the same regardless the changing depth.

These ln-transformed reflectance values from each band can now be used to calculate a depth-independent band ratio Y_{λ_1,λ_2} of band λ_1 and band λ_2 using the attenuation coefficients of both bands (K_{λ_1} and K_{λ_2}) according to Lyzenga (1981) (Eq. 2.11):

$$Y_{\lambda_1,\lambda_2} = \frac{K_{\lambda_2} X_{\lambda_1} - K_{\lambda_1} X_{\lambda_2}}{\sqrt{\left(K_{\lambda_1}^2 + K_{\lambda_2}^2\right)}} \tag{2.11}$$

This method has been used for bathymetric applications with known substrate (Mishra et al. 2004) or benthic habitat mapping (Hedley and Mumby 2003; Mumby et al. 1998; Tassan 1996). The index allows the calculation of $(n^2 - n)/2$ possible band combinations for n bands and adapts typical values for different bottom types. Including the seasonal varying reflectance of SAV and concentrations of water constituents (from *in situ* derived attenuation coefficients) enhances the bottom unmixing result. A detailed description of this method is given in **Chapter 3**.

2.4.5 Retrieval of water constituent concentrations

If the bottom reflectance r_{rs}^b is well known, *in situ* measurements can be used to perform water constituent retrieval using physically based inversion methods. In **Chapter 5**, the application of submerged white and a black plastic foils is presented. The physically based model is the same as in BOMBER (Giardino et al. 2012) which uses the radiative transfer model of Lee et al. (1998, 1999). Since the sensors are not aligned at the same depth (measurement setup of 2011), the least-squared optimization is performed on L_u measurements. Therefore, the radiance at a sensor depth z_1 is separated in a part originating from the bottom (L_u^b) and a part originating from the water (L_u^w) (Eq. 2.12):

$$L_u(z_1) = L_u^b(z_1) + L_u^w(z_1) \tag{2.12}$$

E_d is measured simultaneously in the sensor depth z_2 ($z_2 = z_1 - 0.455m$) and $E_d(z_1)$ can thus be calculated using Eq. 2.13:

$$E_d(z_1) = E_d(z_2) \exp[-K_d \cdot 0.455] \tag{2.13}$$

Since K_d depends also on the IOPs, it is included as fit parameter. Involving this in the shallow water model of BOMBER (Eq. 2.2), $L_u^b(z_1)$ can be expressed as (Eq. 2.14):

$$L_u^b(z_1) = \{E_d(z_2) \exp[-K_d(H - z_2) A_1 r_{rs}^b]\} \exp[-K_{ub}(H - z_1)], \tag{2.14}$$

where H is the water depth, z_1 the sensor depth of L_u and z_2 the depth of the E_d sensor. The contribution of L_u^w can be expressed as (Eq. 2.15):

$$L_u^w(z_1) = \frac{\{r_{rs}^{\infty}(1 - A_0 \exp[-(K_d - K_u^w)(H - z_1)])\} \cdot \{E_d(z_1)(1 - A_0 \exp[-K_d(H - z_1)])\}}{1 - A_0 \exp[-K_u^w(H - z_1)]} \tag{2.15}$$

A least squared optimization is now performed to find best fitting values of IOPs and bottom depth H to minimize the error between modeled L_u^* and measured L_u using Eq. 2.16:

$$\text{err} = \sqrt{\sum_{\lambda_{min}}^{\lambda_{max}} [L_u(\lambda) - L_u^*(\lambda)]^2} \tag{2.16}$$

For the comparison with reflectance derived concentrations, measurements of E_d under water were inverted using the Water Colour Simulator (WASI) of Gege (Gege 2004, 2012; Gege and Pinnel 2011). It enables the separation of direct and diffuse incident light and delivers water constituent concentrations with a high accuracy.

2.5 Image analysis

2.5.1 Atmospheric correction and surface correction

Atmospheric correction of hyperspectral airborne HyMap and APEX images was performed by the German Aerospace Center (DLR) and the APEX processing and archiving facility (Hueni et al. 2009) at VITO (Mol, Belgium), respectively. Both use ATCOR 4 (Richter 1996) which incorporates MODTRAN (MODerate resolution atmospheric TRANsmission), a radiative transfer code with various atmosphere and aerosol types which is used to calculate unique solutions for each image. For hyperspectral AISA Eagle data, *in situ* reflectance measurements were used for atmospheric correction according to the empirical line method (Moran et al. 2001). This method can also be used to refine previous atmospheric corrections (Conel et al. 1987). Thiemann and Kaufmann (2002) found that best results of the the empirical line calibration were achieved by using very dark and very bright surfaces as well as an intermediate reflecting surface. Therefore, white and black silo foils were spread over a meadow next to the main research area at Bernried (Lake Starnberg) and their reflectances were measured with an ASD spectroradiometer. The submerged white plastic foil in shallow water acted as an intermediate surface. In ENVI™ (version 4.7) the field-measured reflectance spectra were paired with the corresponding radiance values from the image and a liner regression was performed to derive best fitting values (gains and offsets) for each spectral band.

For the multispectral imageries of RapidEye and WorldView-2, the results of ATCOR were not satisfying, as resulting in excessive correction of the Red and Blue channel (reflectance values of zero or below) and too high reflectances in the NIR. Thus, the method of Mishra (2005) was used to derive water-leaving radiances from the top-of-atmosphere radiance. It is based on atmospheric correction procedures which were originally developed for the coastal zone color scanner (CZCS), SeaWiFS and MERIS data but can also be applied to other sensors and inland water bodies. According to Gordon and Clark (1981), the radiance received at the sensor is the sum of radiance originating from molecular Rayleigh scattering, aerosol scattering and the water-leaving radiance lowered by the transmittance of the atmosphere. The radiance of aerosol is most difficult to determine from image data without auxiliary measurements. Hence, atmospheric correction procedures were developed where the contribution of aerosol is derived from Rayleigh-corrected images. The contribution of Rayleigh radiance was calculated as a function of wavelength and surface pressure, as well as the viewing- and illumination-geometry (Doerffer 1992; Hansen and Travis 1974; Mishra et al. 2005).

For marine applications, the Angstrom exponent is set to unity which is typical for marine aerosols (Gordon and Voss 1999). In southern Germany, the more continental aerosols have higher Angstrom exponents. The information on aerosol properties are taken from the Aerosol Robotic Network (AERONET), a worldwide network of sun/sky radiometers (Holben et al. 1998). The AERONET station “Munich University” is located

25 km northeast of Lake Starnberg at an altitude of 533 m AMSL. Besides the aerosol properties, additional information provided by AERONET was used to enhance atmospheric correction, such as the ozone concentration, the atmospheric pressure and the water vapour content. Knowing the AOT (τ_a) for a given date, the contribution of aerosol scattering (L_a) to the total radiance received by the sensor can be calculated using the formula of Gordon et al. (1983) (Eq. 2.17):

$$L_a = \omega_a(\lambda)\tau_a(\lambda)F_0'(\lambda)p_a(\theta_0, \theta_v, \lambda)/4\pi \quad (2.17)$$

Where ω_a is the single scattering albedo of aerosol, F_0' is the instantaneous extraterrestrial solar irradiance (F_0) reduced by two trips through the ozone layer and p_a is a function of the Fresnel reflectance and the scattering phase function of aerosol dependent of the wavelength λ and the solar and viewing zenith angles (θ_0 and θ_v), respectively.

The second step of image preparation is the correction of effects at the water surface. Sun glint can appear at the slope of waves and impedes the retrieval of a useable signal (Bostater et al. 2004; Mertes et al. 1993; Morel and Bélanger 2006). For airborne missions, this can be avoided by choosing acquisition times with less sun glint. Risk decreases if the flight lines are directed towards or away from the sun. Sun glint can be estimated from the satellite azimuth and the sun azimuth angle and is highest at a relative azimuth (difference between sun- and satellite-azimuth angles) of ± 90°. This leads to sensors facing towards the sun with highest sun glint effects (Beisl 2001; Wolf et al. 2013b). The algorithms to correct sun glint-affected areas in shallow waters has been developed by Hedley et al. (2005) and Hochberg et al. (2003). Sun-synchronous sensors like RapidEye always crosses the equator at the same local time (Lillesand et al. 2008), thus the sun glint-probability remains constant. RapidEye has a relative bad acquisition constellation since the relative azimuth is mostly ± 90° (highest risk). However, most images are not affected. Only scenes were the relative azimuth ($\Delta\phi = \phi_v - \phi_0$) is greater than zero, forward scattered light can reach the sensor due to specular reflectance – nadir-viewing ($\theta_v \approx 0°$) acquisitions have increased sun glint risk (**Figure 2-11**).

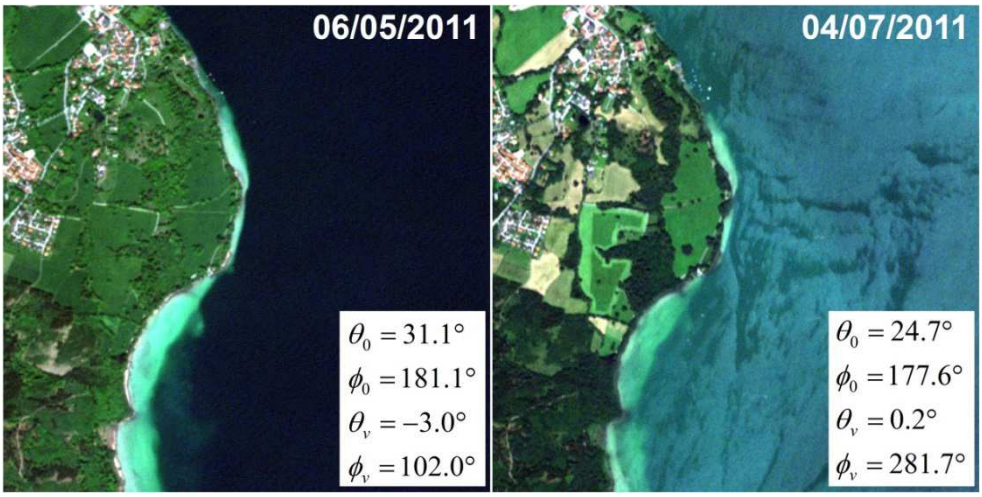

Figure 2-11: examples of a RapidEye scene without sun glint (06/05/2011) and with sun glint (04/07/2011) showing the test site Bernried (Angles: θ_0 sun zenith; θ_v satellite zenith; ϕ_0 sun azimuth; ϕ_v satellite azimuth)

The resulting reflectance above the water surface R_{rs} can be directly calculated from *in situ* measured E_d and L_u-intensities as well as any remote sensors after atmospheric correction and is therefore an AOP. R_{rs} is related to the subsurface reflection r_{rs} (which is measured *in situ* as well). Their relation depends on the individual reflection factors of the downwelling irradiance and the subsurface reflection factors for upwelling irradiance and radiance. Also the refractive index of water ($n = 1.33$) has to be taken into account. The approximation of Lee et al. (1998) relates the remote sensing reflectance above water (R_{rs}) to the remote sensing reflectance just below the water surface (r_{rs}) based on Hydrolight-generated reflectance spectra for nadir-viewing sensors. Solving for r_{rs} leads to Eq. 2.18 (see **Chapter 3**):

$$r_{rs} \approx \frac{R_{rs}}{0.518 + 1.562R_{rs}} \tag{2.18}$$

2.5.2 Water column correction

After air-water interface correction, the remote sensing reflectance of shallow water ($r_{rs}(0-,z)$) now only contains information about the water column (deep water reflection reduced according to the attenuation) as well as the bottom reflectance r_{rs}^b (see Eq. 2.2). To retrieve information about the bottom, the disturbing effects of the water constituents were removed using correction methods.

In this thesis, two different methods were used as described in **Chapter 2.4** for *in situ* data processing. The semi-empirical method based on ln-transformed band ratios according to Lyzenga (1978) needs the vertical diffuse attenuation coefficients as auxiliary data which were taken from *in situ* measurements (**Chapter 2.4.2**). The image based calculation of depth-invariant bands is the same as for the *in situ* data (compare **Chapter 2.4.3**). The resulting image was processed towards pixel based spectral unmixing using the matched filtering method (Manolakis and Shaw 2002) and contains six depth-invariant bands (the near-infrared band of RapidEye was omitted due to strong water absorption). In **Chapter 3**, the possibilities of using multi temporal datasets in combination with multitemporal *in situ* measurements are shown for Lake Starnberg.

The second method is the application of the bio-optical model BOMBER as described in **Chapter 2.4.1**. It has been applied on multitemporal RapidEye data (**Chapter 4**) and on hyperspectral airborne APEX data (**Chapter 5**) using *in situ* measured bottom reflectances.

2.6 Foil experiment

In an experimental approach, artificial surfaces (white and black plastic foils) with known reflectance behaviour (measured in a spectral laboratory) were used during hyperspectral airborne flight campaigns to create controlled test sites for depth estimation and IOP retrieval. This experiment was inspired by the approach of Cho and Lu (2010) who made reflectance measurements in a water tank using light and dark bottoms. The idea behind this is a simplified understanding of the reflectance in shallow water (**Figure 2-12**): A very bright surface has a high bottom reflectance (r_{rs}^b) and reflects nearly the entire incident light ($r_{rs}^b \approx 100\%$), thus the measured reflectance above the submerged white foil (R_{rs}^{white}) is mostly affected by the absorption a of the water column above the foil since r_{rs}^b

is much larger than the sum of water body reflection (r_{rs}^{∞}) and surface reflection (approximated of 2%). If the incident light is measured, a can be derived from the measured reflectance (R_{rs}^{white}). Over the black foil, the contribution of r_{rs}^{b} can be neglected, thus R_{rs}^{black} is approximatelyr_{rs}^{∞}. If measurements of both foils exists at same water depths (as is the case in the experimental setup), b_b can be also estimated since r_{rs}^{∞} and a are known.

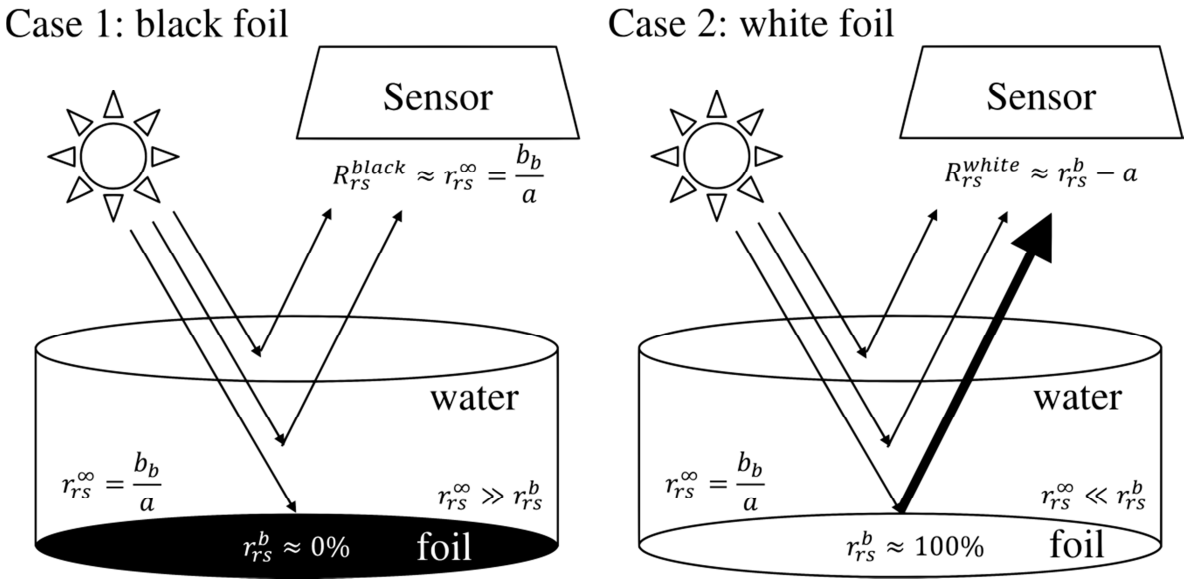

Figure 2-12: Schematic presentation of the foil experiment (modified after Cho and Lu, 2010). r_{rs}^{∞} is the volume reflection of the water (backscattering b_b divided by absorption a), r_{rs}^{b} the bottom reflectance and $R_{rs}^{white/black}$ the reflectance measured directly above the water surface.

Considering this, the black foil should be ideally suited to quantify the predominantly scattering water constituent SPM and the white foil to determine the concentrations of the absorbing water constituents CHL and cDOM. An evaluation based on *in situ* measurements, simulated datasets and APEX imagery is given in **Chapter 5.**

The next three chapters are the embedded original publications. **Chapter 3** starts with the presentation of the semi-empirical method for bottom differentiation; **Chapter 4** presents the use of bio-optical model inversions for multiseasonal datasets. Finally, the results of the foil experiment are presented in **Chapter 5**.

3. MULTISPECTRAL REMOTE SENSING OF INVASIVE AQUATIC PLANTS USING RAPIDEYE

S. Roessler[1], P. Wolf[1], T. Schneider[1], A. Melzer[1]

[1]Limnological Institute, Technische Universität München, München, Germany

J. M. Krisp et al. (eds.), Earth Observation of Global Changes (EOGC), Lectures Notes in Geoinformation and Cartography, pp. 109-123, DOI: 10.1007/978-3-642-32714-8_7

3.1 Abstract

Some invasive aquatic plants are thought to benefit from recent climate warming. Their frequent observation is only feasible using satellite data. Earlier studies used airborne hyperspectral sensors like HyMap to discriminate different plant species – this is a very cost intensive method with an environmental impact through numerous flights. A fully automated processing chain to assess the distribution of invasive species, as well as their abundances and biomass is restricted to spaceborne sensors. The research presented here investigates the ability of multiseasonal multispectral remote sensing data (RapidEye) to differentiate between vegetated and non-vegetated areas, as well as species composition at a subpixel level. This is done by combining *in situ* derived information about the apparent optical properties of the water body and reflectance measurements of *Elodea nuttallii* and *Najas marina*. The information about the current state of the water body is used to produce depth-invariant combinations of spectral bands using a simple physically based semiempirical method. *In situ* reflectance measurements were processed with the same method and subsequently used in a Matched Filtering spectral unmixing approach. The results show a good separation between vegetated and bare littoral areas. A reliable differentiation of plant species still requires further method development.

3.2 Introduction

Submerged macrophytes in freshwater lakes are used as longterm indicators for nutrient conditions (Melzer 1999). Climate change is thought to favour invasive submersed macrophytes in freshwater ecosystems (Rahel and Olden 2008) and therefore to have profound influence on lake ecosystems. Two invasive species, *N. marina* and *E. nuttallii* have been subject of multidisciplinary research for several years, as it is assumed that increasing water temperature promotes their expansion. *N. marina* is indigenous to Europe, while *E. nuttallii* is a neophytic species originating in North America. The species differ in their expansion speed with *E. nuttallii* expanding much faster. Since the trophic state of these ecosystems is strongly correlated to water temperature, adequate monitoring of these species will give important information about the development of lakes in a warming climate. In this study the application of different space- and airborne sensors for identification and monitoring of invasive aquatic plants have been tested.

Until now, a frequent observation of the expansion behaviour of invasive species is restricted to hyperspectral airborne remote sensors which provide the needed geometric and spectral resolution (Pinnel 2007). This is – for frequent observations – a very expensive method and has major ecological impact through flight related emissions of greenhouse

gases. Therefore, a fully automated monitoring system must be based on spaceborne sensors with satisfying spectral, radiometric and geometric resolutions and a short revisit time, enabling on demand information about the current state. The multispectral data provided by RapidEye fulfils these requirements.

The questions we addressed were: Can multispectral remote sensing combined with frequent *in situ* observations and/or model prediction help to distinguish submerse macrophytes in shallow freshwater environments? Which statements can be made in terms of species composition, abundance of invasive species, as well as their expansion behaviour and vitality? RapidEye is ideally suited to address this problem. Moreover, the short revisit time at a geometric resolution of 5 metres allows a realistic description of the spatially and temporally heterogeneous vegetation communities. Multiseasonal RapidEye data were obtained from the RapidEye Science User Archive (RESA) covering the vegetation period from May to September 2011.

3.3 Materials and Methods

3.3.1 Study Site

The study site was Lake Starnberg (47°55'N, 11°19'E) situated 25 km southwest of Munich (**Figure 3-1**). It covers an area of 56 km^2 and is Germany's fifth largest lake. The length is 20 km, the maximum width 4.7 km and the maximum depth is 127.8 m (on average 53.2 m). The lake was formed by the Isar-Loisach-Glacier during last glacial period (Fesq-Martin et al. 2008). Extended littoral terraces are situated on the western shore. At this lakeside, test sites were selected according to high abundances of *Najas marina* and *Elodea nuttallii*, as well as other common macrophytes like *Potamogeton perfoliatus* and *Chara* spec., which were also spectrally measured to compare their reflectance properties.

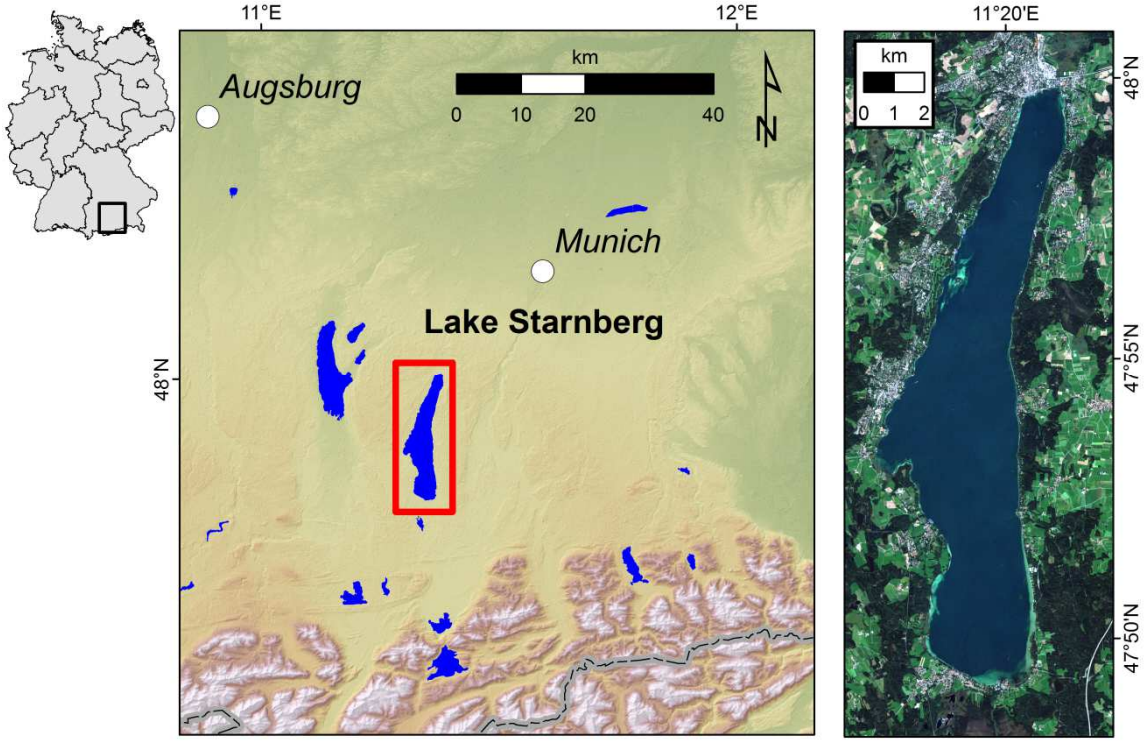

Figure 3-1: Location of Lake Starnberg and RapidEye subset from 03/09/2011

The former oligotrophic lake turned into a mesotrophic state after 1950 due to discharge of wastewater. After installation of a sewage disposal system, water quality improved. Present Phytoplankton concentrations range between 2.4 and 4.8 µg l^{-1} in winter and 6–12 µg l^{-1} in summer, respectively. The average annual primary production is 889 g C m^{-2} y^{-1} (Pinnel 2007).

3.3.2 In Situ Data and Processing

In situ measurements were performed using three RAMSES submersible spectroradiometers (TRIOS GmbH), which were triggered simultaneously. The sensors recorded hemispherically the downwelling (E_d) and upwelling (E_u) irradiance, and the upwelling radiance (L_u) with a field of view of 7°, respectively.

Data acquisition took place during the growing season between August and Oktober 2010 at solar noon (± 2 hours) to get reflectances at low sun zenith angles (30° at maximum). Above each of the patches measurements were made at two different water depths (i.e. to include the water column with its constituents). The first measurement was just beneath the water surface (R_{0-}), the second just above the vegetation surface (R_b). In both sensor positions 20 single spectra were recorded. In **Figure 3-2**, pictures taken from an attached stereo camera system are shown. The photos were taken at the lower sensor position, located approximately 20 cm above the vegetation surface.

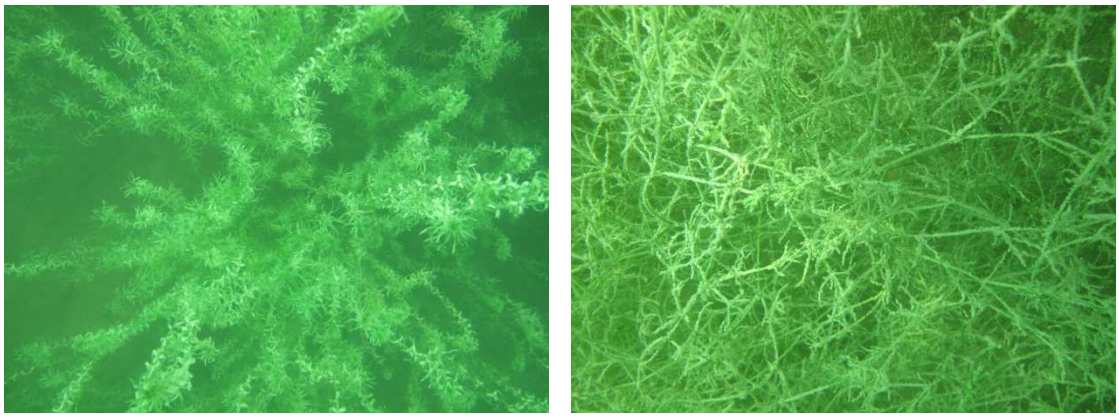

Figure 3-2: Photos taken under water of *Elodea nuttallii* (left) and *Najas marina* (right)

After an automatic calibration with MSDA_XE software (version 8.5) by TRIOS GmbH, the data were resampled to an equal wavelength raster, ranging from 320 to 950 nm with a spectral sampling interval of 3.3 nm. Further calculations (i.e. the remote sensing reflectance, attenuation) were performed with Python(x,y).

Apart from *in situ* spectral measurements, sediment samples were taken during diving trips and spectrally characterized in the laboratory using an ASD-FR field spectrometer (Analytical Spectral Devices Inc.). Samples were taken at 18 locations on the western shore at three different depths to generate a complete spectral library for all common sediment types.

Further biophysical parameters such as coverage (percentual amount of leaves, stalks, sediment and shade), growth height, biomass and pigment composition were collected at each penological state when spectral measurements were performed. The database serves as a basis for the development of a coupled reflection/ growth model for the macrophytes of interest (*E. nuttallii* and *N. marina*).

3.3.3 RapidEye Data and Processing

Multispectral remote sensing data were obtained from the RapidEye Science Archive (RESA) within the project no. 455. A time series of Lake Starnberg was recorded between 6th May and 3rd September 2011. The scenes were delivered as level 3A products including standard radiometric and geometric corrections. Atmospheric correction was performed using ATCOR 2 (Richter 1996) for flat terrain implemented in PCI Geomatics™ (version 10.2.3). The resulting bottom-of-atmosphere (BOA) reflectance images were mosaiced and further processed to correct for water specific properties. **Figure 3-3** gives an overview of how *in situ* measurements were included in the processing of RapidEye images.

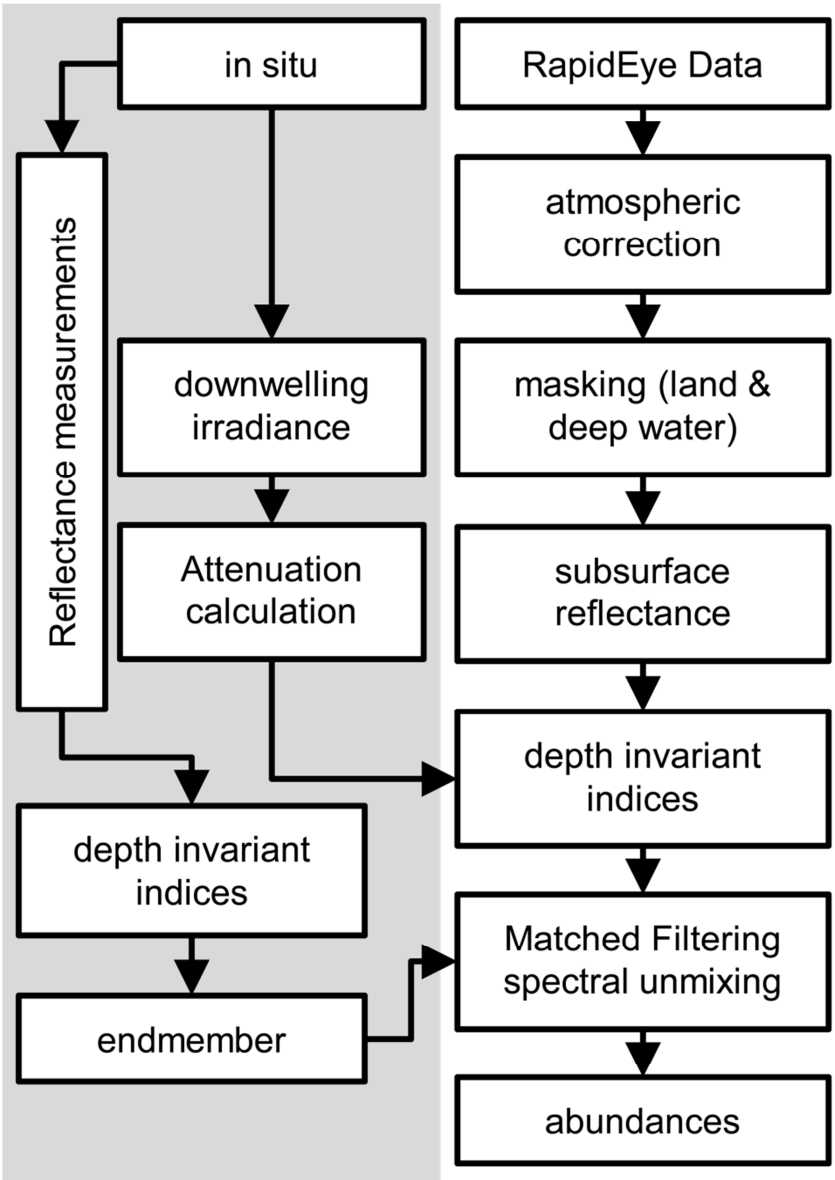

Figure 3-3: Processing flow chart showing the combination of *in situ* measurements and RapidEye data

Due to low variation of the reflectance signal in the near-infrared over optically deep water (Kay et al. 2009), sun glint correction was not carried out. To identify water bodies, a normalized difference water index (NDWI) was calculated using the reflection in the Green and near-infrared wavelength domain (McFeeters 1996) using Eq. 3.1:

$$NDWI = \frac{\rho_{green} - \rho_{NIR}}{\rho_{green} + \rho_{NIR}} \tag{3.1}$$

Although other authors (Lira 2006) propose a principal component analysis, we achieved good segmentation results with a NDWI threshold of 0 to delineate water bodies (pixel with values greater than 0 are assigned to water). Since only shallow water areas are of interest, a further threshold was applied using a deepwater corrected Red Index (RI) calculated with Eq. 3.2 (Spitzer and Dirks 1987).

$$RI = \frac{\rho_{red} - \rho_{\infty,red}}{\rho_{red}} \tag{3.2}$$

With ρ_{red} being the reflection value of each pixel in the Red and $\rho_{\infty,red}$ the mean Red reflection over optically deep water. Taking the variations of deepwater reflectance into account, an influence of the bottom signal was found if the Red Index value exceeded 0.15. This value is empirically defined for Lake Starnberg depending on the water constituents. Pixels with an NDWI value greater than 0 and a Red Index values greater 0.15 were further assigned to shallow water and processed.

The water leaving reflectance measured by the sensor above the surface (R_{rs}) is including the reduction of the signal due to the refraction of the upwelling radiance at the water surface. This decrease of water leaving signal intensity is described by dividing the signal with the squared refractive index of water (n_w^2 = 0.56). Taking the reflection factors of E_d (σ), L_u^- (σ_L^-) and E_u (σ^-) into account, the water leaving Remote Sensing reflectance can be calculated with Eq. 3.3 (Lee et al. 1998):

$$R_{rs} = \frac{(1-\sigma)(1-\sigma_L^-)}{n_w^2} \cdot \frac{r_{rs}}{1 - \sigma^- \cdot Q \cdot r_{rs}} \tag{3.3}$$

Lee et al. (1998) found as typical values for nadir viewing sensors $(1-\sigma)(1-\sigma_L^-)/n_w^2$ = 0.518 and $\sigma^- \cdot Q$ = 1.562 for transforming reflectances from beyond to above the water surface. Solving Eq. 3.3 for r_{rs} – which is measured *in situ* – leads to the Eq. 3.4 which can be used as approximation (Lee et al. 1999):

$$r_{rs} \approx \frac{R_{rs}}{0.518 + 1.562 R_{rs}} \tag{3.4}$$

In order to get information about subsurface bottom types at different depths, the exponentially decreasing light intensity has to be considered. This loss of radiation (vertical diffuse attenuation) is a function of scattering due to suspended particles and absorption of water constituents (phytoplankton, suspended particulate matter, gelbstoff and the water itself). Models have been developed to retrieve water constituents from remotely sensed or *in situ* data (Gege 2004). The correction of the decrease of light beam due to properties of the water column requires the knowledge of wavelength-dependant attenuation coefficients, water depths or the reflectance spectra of the substrate, respectively. Heege et al. (2003) developed a physically based process chain to derive bottom reflectances using a spectral library of known substrate albedo spectra. Instead of predicting the bottom reflectance, Lyzenga (1978, 1981) used a semi-empirical method that compensates the effects of variable depths by calculating depth-invariant indices. This method has been used

successfully for bathymetric studies with known substrate (Mishra et al. 2004), but can also be used to map different benthic habitats of varying depths (Hedley and Mumby 2003; Mumby et al. 1998; Tassan 1996). To account for the exponential depth dependance of the received signal, a linearization of each band was performed using the natural logarithm of each spectral band (Lyzenga 1978). Linear combinations of the log-transformed reflectance values were used to produce depth-invariant indices (Eq. 3.5) as described by Lyzenga (1981):

$$Y_{i,j} = \frac{K_j \ln(\rho_i - \rho_{\infty i}) - K_i \ln(\rho_j - \rho_{\infty j})}{\sqrt{(K_i^2 + K_j^2)}} \tag{3.5}$$

where K_i and K_j are the attenuation coefficients in band i and j, and $Y_{i,j}$ the calculated depth-invariant index between these bands. The natural logarithm is calculated from the reflectance values of shallow water areas reduced by the reflectance of deep water in the same band $(\rho_i - \rho_{\infty i})$.The index $Y_{i,j}$ is related to the bottom reflectance (r_i) as follows (Eq. 3.6) (Lyzenga 1981):

$$Y_{i,j} = Y_{i,j0} + \frac{K_j \ln r_i - K_i \ln r_j}{\sqrt{(K_i^2 + K_j^2)}} \tag{3.6}$$

The value $Y_{i,j0}$ is a constant for fixed illumination conditions and concentrations of water constituents. However, it can be omitted by adding an artificial water column to the *in situ* measured reflectance using known attenuation coefficients (K_d) and deepwater reflection (r_∞). The simulated shallow water reflection is calculated using Eq. 3.7 (Philpot 1989):

$$r_{shallow} = r_{bottom} \exp(-2K_d z) + r_{deepwater}[1 - \exp(-2K_d z)] \tag{3.7}$$

From the simulated reflectances of known substrates (derived from *in situ* spectral measurements), depth-invariant indices were calculated for each RapidEye scene representing the current conditions of water constituents and illumination geometry. The indices were used as endmembers in subsequent spectral unmixing of image derived depth-invariant indices.

The required diffuse attenuation coefficients (K_d) for the downwelling irradiance of the five spectral bands of RapidEye can either be derived from image data with known substrate at different depths (Armstrong 1993) or can be calculated with *in situ* measured spectra. We used measurements of the downwelling irradiance (E_d) at different depths $(z_2 > z_1)$ recorded for the different times RapidEye data were achieved. The attenuation coefficients were calculated using the Eq. 3.8 (Maritorena 1996):

$$K_d = \frac{\ln\left[\frac{\bar{E_d}(z_1)}{\bar{E_d}(z_2)}\right]}{z_2 - z_1} \tag{3.8}$$

The RAMSES derived hyperspectral attenuation coefficients (**Figure 3-4**, left) were spectrally averaged according to the channel specific sensitivity of RapidEye using the

spectral response functions of each band. Averaging was performed using ENVI™ 4.7. The resulting attenuation coefficients for 4 selected RapidEye Scenes are shown in **Figure 3-4** (right).

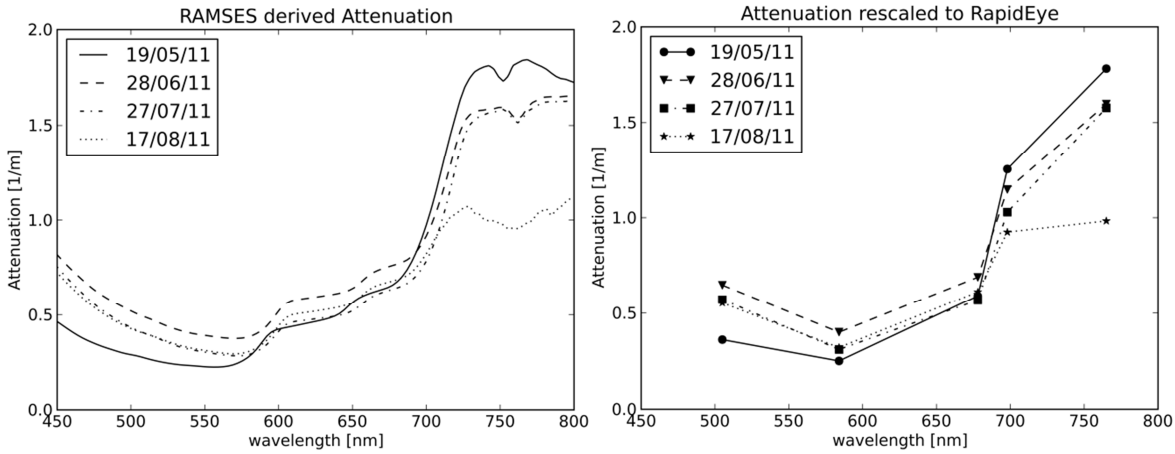

Figure 3-4: Attenuation coefficients derived from *in situ* measurements (left) and spectrally rescaled to the five bands of RapidEye (right)

Depth invariant indices according to Eq. 3.5 were calculated after preprocessing for all possible six band combinations between channels 1-4 (the NIR band was omitted due to strong water absorption). Subsequently, linear spectral unmixing was performed using the Matched Filtering method (Manolakis and Shaw 2002). This method was chosen since the three *in situ* derived endmembers (*E. nuttallii*, *N. marina* und uncovered sediment) presumably do not represent all possible coverages of Lake Starnberg's littoral zone. Every pixel was assigned a score value for the possible endmembers affiliation. Values near 1.0 indicate a perfect match (abundance of 100 %), values between 0.0 and 2.0 suggest a contribution of the endmember to the overall signal to a certain extent. Score values below 0 rule out an affiliation of this endmember.

3.4 Results and Discussion

3.4.1 In Situ Data

The *in situ* reflectance measurements above vegetation patches of *E. nuttallii* and *N. marina* show strong variations especially in the Red Edge and the near-infrared region. The main explanation for this is the strong variation of the downwelling irradiance caused by waves. In **Figure 3-5**, the deviation factor for different sensor depths is shown. It is calculated by dividing all recorded spectra with the lowest measured intensity.

With increasing depth the variation decreases, since the influence of waves decreases with increasing water column. At a depth of 5 m almost no deviations appear. Unlike the irradiance intensities, the radiance measurements are less influenced by waves. However, there are certain variabilities caused by plant movement. As meadow-like growing *Characea* are less influenced by waves, measurements are more stable. Variabilities of high growing macrophytes like *E. nuttallii* and *N. marina* increase with waves.

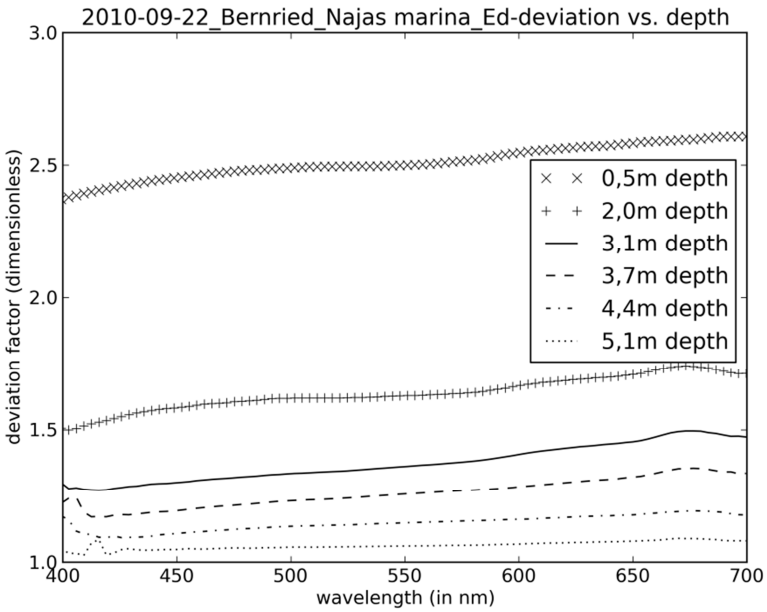

Figure 3-5: Deviation factor of the downwelling irradiance for different sensor depths

Due to the high standard deviation of measured reflectance spectra from different macrophytes or sediment coverages there is a great overlap between *N. marina* and *E. nuttallii* (**Figure 3-6**, left). However, the calculated depth-invariant ratios between the spectral bands of RapidEye are less affected by variations and provide good separability in certain artificial bands. The right panel of **Figure 3-6** shows the six possible depth-invariant band combinations.

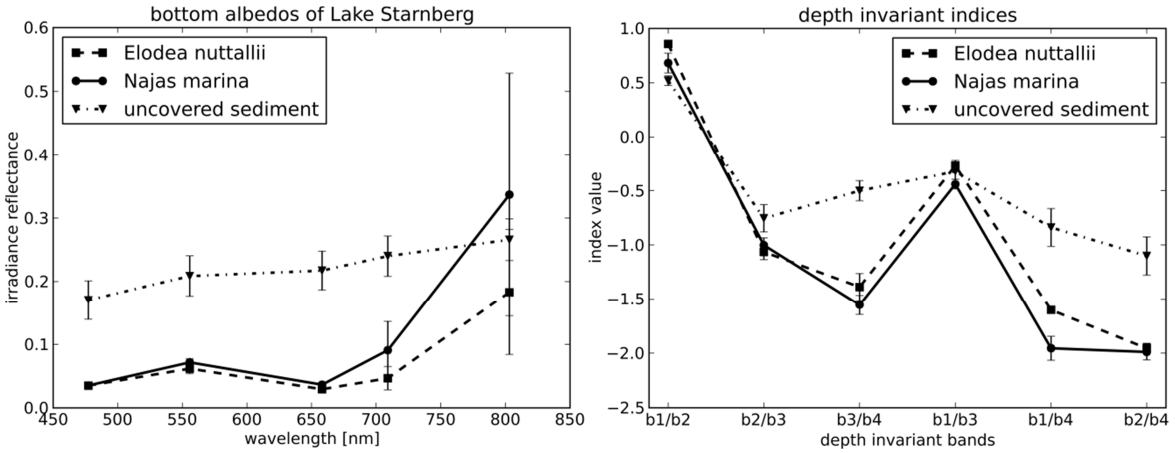

Figure 3-6: Reflectance measured above the bottom over different targets (left panel) and calculated depth-invariant indices (right panel)

The calculated indices indicate that band combinations may exist for which a separation of different species is possible as well as a discriminatation of bare soil and vegetated surfaces. To identify band combinations best suited for the identification of macrophytes (i.e. *N. marina* and *E. nuttallii*) as well as uncovered sediment, separability measures were calculated for all possible band combinations. As typical measures for Remote Sensing applications the Jeffries-Matusita Index (Richards 1999) was calculated using the software ENVI™ 4.7 (**Table 3-1**).

Table 3-1: Calculated separability measure for possible band combinations for the depth-invariant indices

Used depth-invariant Bands	Jeffries-Matusita index		
	Elodea nuttallii / Najas marina	***Elodea nuttallii* / uncovered sediment**	***Najas marina* /uncovered sediment**
All	1.56931166	2.00000000	1.98296533
(1) b1/b2	1.07808005	1.99998320	1.91085016
(2) b2/b3	1.17638898	1.99999987	1.93642036
(3) b3/b4	1.32375258	1.99999997	1.91254893
(4) b1/b3	1.24110761	1.99999989	1.94254478
(5) b1/b4	1.18262100	1.99999186	1.84942206
(6) b2/b4	1.05027142	1.99999438	1.84366436

Between *E. nuttallii* and *N. marina*, only depth-invariant band 3 (Red / Red Edge) and band 4 (Blue / Red) show comparatively good separability, however according to Richards (1999) only index values greater than 1.9 indicate good separability.

Between uncovered sediment and *E. nuttallii*, almost all calculated depth-invariant indices are well suited for separation. However, as seen in **Figure 3-6** (bottom panel), especially the depth-invariant bands 3 (Red / Red Edge), band 5 (Blue / Red Edge) and band 6 (Green / Red Edge) show completely different values compared to vegetated surfaces. Since it is less affected by absorption of coloured dissolved organic matter (cDOM), the depth-invariant band 3 can be used to differentiate between vegetated surfaces and bare bottom.

To evaluate the non-linear development of the index value of depth-invariant band 3, different coverages of *N. marina* were used to calculate depth-invariant indices (**Figure 3-7**, left). The different index values of depth-invariant band 3 shown in **Figure 3-7** (right) serve as threshold values to assess vegetation coverage from image data.

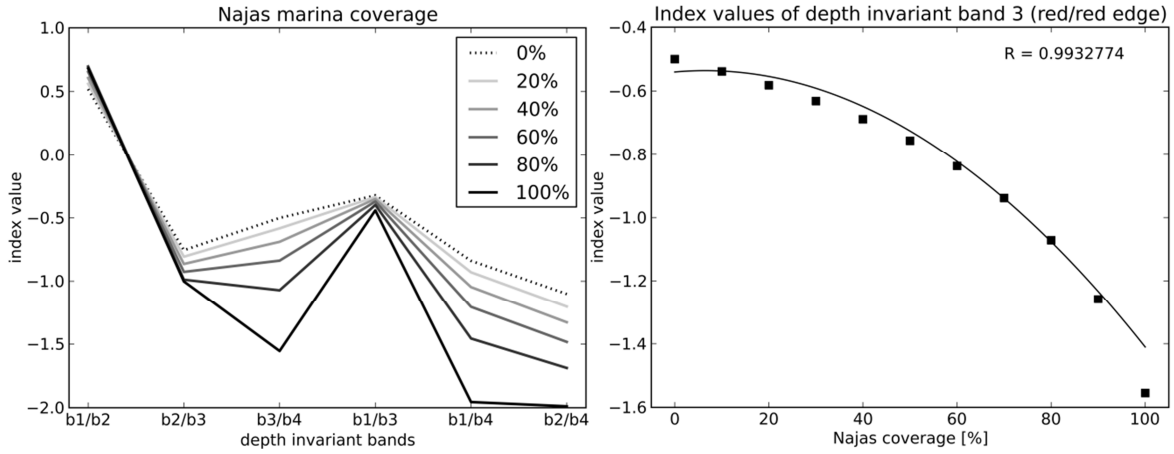

Figure 3-7: Depth-invariant indices calculated for different coverages of *Najas marina* (left) and relationship between vegetation coverage and index value of depth-invariant band 3 (right)

3.4.2 Remote Sensing Data

The Lyzenga (1978, 1981) based method for calculating depth-invariant bands was applied to 4 RapidEye scenes from summer 2011 (06/05/2011, 28/06/2011, 16/07/2011, and 20/08/2011). After masking of land and optically deep water areas (using Eqs. 3.1 and 3.2), depth-invariant indices were calculated with the attenuation values derived from *in situ* measurements for the subsurface reflectance (Eq. 3.5) of shallow water areas with the values given in **Figure 3-4** (right). The artificial band 3 (Green / Red Edge) was shown to be best suited to differentiate bare sediment from vegetated areas. In **Figure 3-8**, this index is shown for the area surrounding the Roseninsel (situated at Lake Starnberg near the town Tutzing). This area is known for large meadows of *Characea* spec. in the northern littoral zone as well as bare soil at the northern edge of the island. *Characea* are annual plants and therefore ideally suited to test the detection of bare sediment at the beginning of the growth period. Low index values (up to -1.5) indicate vegetation, higher index values (greater -0.9) larger percentages of bare soil. The colour bar is adapted to the values given in **Figure 3-8** (right) and scaled to coverages from 0 to 100 % (note the non-linear relationship).

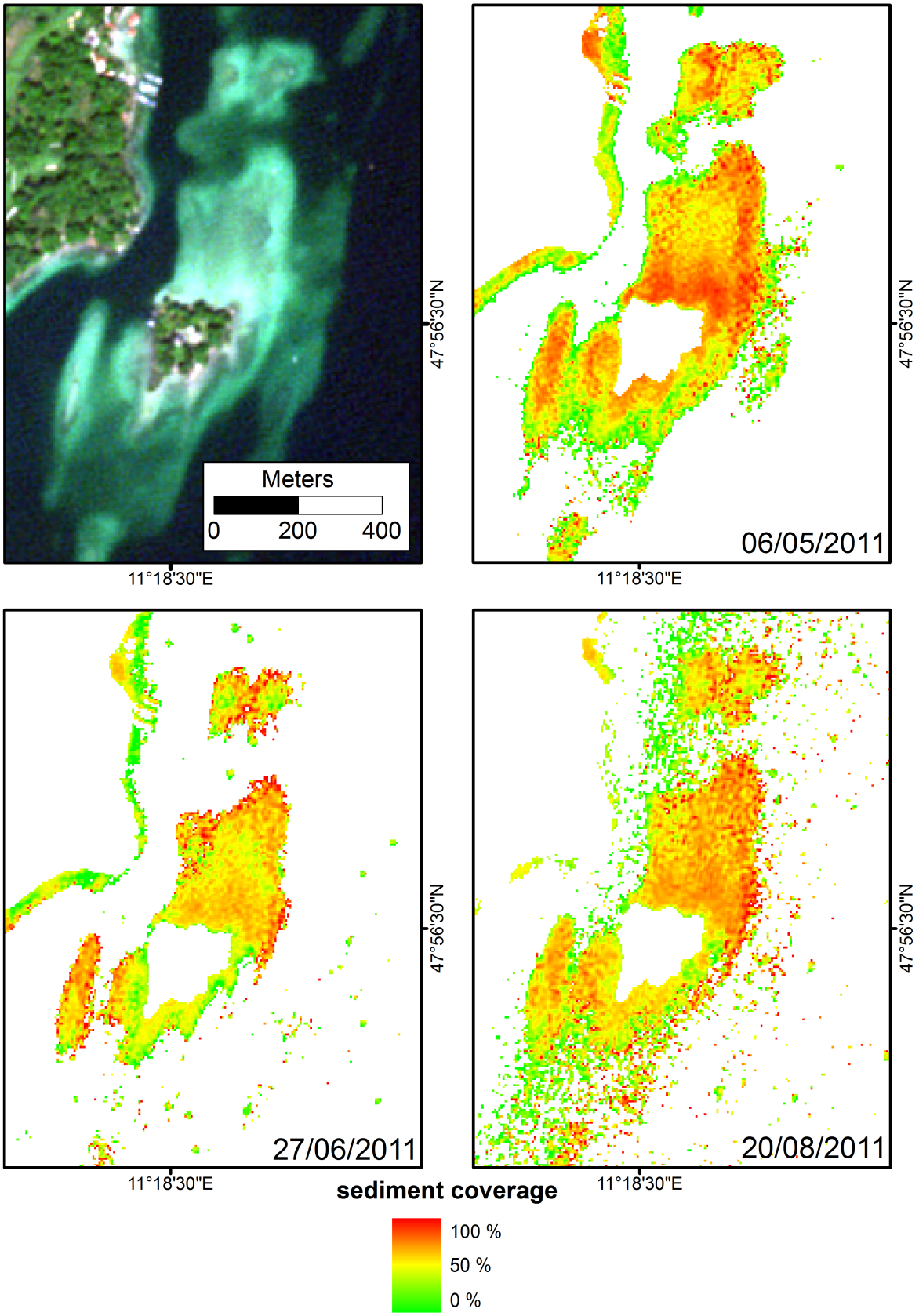

Figure 3-8: Depth-invariant band 3 (Red / Red Edge) for three selected dates during vegetation period 2011 (low values: vegetated, high values: bare soil)

Vegetation coverage increases from May onwards, although areas covered by plant detritus can also lead to low index values which would be interpreted as vegetation

coverage. In June large areas in the northern littoral were already covered by plants. The vegetation coverage decreased in August.

The Matched Filtering spectral unmixing approach also showed good results for the differentiation of bare soils and vegetated areas. However, the distinction between *E. nuttallii* and *N. marina* is difficult. Unmixing was performed for all four scenes using endmember derived from Eq. 3.6 for the scene specific attenuation coefficients. Results for 6th of May (**Figure 3-9**), as well as 20th of August (**Figure 3-10**) are shown.

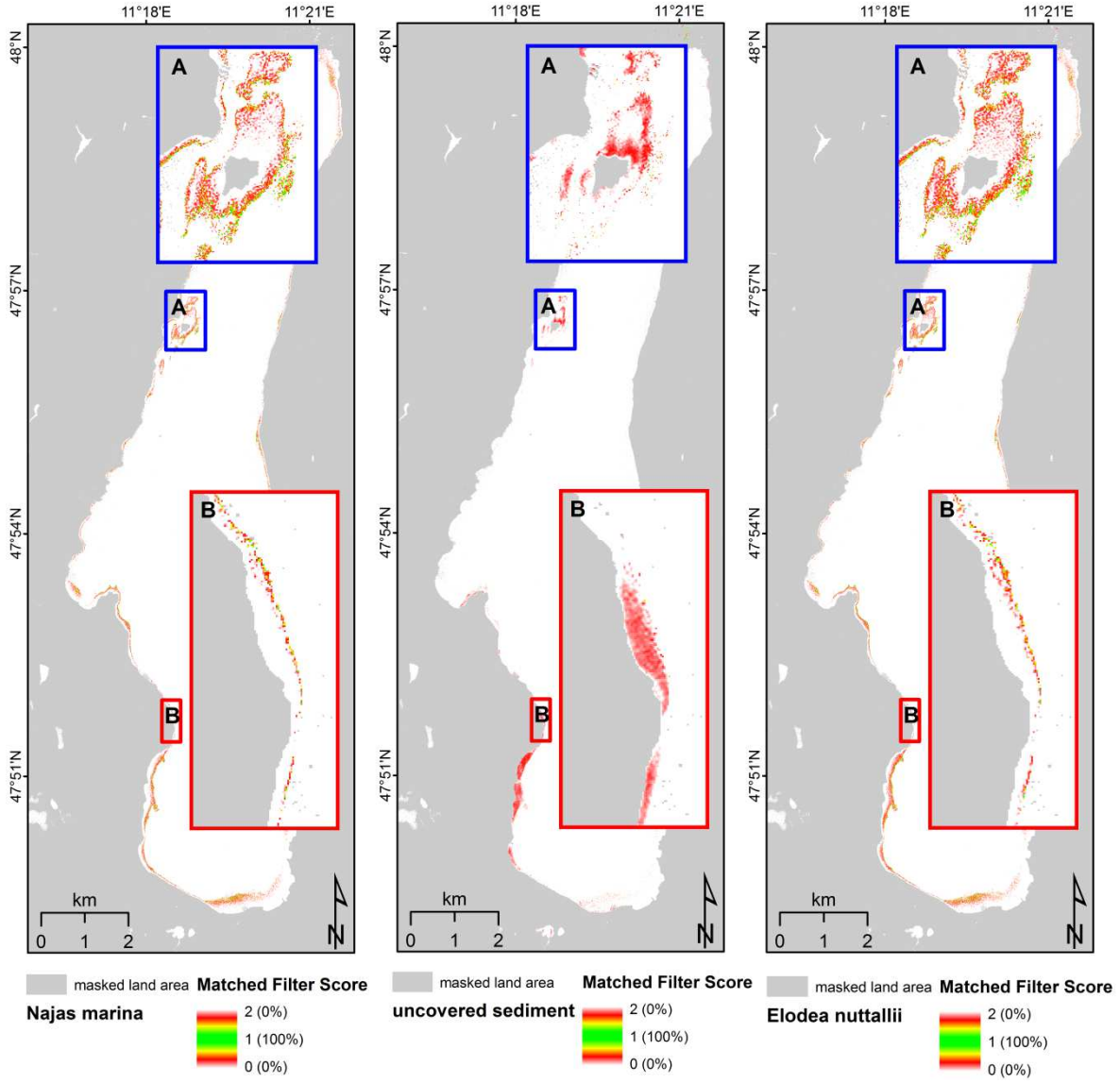

Figure 3-9: Matched filter spectral unmixing result for the RapidEye scene from 06/05/2011

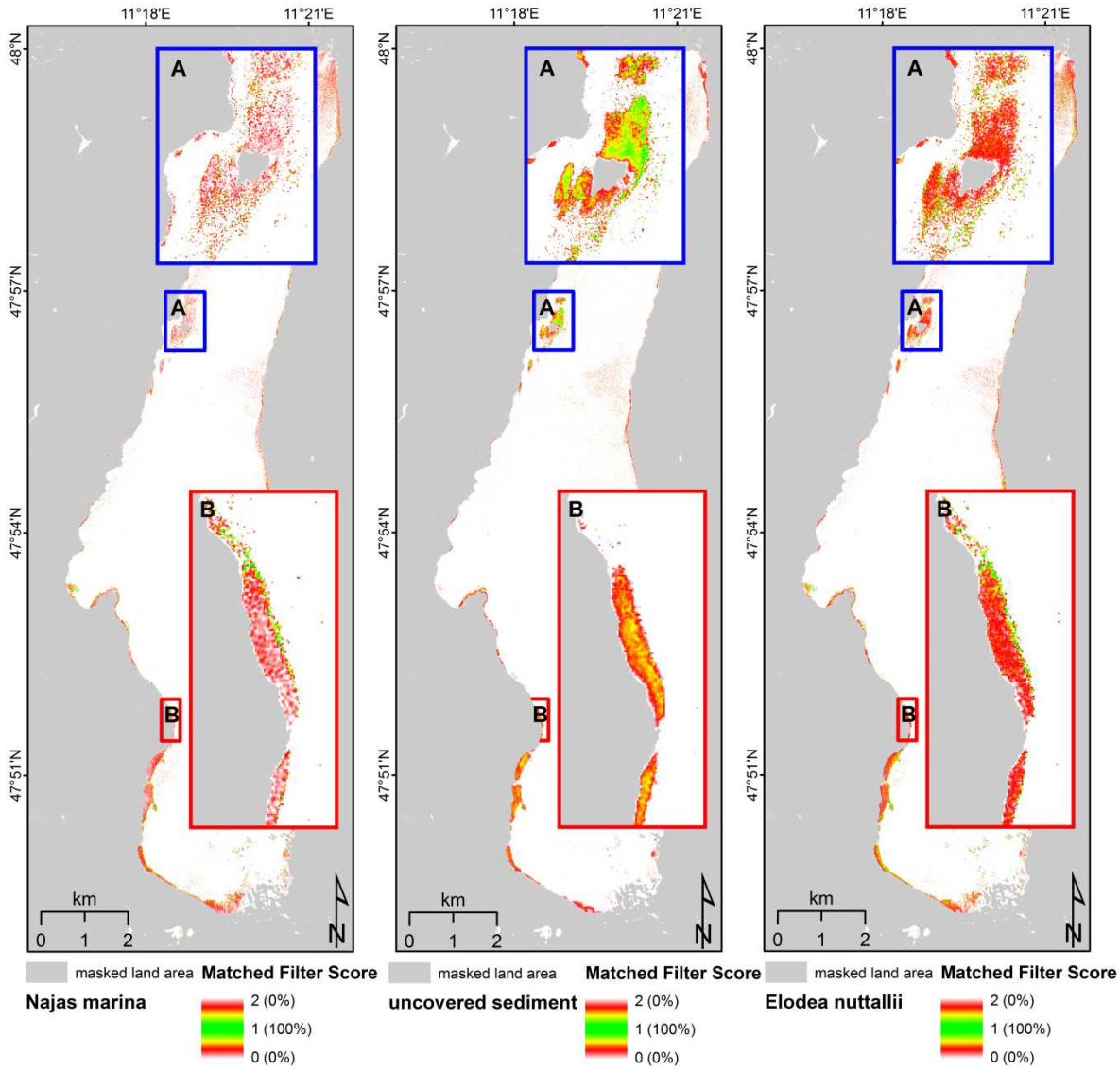

Figure 3-10: Matched filter spectral unmixing result for the RapidEye scene from 20/08/2011

For a better visualisation, the area ‘‘Roseninsel’’ (A) and ‘‘Bernried’’ (B) are enlarged. As discussed above, large areas of uncovered sediment appeared north of the Roseninsel, Bernried was characterized by dense coverage of *N. marina* from July onwards. However, the score values for uncovered sediment do not show a complete coverage of soil. This is probably caused by detritus over bare ground. The shallow area of Bernried was also covered by bare silty sediment. Plants only occurred below a water depth of 3 m.

The results of the 20th of August (**Figure 3-10**) show better identification of bare sediment compared to vegetated areas. The uncovered regions around the Roseninsel were identified as those. The differentiation of *E. nuttallii* and *N. marina* is currently not reliable. However, it can be stated, that most areas identified as *E. nuttallii* have also high values of the endmember *N. marina*. Since 2011 was a very poor year for the growth of *E. nuttallii* (littoral mapping by scientific divers showed almost no pure stands of *E. nuttallii*) the areas classified as *Elodea* may include *Najas* patches as well.

3.5 Conclusion

The applied method for processing multispectral remote sensing data yields good results for the elimination of the water column provided that accurate attenuation coefficients are known or measured. An additional assumption is that the properties of the water constituents are homogenous throughout the water column. The *in situ* measured reflectance spectra are – despite the discussed problems – an ideal basis to create a multiseasonal database throughout the growing period. During summer 2012, with ongoing RapidEye data acquisition, ground truth measurements will be carried out to obtain reliable endmember spectra for supervised classifications with spectral unmixing methods. Further methods will be tested to retrieve the necessary information about the apparent optical properties (i.e. attenuation coefficients) from optical deep water reflectances according to Lee et al. (2002). Littoral mapping by scientific divers will be carried out 2012 to find larger areas with pure stands of *N. marina* and *E. nuttallii* to perform an accuracy assessment of the presented method.

3.6 Acknowledgments

This project is founded by the Bavarian State Ministry of Environment and Health under the number ZKL01Abt7_18457. Thanks to the colleagues from the Limnological Institute who helped us during field work and to the Rapid Eye Science archive (RESA) who thankfully provided us with the data within the project no. 455.

4. LITTORAL BOTTOM MAPPING IN LAKES USING MULTITEMPORAL RAPIDEYE DATA

S. Rößler[1], P. Wolf[1], T. Schneider[1], A. Melzer[1]

[1]Limnological Institute, Technische Universität München, Iffeldorf, Germany

E. Borg et al. (eds.), RapidEye Science Archiven (RESA) - From the Basics to the Service, pp. 107-127, ISBN: 978-3-95545-002-1

4.1 Abstract

Global warming increases the water temperatures of the Central European lakes. This may alter the composition of optical active water constituents – the inherent optical properties (IOPs) of the water column, but can also lead to change in species composition of submersed aquatic macrophytes. In Bavaria (southern Germany), an increasing spread of endemic species like *Najas marina* and invasive plants like *Elodea nuttallii* can be observed which supports the assumption that this species benefits from rising water temperatures. Spatial and temporal high-resolution spaceborne sensors like RapidEye can be used to observe the seasonal highly variable growth of macrophytes on littoral areas. During the growing season 2011, RapidEye imagery was acquired monthly and processed towards littoral bottom coverage and IOPs using the bio-optical inversion model BOMBER and additional spectro-radiometrical *in situ* measurements carried out with RAMSES underwater spectrometers. The results show a good performance for the separation between vegetated areas and bare sediment, however a discrimination of species is still challenging.

4.2 Introduction

The water quality (nutrient conditions) of lakes can be coupled to the occurrence of specific macrophytes (Melzer 1999), and thus monitoring of these indicators for the trophic state are useful to detect changes in entire lake ecosystems at an early stage. Some invasive submersed aquatic plants are suspected to benefit from rising water temperatures due to global warming (Rahel and Olden 2008) and therefore offer the possibility to monitor these thermal changes as well. In the freshwater lakes of Bavaria (southern Germany), an increased spread of invasive species like *Elodea nuttallii* and the expansion of indigenous species like *Najas marina* can be observed.

The spatially and temporally highly variable growth of these plants requires monitoring methods to cover large areas and rapid deployment. Until now, the identification of submersed macrophytes by remote sensing is only possible using hyperspectral airborne sensors (e.g. HyMap, ROSIS, APEX, HySpex) which offer the needed spectral and geometric resolution (Heege et al. 2003; Pinnel 2007).

Multispectral spaceborne imagery has been used successfully for bathymetric applications using Landsat TM (Bierwirth et al. 1993; Philpot 1989), IKONOS (Mishra et al. 2004; Stumpf et al. 2003) or SPOT (Lafon et al. 2002). The mapping of benthic habitats by using multispectral data is mainly focussed on coral reefs (Andréfouët et al. 2003; Kanno 2011; Mumby et al. 1997) and marine macrophytes (Phinn et al. 2008). Only few works were performed on the littoral bottom mapping of lakes (Ackleson and Klemas

1987; Dogan et al. 2009; Sawaya et al. 2003). The integration of field investigations and spatially high resolution satellite imagery for the monitoring of macrophytes development with focus on the EU water framework directive has also been discussed (Malthus and Karpouzli 2003).

In this study, multiseasonal RapidEye data in combination with multi seasonal field investigations were used to derive bottom information like coverage and colonization of submerged macrophytes as well as inherent optical properties (IOPs) of the water column throughout the year. For this, *in situ* measured bottom reflectances were implemented in the bio-optical software BOMBER (Giardino et al. 2012) which corrects for the exponential decrease of light intensity due to the optically active water constituents Phytoplankton (CHL), suspended particulate matter (SPM) and coloured dissolved organic matter (cDOM) and finally performs a depth retrieval as well as spectral bottom unmixing.

4.3 Methods and Material

4.3.1 Study area

The study area is Lake Starnberg (47°55'N, 11°19'E) in Bavaria, southern Germany (**Figure 4-1**) covering an area of 56 km². The lake was formed by the Isar-Loisach-Glacier during last glacial period (Fesq-Martin et al. 2008), which explains its great depth of 127.8 metres (on average 53.2 m). Spacious littoral terraces lie on the western shore of the lake and guided the selection of the test sites. For the demonstration purposes of this study an area near the municipality of Bernried was chosen due to dense coverage of *Najas marina* in depth from 1 to 5 metres. In shallow water areas, large populations of *Chara* spec. occur and are therefore also subject in this study for comparison of low and high growing macrophytes and as competitors within the ecosystem.

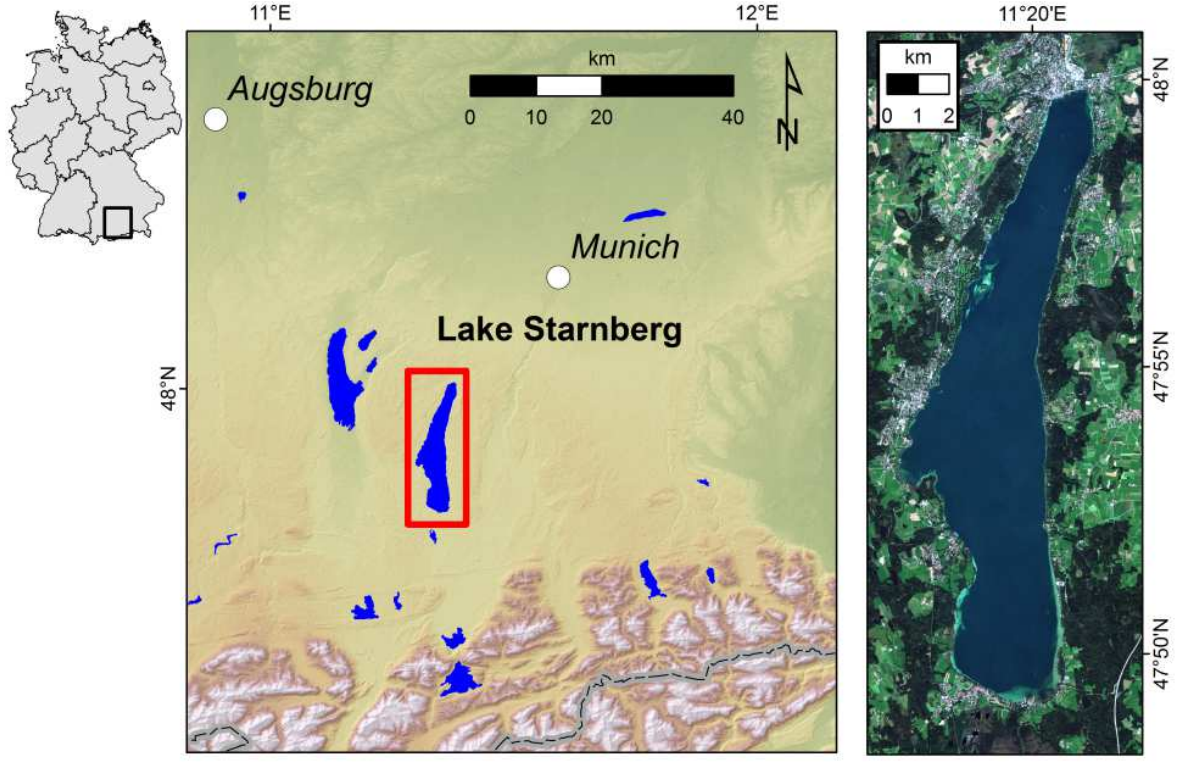

Figure 4-1: Location of Lake Starnberg and RapidEye image from 03/09/2011

According to the nutrient content, Lake Starnberg can be classified as oligotrophic with an average primary production of 889 g C m^{-2} y^{-1}. Phytoplankton concentrations range between 2.4 to 4.8 µg l^{-1} in winter and 6 to 12 µg l^{-1} in summer, respectively (Pinnel 2007).

4.3.2 In situ data collection and processing

Spectro-radiometrical *in situ* measurements were performed in 2011 during the growing period of submersed aquatic plants (May to October) using three submersible RAMSES spectrometers (TRIOS). Two irradiance devices (ACC) and a radiance sensor (ARC), covering a spectral range from 320 to 950 nm with 3.3 nm intervals were used to measure hemispherical the upwelling (E_u) and downwelling irradiance (E_d) as well as the upwelling radiance (L_u) with a field of view of 7°.

Besides the mentioned invasive and expanding indigenous species, two other common macrophytes in Lake Starnberg were observed. Above $(0+)$ and just below the water surface $(0-)$, as well as just above the vegetation patches (b) simultaneous measurements of all three sensors were made from populations of *Chara* spec., *Elodea nuttallii*, *Potamogeton perfoliatus* and *Najas marina* as well as from uncovered sediment. The data was further processed to calculate subsurface remote sensing reflectance (r_{rs}), irradiance reflectance (r) of plants and the anisotropy of the underwater light field (Q).

The measurements below the water surface were made to include the water column and to obtain variations of concentration and of the IOPs during the year. Therefore, the E_d-measurements were inverted using the software WASI (Gege 2012) which is mainly based on the bio-optical model of Albert and Mobley (2003) for the radiative transfer in shallow waters. From r_{rs} measurements just below the water surface and directly above the macrophytes r_{rs}^b (with nearly no water column in between) the deep-water remote sensing reflectance r_{rs}^{dp} was estimated. For the latter, the equation of Lee et al. (1998) is solved for r_{rs}^{dp} according to Eq. 4.1:

$$r_{rs}^{dp} = \frac{r_{rs} - r_{rs}^b \exp(-2K\Delta z)}{1 - \exp(-2K\Delta z)} \tag{4.1}$$

The depth difference Δz is obtained from the pressure sensor of the RAMSES E_d device (SN: 8109). The attenuation coefficient K is calculated from E_d-measurements in different depths (z_1 and z_2) using Eq. 4.2 (Maritorena 1996):

$$K = \frac{1}{\Delta z} \ln \frac{E_d(z_1)}{E_d(z_2)} \tag{4.2}$$

To evaluate the spectral separability of common macrophytes, their seasonal changing reflectances obtained by the above described RAMSES-measurements were resampled to the spectral resolution of RapidEye and the M-statistic of Kaufman and Remer (1994) was used to calculate separability for all possible combinations of macrophyte classes. This index has been used in other studies for benthic mapping (O'Neill et al. 2011). μ is the mean and σ the standard deviation of r_{rs} for each spectral band of the classes 1 and 2 (Eq. 4.3):

$$M = (\mu_1 - \mu_2)/(\sigma_1 - \sigma_2) \tag{4.3}$$

To account for the seasonal development of different macrophyte reflectance (related to phenology), a wavelength dependent polynomial fit (2nd degree) was applied to the r_{rs}-spectra of vegetation. The time was used as x-value, each wavelength of the corresponding r_{rs}-spectra as y-value. Reliable bottom r_{rs}-spectra for each day of the year (DOY) were obtained as required for multiseasonal RapidEye data processing.

4.3.3 RapidEye data and pre-processing

Within the RapidEye Science Archive (RESA) project no. 455, several scenes were acquired between May and October 2011 covering Lake Starnberg. The data were delivered as level 3A product tiles including standard radiometric correction and geocoding. The images were further normalized to top-of-atmosphere (TOA) reflectance using the recommendation given in the Product Specifications (RapidEye 2011) and subsequently mosaicked.

A simple atmospheric correction was applied assuming that the TOA-reflectance is the sum of contributions from Rayleigh scattering, aerosol scattering and the water leaving reflectance (R_w) lowered by the transmittance of the atmosphere (Gordon and Clark 1981). The wavelength dependent Rayleigh scattering was computed using the Rayleigh optical thickness (Hansen and Travis 1974), the Rayleigh scattering phase function (Doerffer 1992) and its relation to the forward/backward scattering angle (Gordon et al. 1983) depending on viewing and solar illumination directions (Mishra et al. 2005). The contribution of the aerosol was computed assuming that the water leaving reflectance in the near-infrared (RapidEye Band 5) is essentially zero. The aerosol contribution to the other bands is calculated pixel based from the NIR-value using empirically defined factors from Gordon and Wang (1994) and has been developed on the combination of maritime and continental aerosol. Atmospheric correction was only applied to water areas which were extracted from the whole image using a threshold of the normalized difference water index (McFeeters 1996) greater than zero.

4.3.4 The bio-optical model BOMBER

The ENVI add-on BOMBER (Bio-Optical Model Based tool for Estimating water quality and bottom properties from Remote sensing images) has recently been published by Giardino et al. (2012) and relies on the model developed by Lee et al. (1998, 1999) with HYDROLIGHT (Mobley 1994) simulations. It can be run in a shallow water and a deep water mode. The shallow water mode requires additional bottom albedos for spectral unmixing as well as the apparent underwater sun zenith angle. Equation 4.4 summarizes the different contributions of the IOPs and the bottom reflectance (r_{rs}^b) as well as the attenuation coefficients for the up- and downwelling light to the subsurface remote sensing reflectance (r_{rs}) at a given depth (z) which are implemented in the shallow water model of BOMBER:

$$r_{rs} = r_{rs}^{dp}(1 - A_0 \exp[-(K_d + K_{uw})z]) + A_1 r_{rs}^b \exp[-(K_d + K_{ub})z] \qquad (4.4)$$

The contribution of the deep water (r_{rs}^{dp}) depends only on the IOPs (Lee et al. 1999), the factors A_0 and A_1 are weighting factors for the contribution of the water and the bottom to the received overall signal (Albert and Mobley 2003). The parameterization of the

attenuation of downwelling irradiance (K_d) and the upwelling radiance coming from the water (K_{uw}) and the bottom (K_{ub}) is adapted from Lee et al. (1999). The transformation from the reflectance above (R_{rs}) to below the water surface (r_{rs}) is based on Lee et al. (1998).

BOMBER was only applied on shallow water areas. Land was masked using the normalized difference water index (NDWI) according to McFeeters (1996), values greater than 0 were assigned to water. Deep water was excluded based on a R_{rs}-threshold of 3% in the Green wavelength region, lower values were masked. This masking results in different masks for each scene, thus only percent coverage was compared using the subpixel abundance of every pixel.

4.4 Results and Discussion

4.4.1 In situ measurements

In situ measurements over different common macrophytes (*Chara* spec., *Elodea nuttallii*, *Potamogeton perfoliatus* and *Najas marina*) were carried out at Lake Starnberg during 2011 (**Figure 4-2** shows the reflectance development for three selected months).

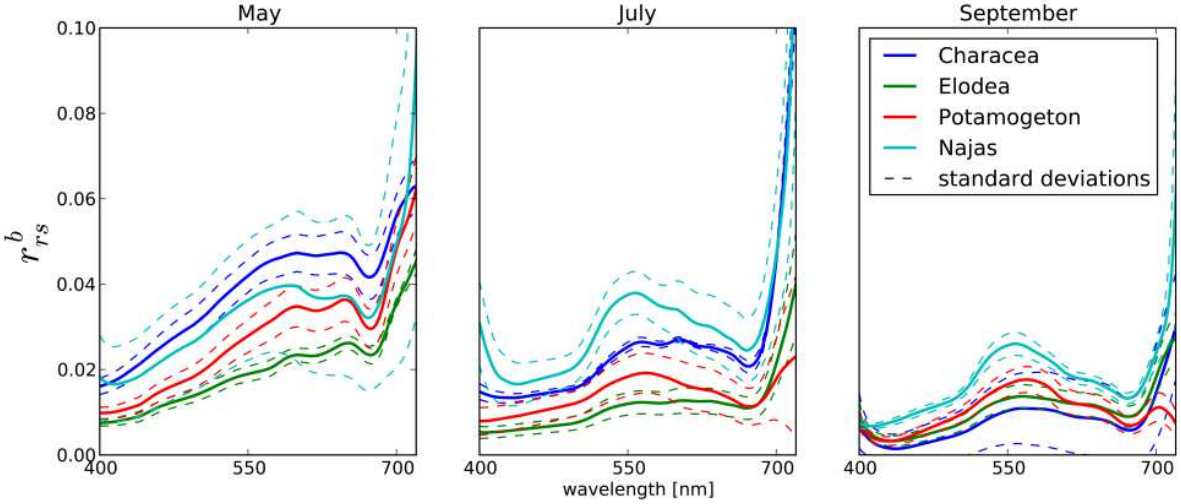

Figure 4-2: Seasonal variability of bottom r_{rs} of different macrophytes from May to September measured with RAMSES. The solid line shows the mean values, the dashed line shows the mean ± standard deviation.

In May, the differences in reflectance are caused mainly by the sediment since plants occur only sparsely. Regarding the standard deviations and the spectral shape, the curves are very similar. In July and September the coverage of *Characea*, *Elodea* and *Najas* was dense; only *Potamogeton perfoliatus* grows sparsely. The M-statistic (according to Eq. 4.3) was calculated for spectra shown in **Figure 4-2** (resampled to the spectral resolution of RapidEye) and compared in terms of species differentiation (**Table 4-1**, values greater than 1 indicate good separability, smaller values bad separability).

Table 4-1: M-statistic for all possible combinations of measured macrophytes reflectances (resampled to RapidEye), grey areas indicate bad separability (M < 1)

		Characea/ Elodea	*Characea/ Potamogeton*	*Characea/ Najas*	*Elodea/ Potamogeton*	*Elodea/ Najas*	*Potamogeton/ Najas*
		May					
RapidEye Band	1	7.32	11.29	**0.49**	3.66	1.22	**0.91**
	2	10.16	694.18	**0.57**	4.13	1.37	**0.76**
	3	6.20	108.04	**0.74**	2.72	**0.63**	**0.14**
	4	5.10	1.56	**0.37**	2.91	**0.74**	**0.45**
	5	3.10	5.09	**0.84**	4.61	**0.92**	**0.30**
		July					
RapidEye Band	1	10.44	1.70	1.29	2.72	4.79	7.79
	2	8.04	1.94	2.73	3.37	10.14	35.54
	3	6.80	2.96	**0.62**	**0.67**	3.21	4.71
	4	42.72	9.78	**0.42**	1.94	2.38	3.41
	5	18.56	52.46	26.70	4.96	4.04	10.06
		September					
RapidEye Band	1	**0.67**	1.13	2.25	199.42	11.30	8.59
	2	**0.53**	1.23	2.59	12.26	50.11	16.19
	3	**0.55**	**0.31**	1.17	4.39	3.88	6.21
	4	**0.08**	1.62	3.07	7.74	1.66	2.31
	5	9.17	6.42	1.73	4.36	2.81	3.06

The following results concentrate on monitoring aspects for *Najas marina* and the competing *Chara* spec. population at the Bernried demonstration site since they are the dominant species at this littoral region of Lake Starnberg and BOMBER supports only three endmembers (including uncovered sediment) for spectral unmixing. According to the M-statistic, a best differentiation between *Chara* spec. and *Najas marina* can be made in September when all bands show a good separability.

For the application of BOMBER at the demonstration site Bernried, all measurements above *Najas marina* (19/05/11, 28/06/11, 27/07/11, 12/08/11, 03/09/11, 16/09/11 and 18/10/11) were interpolated according to the methods described above to derive bottom reflection for each day of the year (**Figure 4-3**, right).

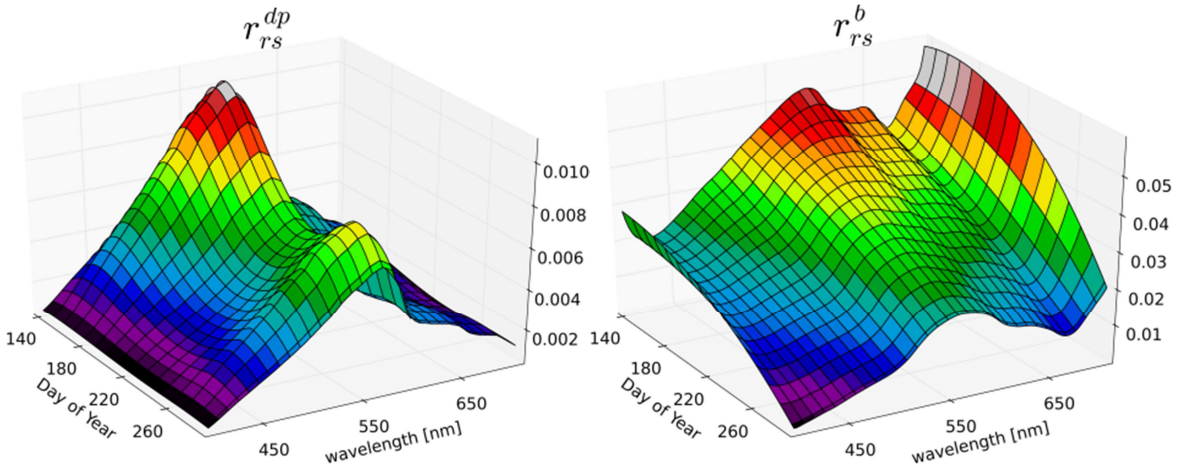

Figure 4-3: interpolated deep water r_{rs}^{dp}-spectra (left) and bottom r_{rs}^{b}-spectra of *Najas marina* (right) during growing season 2011 (based on *in situ* measurements)

The r_{rs}^{dp}-spectra (**Figure 4-3**, left) were used to evaluate the atmospheric correction results (see **Chapter 4.4.2**). From the interpolated bottom reflectances of *Najas marina* for the growing period 2011 the spectra corresponding to the acquisition dates of RapidEye were resampled to the spectral resolution of RapidEye and included as possible endmember

for the unmixing within the BOMBER processing. In the shallow water model of BOMBER, only three endmembers can be selected for bottom unmixing, thus only the dominant species for the test site were chosen next to a measured spectrum of pure sediment. In BOMBER, two bottom types (endmembers) are treated as fit-parameters, the third bottom type is adjusted that the sum equals 1 (100% coverage). Besides *Najas marina*, the low growing *Chara* spec. was chosen as endmember to be fitted. The adjusted third endmember was uncovered sediment (silty sand) measured at the test site in spring 2011 (**Figure 4-4**).

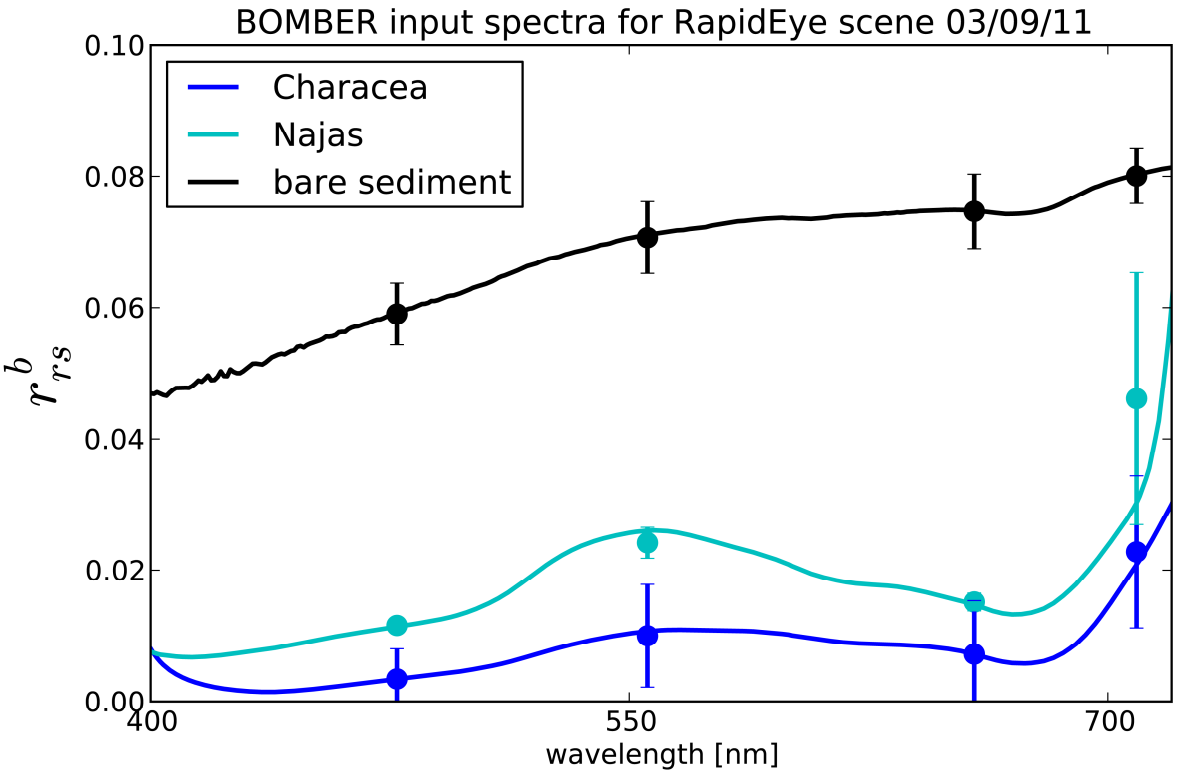

Figure 4-4: Bottom r_{rs} used for unmixing of the RapidEye Scene from 03/09/11, circles show the spectra resampled to RapidEye, error bars show standard deviation.

4.4.2 RapidEye data

The performance of the atmospheric correction was tested on the result of the RapidEye scene from 3rd September 2011. R_{rs} spectra were measured simultaneously to image acquisition over shallow water and the associated deep water reflection R_{rs}^{dp} was estimated from measured subsurface reflectance (r_{rs}) using Eq. 4.1. Both spectra were compared to image derived RapidEye spectra after atmospheric correction (**Figure 4-5**). The image derived R_{rs} are slightly higher than the in situ measured ones (mean difference of +0.13% reflectance for all bands).

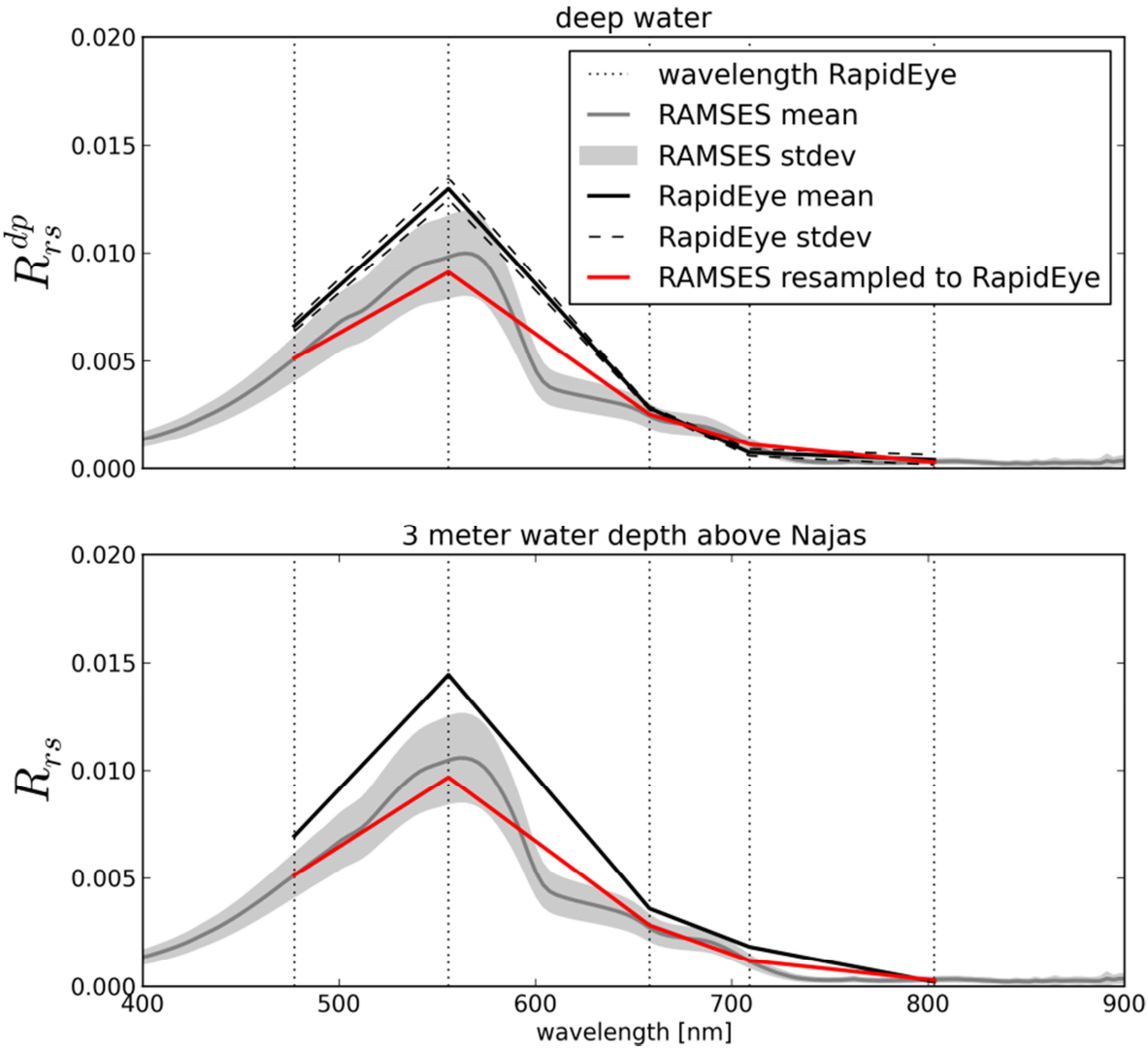

Figure 4-5: *in situ* measured R_{rs} over a *Najas marina* patch in 3 metre water depth (below) and derived deep water reflectance R_{rs}^{dp} (above) were resampled to the spectral resolution of RapidEye (red curves) and compared to the image derived R_{rs} spectra after atmospheric correction (black lines). For the shallow water area only one pixel centered at the measurement site was used, the deep water reflection is the mean of 100 pixels (shown ± standard deviation) located nearby the test site.

For the shallow water mode of BOMBER, endmember spectra for *Najas marina* are taken from modelled reflectance spectra (**Figure 4-3**, right) corresponding to the acquisition date. The resulting inversion and bottom unmixing result of the three allowed endmembers (in this case *Najas marina*, *Chara* spec., and uncovered sediment) is shown in **Figure 4-6** for three selected scenes acquired in 2011.

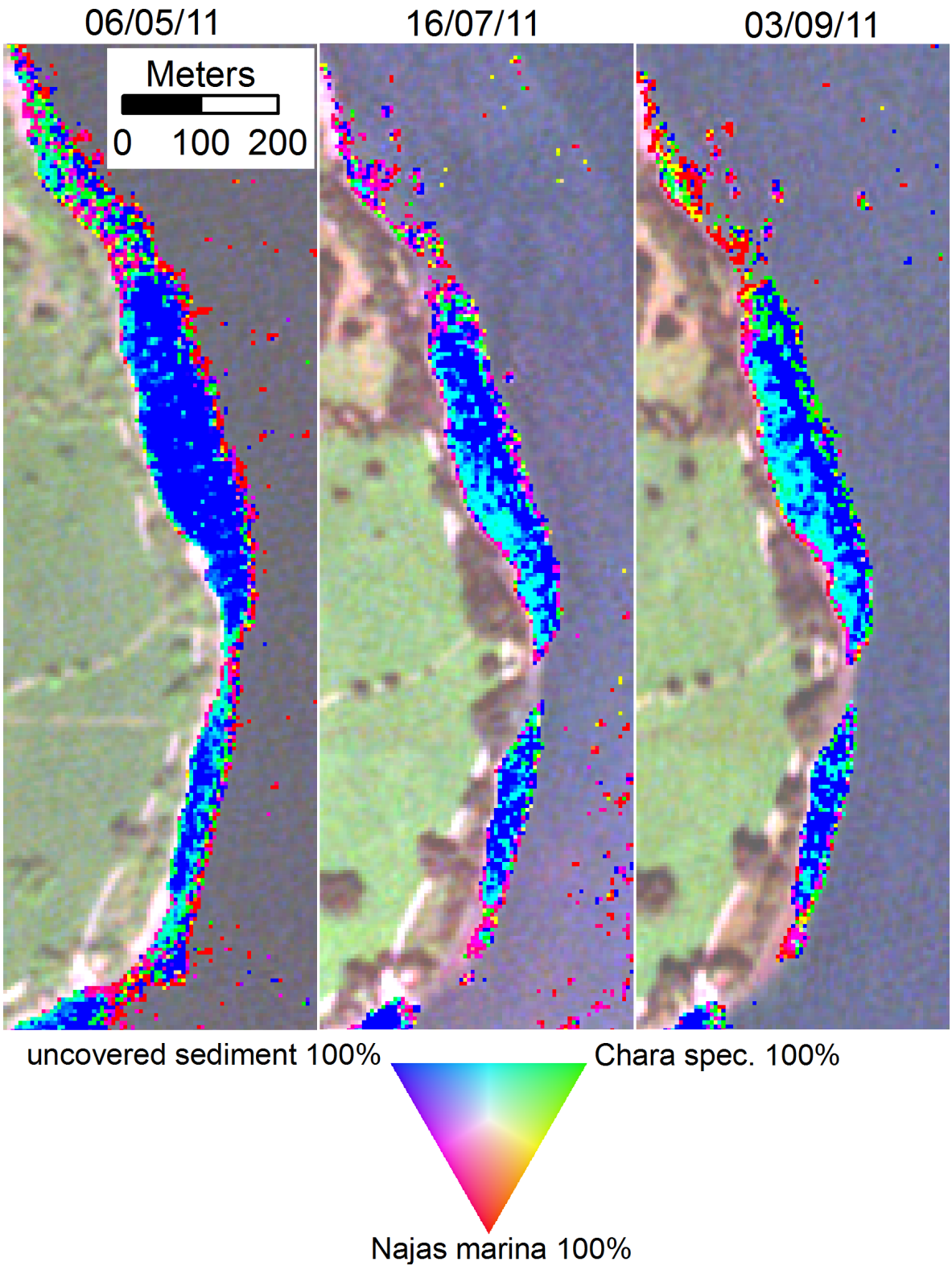

Figure 4-6: result of bottom unmixing for three selected RapidEye subsets showing the test site Bernried

A decreasing proportion of uncovered sediment can be observed from May to September: the sum of subpixel abundance of uncovered sediment multiplied with pixel area and divided with the whole classified area changed from 69.9% in May to 60.1% in September. Consequently, the fractions of submersed macrophytes increase (*Najas marina*: 16% to 17.1%; *Chara* spec.: 14.8% to 22.9%). *Chara* spec. occurs predominantly sparsely

at lower water depths (cyan areas in **Figure 4-6**) and interspersed in *Najas marina* patches. Areas classified as *Chara* spec. in greater depths (2 – 5 m) are incorrectly classified *N. marina* patches which are known here to cover the whole shore area at this depth (mapped by diving). This misclassification of macrophytes with multispectral sensors has also been observed in other studies (Vahtmäe and Kutser 2007).

The resulting BOMBER derived concentrations for the shallow water area at the test site Bernried were compared to the concentrations derived by E_d-measurement inversions with WASI (**Figure 4-7**). An overestimation of CHL and simultaneous underestimation of cDOM can be explained by their overlapping absorption bands in the Blue wavelength domain (Mobley 1994). The large standard deviations show that an accurate estimate of water constituent concentrations is not possible. The WASI derived concentrations show lower errors and a seasonal development (expect for SPM).

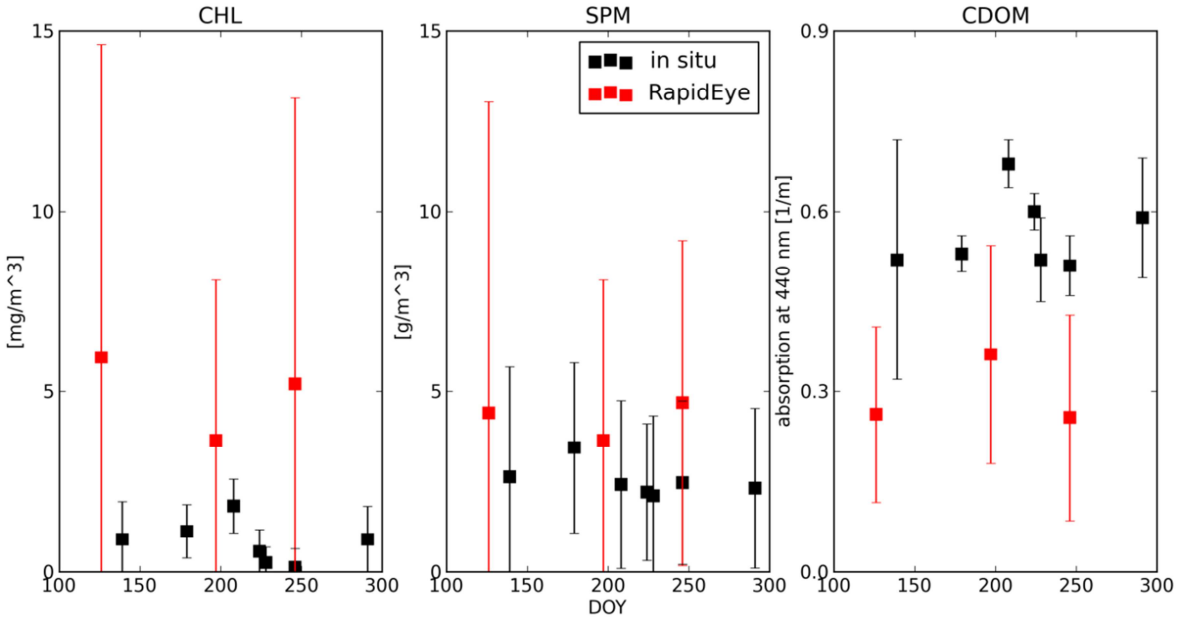

Figure 4-7: seasonal variability of the concentrations of phytoplankton (CHL), suspended particulate matter (SPM), and coloured dissolved organic matter (cDOM) from WASI inverted E_d-measurements (black squares) and BOMBER processed RapidEye images (red squares), error bars show standard deviation

4.5 Conclusion

In this study, it has been shown that the bio-optical inversion model BOMBER (originally designed for hyperspectral images) can be applied on RapidEye imagery for littoral bottom mapping and the observation of seasonal changes in littoral coverage. In this study, this was achieved by building time dependent spectral libraries for *Chara* spec. and *Najas marina* for the growing season 2011.

Applying BOMBER to multitemporal RapidEye imagery can help to monitor the seasonal development from sparsely vegetated areas (May) to larger vegetated areas (September). In 2011, the maximum of macrophytes growth was assessed in September (mapped by diving). The retrieval of concentrations of water constituents using BOMBER didn't reveal good results. The derived concentrations showed strong deviations to the WASI inverted *in situ* measurements of E_d and the standard deviations were very high.

The main limitation of multispectral sensors like RapidEye is the spectral resolution which prevents a differentiation between different macrophytes. Here, the combination of

multitemporal imagery and a phenological reflectance database presented in this study can be used to find a moment where the plants are best separable even on a multispectral image with broad bands. Another limitation of the BOMBER algorithm is caused by the attenuation which depends on IOPs and illumination conditions and controls the maximal depth of application due to scattering and absorption of the water body (approximately 5 metres in the case of Lake Starnberg). However this limitation also offers new possibilities. The *in situ* observations let expect a good separability chance when depth is used as decision threshold for species differentiation of *Chara* and *Najas*. This approach may be useful for implementation in object-based image analysis (OBIA) knowledge based rule sets.

Further works will focus on the investigation of water constituent concentrations by laboratory analysis to evaluate inversion results and to regionalize existing radiative transfer models. Echo sounders will be used to validate retrieved depths and to estimate biomass by distinguishing between vegetation surface and the bottom echo. A combination of the presented method with semi-empirical models based on logarithmic transformation (Roessler et al. 2013; Rößler et al. 2012) is envisaged in order to include the biomass of invasive aquatic plants as well.

4.6 Acknowledgments

This project is funded by the Bavarian State Ministry of the Environment and Public Health under the number ZKL01Abt7_18457. Thanks to the RapidEye Science Archive (RESA) who provided us with data within the project no. 455. A special thanks to Claudia Giardino for providing the software BOMBER and to all colleagues from the Limnological Institute who helped us during field work.

5. WATER CONSTITUENT RETRIEVAL AND LITTORAL BOTTOM MAPPING USING HYPERSPECTRAL APEX IMAGERY AND SUBMERSED ARTIFICIAL SURFACES

S. Rößler[1], P. Wolf[1], T. Schneider[1], S. Zimmermann[1], A. Melzer[1]

[1]Limnological Institute, Technische Universität München, Iffeldorf, Germany

EARSeL eProceedings, 12(1): pp. 44-57, ISSN: 1729-3782

5.1 Abstract

The analysis of littoral bottom properties such as bathymetry and coverage (i.e. plant identification) often requires knowledge about the composition of relevant optically active water constituents like phytoplankton, suspended particulate matter and coloured dissolved organic matter, which influence the radiative transfer in water due to scattering and/or absorption. These inherent optical properties (IOPs) of the water column can be retrieved in optically deep water (i.e., with no reflectance contribution of the bottom) by using physically based inversion techniques. In shallow water – which often differs from deep water in the amount of water constituents due to terrestrial input from the shore – a reliable estimation of IOPs requires at least a valid bottom reflectance, which is difficult to measure in water. An accurate estimation of water constituents is essential to the retrieval of bottom reflectance and subsequent identification of invasive aquatic plants, which was the main goal of this project.

In an experimental approach, the application of artificial surfaces for retrieving water constituents as well as bottom depth was tested during the hyperspectral APEX campaign 2011 covering Lake Starnberg in southern Germany. Two silo foils (10 metres wide and 50 metres long) were spread on the littoral bottom covering depths from 0.5 to 16 metres and acting as a very bright (white side of the foil) as well as a very dark (black side of the foil) reflective bottom albedo for the ENVI add-on BOMBER in terms of water constituents retrieval and bottom depth estimation. Reflectance spectra of the foils are known from laboratory measurements. *In situ* measurements were performed in water using RAMSES spectrometers and processed using the algorithms implemented in BOMBER as well as the inversion software WASI. The results show best performance for the black sided foil regarding pixel unmixing, water constituent retrieval and depth estimation, which agreed well with the WASI inversion results of the downwelling irradiance, which was used for validation due to lacking bottom influence.

5.2 Introduction

In water remote sensing applications focussing on shallow littoral areas a large reflectance contribution originates from the water column itself. The inherent optical properties (IOPs) of the water column depend on the concentrations of the optically active constituents namely phytoplankton (CHL), suspended particulate matter (SPM) and coloured dissolved organic matter (cDOM) (Mobley 1994). They influence the radiative transfer in water due to scattering and absorption of incident radiation. Depending on the illumination conditions, they can be related to apparent optical properties (AOPs) such as

the vertical attenuation coefficient and the reflection of optically deep water. Several parameterizations exist for relating IOPs to AOPs (Albert and Mobley 2003; Gordon et al. 1975; Kirk 1984; Morel 1980; Morel and Gentili 1993) for optically deep water. For shallow water, additionally the depth and the bottom albedo have to be taken into account.

Although water constituent retrieval approaches are mainly focussed on marine environments using multispectral sensors enabling a large coverage like SeaWIFS (Gordon and Wang 1994), CZCS (Gordon and Clark 1981), MODIS (Carder et al. 2004; Kallio et al. 2005), MERIS (Kallio et al. 2005) and ETM+ (Doxaran et al. 2006; Kallio et al. 2005), several algorithms have been adapted to be used on inland water bodies as well. A review of spaceborne remote sensing studies focussing on water constituents is given by Odermatt et al. (2012). The application of hyperspectral airborne remote sensing for water quality in inland waters has also been shown in several studies (Kallio et al. 2001; Koponen et al. 2002; Thiemann and Kaufmann 2002). Inland water applications in shallow water areas either focus on the retrieval of water constituents (Albert 2004; Hakvoort et al. 2002; Hooker et al. 2004; Van Stokkom et al. 1993) or on the retrieval of bottom properties like vegetation coverage (Gullström et al. 2006; Heege et al. 2003; Lu and Cho 2010; Pinnel 2007) or bathymetry (McIntyre et al. 2006).

One main issue with the application of physically based modelling of IOPs from shallow water like WASI (Gege 2004), MIP (Heege et al. 2003) and BOMBER (Giardino et al. 2012) is a reliable bottom albedo that is used as a reference for depth and constituent retrieval. In this study, the application of artificial bottom albedo of very bright and dark surfaces was tested to evaluate the retrieval of water constituents and depth using the bio-optical software BOMBER (Giardino et al. 2012). A similar study has already been carried out by Tolk et al. (2000) using a tank with black and white bottom for different SPM concentrations. According to their findings, the wavelength range between 740 and 900 nm is least affected by the bottom due to strong absorption of the water itself and thus the remaining scattering results from SPM and not from the bottom. Another tank experiment with dark and bright surfaces (and constant water constituents) was used to correct *in situ* measured vegetation reflectance (Cho and Lu 2010).

In our approach, a combination of artificial dark and white surfaces (silo foils) in a natural environment (lake shore) and intensive spectroradiometric *in situ* measurements were performed simultaneously with a hyperspectral APEX flight. Through this a large data set was acquired covering the same targets (foils) with known reflectance behaviour which was processed further using WASI and BOMBER and compared with regard to uncertainties of water constituent retrieval and depth estimation.

5.3 Study site

Lake Starnberg (47°55’N, 11°19’E) in southern Bavaria occupies an area of 65 km² and is Germany’s fifth largest lake (**Figure 5-1**). Its expansion is 20 km, its maximum width 4.7 km. The lake was formed by the Isar-Loisach glacier during the last glacial period (Fesq-Martin et al. 2008) and has an average depth of 53.2 metres (maximum 127.8 metres).

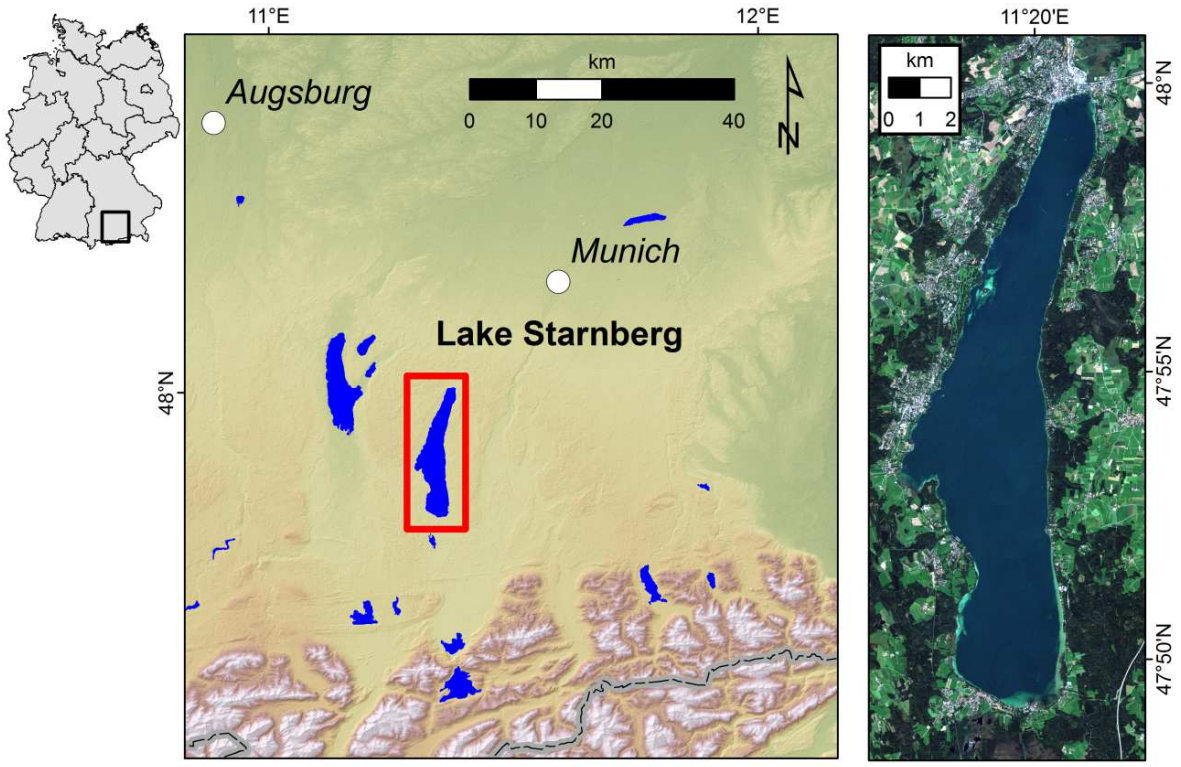

Figure 5-1: Location of Lake Starnberg and RGB composite of a RapidEye scene from 03/09/2011.

Large shallow littoral terraces are mainly located at the western lakeside and were therefore chosen for *in situ* measurements as well as guiding the orientation of the flight lines during the APEX campaign 2011. At this lakeside, several areas are covered by submersed aquatic macrophytes such as *Potamogeton pectinatus*, *Potamogeton perfoliatus*, *Chara* spp., *Najas marina* and *Elodea nuttallii*. The last two are considered to be invasive plants since increasing water temperatures promote their expansion. The identification of these two species was the main purpose of this study leading to the hypothesis that they can be recognized if artificial surfaces with known reflectances are classified correctly. The main test site near the village of Bernried was chosen due to high abundance of Najas marina at depths between 2 and 6 metres. Submersed foils were spread out here to gather information about IOPs from shallow water areas. In this oligotrophic lake, concentrations of phytoplankton were reported to be between 2 and 5 µg/l in winter and 6 – 12 µg/l in summer, respectively (Pinnel 2007).

5.4 Material and Methods

5.4.1 BOMBER

BOMBER (Bio-Optical Model Based tool for Estimating water quality and bottom properties from Remote sensing images) is an ENVI add-on that was recently published by Giardino et al. (2012). It relies on the model by Lee et al. (1998, 1999) which has been developed with HYDROLIGHT (Mobley 1994) simulations and can be used for optically deep water (i.e. with no influence of the bottom) and shallow water. The deep water mode only requires water leaving reflectance and simplified spectral response functions (Gaussian functions built from central wavelength and FWHM value). In shallow water mode, the underwater sun zenith angle θ_w has to be provided as well as three different

bottom reflectances ρ for linear bottom unmixing. For the shallow water model, a contribution of the water reflectance itself (depending on the IOPs, left term of Eq. 5.1), as well as the bottom contribution (right side of Eq. 5.1) depending on the water depth H are calculated according to Eq. 5.1 (Lee et al. 1998):

$$r_{rs} = r_{rs}^{\infty}(1 - A_0 \exp[-(K_d + K_u^C)H]) + A_1 \rho \exp[-(K_d + K_u^B)H] \tag{5.1}$$

The variables A_0 and A_1 are weighting factors for the contributions of water and bottom to the apparent reflectance (Albert and Mobley 2003; Lee et al. 1998). The parameterization of the attenuation for the downwelling irradiance (K_d) and upwelling radiance from the bottom (K_u^B) and from the water (K_u^C) was adapted from Lee et al. (Lee et al. 1999) based on HYDROLIGHT simulations and can be changed in BOMBER. They relate the IOPs total absorption (a) and total backscattering (b_b) to the AOPs attenuation (K) and deep water reflection (r_{rs}^{∞}) through Eq. 5.2 to Eq. 5.5:

$$K_d = \frac{a + b_b}{\cos\theta_w} \tag{5.2}$$

$$K_u^C = \left[1.03\left(1 + 2.4\frac{b_b}{a + b_b}\right)^{0.5}\right](a + b_b) \tag{5.3}$$

$$K_u^B = \left[1.04\left(1 + 5.4\frac{b_b}{a + b_b}\right)^{0.5}\right](a + b_b) \tag{5.4}$$

$$r_{rs}^{\infty} = \left(0.084 + 0.17\frac{b_b}{a + b_b}\right)\frac{b_b}{a + b_b} \tag{5.5}$$

θ_w is the sun zenith angle under water, a the sum of individual absorption coefficients (CHL, SPM, cDOM and water) and b_b the sum of backscattering coefficients (CHL, SPM and water). Eqs. (5.3) to (5.5) already include the parameterizations of Lee et al. (1999). In BOMBER, a least square optimization is performed to minimize the error (err) between measured (R_{rs}) and modelled reflectance ($\hat{R}_{rs}$) above water for all wavelengths λ under examination (Eq. 5.6).

$$err = \sqrt{\sum_{\lambda_{min}}^{\lambda_{max}} \left(R_{rs}(\lambda) - \hat{R}_{rs}(\lambda)\right)^2} \tag{5.6}$$

5.4.2 Simulated data

The performance of BOMBER on APEX data was tested using a simulated data set. For three different surfaces (white foil, black foil and bare sediment), 30 reflectance spectra were randomly created from a large range of water constituent concentrations (CHL: 1 – 5 µg/l; SPM: 1 – 5 mg/l; cDOM: 0.2 – 0.7 m^{-1}) and depths (0.5 – 16 metres) for each bottom coverage. The radiative transfer equation of Lee et al. (1998, 1999) – which is also the

physical basis of BOMBER – was used for for-ward modelling. The spectra were further resampled to the spectral resolution of APEX.

The simulated reflectance spectra were subsequently inverted using a python (version 2.7) routine which comprises the equations of BOMBER. In contrast to the forward modelling, the inversion has to be performed on a lower spectral resolution and three endmembers (white foil, black foil and bare sediment) were provided for bottom unmixing. The bottom reflectance spectra for these surfaces, as well as the two plant reflectances (*Najas marina*, *Chara* spp.) used for the final classification of the whole image, are shown in **Figure 5-2**.

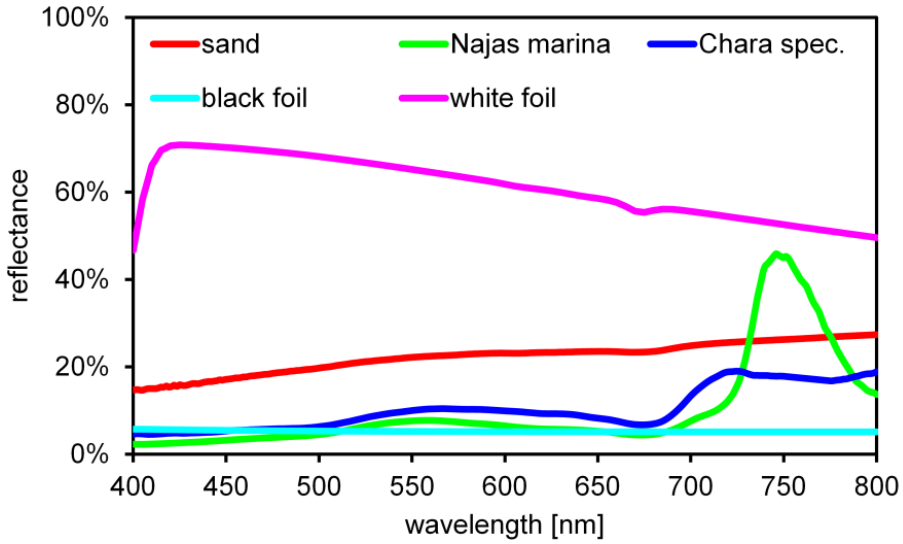

Figure 5-2: Bottom reflectance of possible endmembers for spectral unmixing.

The inversion of the simulated data set was performed to find out whether the three different surfaces were assigned to the right endmember by calculating the classification accuracy (percentage of pixel with 100% coverage of the right endmember). In addition, the accurate determination of depth and water constituents was evaluated by calculating the root-mean-square error ($RMSE$), the mean absolute percentage error ($MAPE$) and the coefficient of determination (R^2) between input values and BOMBER-derived output values (separately for each bottom coverage).

5.4.3 Field data set

Field work during the APEX image data acquisition included bringing out the two foils with the aid of scientific divers as well as spectral measurements. The location for the foils was guided by morphometric aspects. To cover a littoral area with a large range of depths, sites were selected to provide very shallow depths (0.5 m) for the first 20 metres of the total length as well as very deep (>15 m) areas where the reflected signal by the bottom can be neglected. Additionally, the foils were placed at a distance of 50 m from each other to assure comparable quantities of water constituents and avoid overframing of the black foil by the white one. The black foil has an average reflectance of 5% (**Figure 5-2**) so that the apparent reflectance above the water surface clearly differs from the reflectance of optically deep water. However, it can be used to minimize the effect of the bottom due to a missing wavelength dependency and a generally low reflectance.

Spectral *in situ* measurements were performed using three submersible RAMSES spectroradiometers (TriOS). Two hemispherical sensors (ACC) measured the downwelling (E_d) and upwelling irradiance (E_u) and one radiance sensor (ARC) the upwelling radiance (L_u) with a field of view of 7°. The sensors were triggered simultaneously and enabled the irradiance reflectance ($R = E_u/E_d$), remote sensing reflectance ($R_{rs} = L_u/E_d$) and anisotropy ($Q = E_u/L_u$) to be calculated.

Remote sensing ground truth data were collected directly above the foils at four different depths (0.5, 3, 5, 8 m). At each measuring point, in-water measurements were collected at 1 m depth intervals (11 iterations) ranging from just above the foils ($R(b)$) to just below the water surface ($R(0-)$). Above-water measurements ($R(0+)$) were also recorded to be compared with APEX data. A total of 522 individual measurements were made.

5.4.4 Applying BOMBER and WASI on in situ measurements

The bio-optical model BOMBER has also been applied to the *in situ* measured intensities of L_u and E_d to retrieve water constituents and bottom properties (depth, coverage). For inversion it has to be taken into account that the measurements were made in water and that the entrance optics of the sensors were not aligned at the same depth level to avoid instrument shadowing. The intensity of E_d has to be lowered by 0.475 m to correspond to the depth level of the L_u and E_u sensors. To account for this difference, a python routine was created where the sensors measuring L_u and E_d are treated separately and the depth difference between them is taken into account. For the least square optimization, the L_u measurements were chosen as target functions to derive water constituents and bottom properties. Eq. (5.1) was modified according to our requirements (separating L_u and E_d). Therefore, the radiance at a given depth (z_1) is separated into a part originating from the water column (L_u^C) and a bottom contribution (L_u^B) (Eq. 5.7):

$$L_u(z_1) = L_u^C(z_1) + L_u^B(z_1) \tag{5.7}$$

To account for the depth difference between z_1 and z_2, the intensity of $E_d(z_1)$ has to be lowered using the attenuation coefficient K_d (Eq. 5.8):

$$E_d(z_1) = E_d(z_2)\exp[-K_d(z_1 - z_2)] \tag{5.8}$$

The contribution of the water column and the bottom to the apparent radiance at the depth z_1 is then modelled using Eqs. (5.9) and (5.10) and a least square optimization according to Eq. (5.6) is performed using L_u instead of R_{rs}.

$$L_u^C(z_1) = \frac{\{r_{rs}^{\infty}(1-A_0\exp[-(K_d-K_u^C)(H-z_1)])\}\times\{E_d(z_1)(1-A_0\exp[-K_d(H-z_1)])\}}{1-A_0\exp[-K_u^C(H-z_1)]} \tag{5.9}$$

$$L_u^B(z_1) = \{E_d(z_2)\exp[-K_d(H-z_2)]A_1\,\rho\}\exp[-K_u^B(H-z_1)] \tag{5.10}$$

The Water Colour Simulator (WASI) of Gege (2004) was used to estimate the optically active water constituents from *in situ* data. Since only the measured intensity of E_d is used for inversion, there is no influence of the bottom on the recorded signal. WASI allows us to differentiate between direct and diffuse radiation (Gege 2012) which leads to a highly

accurate retrieval of water constituents. Thus, it was used as a validation for the BOMBER inversion results.

5.4.5 APEX data

During the APEX campaign 2011, Lake Starnberg was captured on 10/09/2011 in five strips (two covering the western shore plus three additional east-west orientated strips). The data acquisition took place between 11:49 and 12:21 UTC at low solar zenith angles (43.6° – 45.4°). The airborne imaging spectrometer APEX (Airborne Prism EXperiment) offers 288 spectral bands covering a wavelength range from 380 – 2500 nm (33). With a field of view of 14° and a flight altitude of 4900 metres a spatial resolution of 4 metres was achieved. The data was delivered by VITO as level 3A product including geometric and atmospheric correction as well as additional water-air interface correction (i.e. with resulting water-leaving reflectance). For further water analysis, only the first 70 bands were used covering a spectral range from 413 to 745 nm (central wavelengths) and band-widths (FWHM) between 3.5 and 13.5 nm. Analysis included masking of land and deep water areas as well as inversion using BOMBER to retrieve IOPs and bottom properties with the image analysis software ENVI 4.7 (Exelis).

5.5 Results and Discussion

5.5.1 Inversion of simulated data

The inversion of the simulated data set using the BOMBER implemented algorithms showed very good results regarding the individual RMSE, $MAPE$ and coefficient of determination (R^2) between input and inversion output for the water constituents (CHL, SPM, cDOM) and the depth (**Table 5-1**).

Table 5-1: Accuracy measures (RMSE, MAPE and R^2) between input and inversion results of simulated water constituents concentrations and depths and classification accuracies of the bottom coverage (Pixel with 100% coverage of the input bottom).

Bottom albedo input	CHL	SPM	cDOM	Depth	Classification accuracy
white foil	**0.068** *1.00%* 0.998	**0.054** *0.72%* 0.998	**0.006** *0.16%* 0.998	**0.653** *1.46%* 0.982	84%
black foil	**0.000** *0.00%* 1.000	**0.000** *0.00%* 1.000	**0.000** *0.00%* 1.000	**0.769** *2.05%* 0.976	51%
Sediment	**0.000** *0.00%* 1.000	**0.000** *0.00%* 1.000	**0.000** *0.00%* 1.000	**0.722** *2.59%* 0.985	73%

root-mean-square error (RMSE) *mean absolute percentage error (MAPE)* coefficient of determination (R^2)

The high overall agreement between input and output can be explained with the same models used for both calculations and the high spectral resolution of APEX. An artificial

error (in percentage of standard deviation) was intentionally omitted, since we were especially interested in the unmixing result of undisturbed spectra (accuracy of correct classification in **Table 5-1**). The best classification accuracy of the bottom was obtained over the white foil. However, the water constituents and the depth here showed the highest deviations. This can be explained by the large amount of reflection stemming from the bottom which overframes the water originating part of the reflection and leads to a higher inaccuracy.

The black foil showed low classification accuracy (51%) but a good estimation of water constituents. The RMSE and the R^2-value for the depth showed the worst values for this surface. The classification accuracy over bare sediment is in between the black and the white foil, the water constituents were well retrieved and the depth estimation errors are comparable to the black foil.

The result of the simulated data set showed that the algorithm works best with natural surfaces. This can be explained by the unnatural bright albedo of the white foil compared to natural reflectors (plants, sediment) which were used for the parameterization of Lee et al. (1998, 1999). However, these natural surfaces (especially sediment) have a large spectral variability which causes inaccuracies. Thus, we expect best results for water constituent retrieval above the black foil. The depth estimation will give better results above the white foil.

5.5.2 Inversion of in situ data

In a next step, the *in situ* measured spectra of L_u and E_d were processed using the modified BOMBER algorithm (see above) for three different water depths (3, 6 and 8 m). To provide a large water column which interacts with incident radiation, only the measurements at the uppermost sensor position (sensor depth of 0.5 m) were used for inversion. The measurements at the very shallow littoral terrace (water depth of 0.5 m) were omitted from analysis, since they do not provide a water column large enough for constituent retrieval. The inversion results of L_u (based on Eqs. 5.7 to 5.10) for the retrieved water constituents (CHL, SPM and cDOM) and depths from *in situ* RAMSES measurements are shown in **Table 5-2**.

Table 5-2: BOMBER-derived water constituents and water depth (± standard deviation σ) from *in situ* RAMSES measurements above the white and the black foils at three water depths. The first row shows the real water depth at this position obtained from the attached pressure sensor.

Parameter	**Bottom coverage**					
	white foil			**black foil**		
water depth (real) [m]	8.1	5.6	3.3	8.0	5.5	3.4
Derived water depth [m] ± σ	12.2 ± 0.4	5.8 ± 1.8	3.2 ± 0.1	4.8 ± 0.2	5.4 ± 0.7	4.5 ± 2.2
CHL [mg m^{-3}] ± σ	3.5 ± 0.2	1.5 ± 2.1	3.1 ± 0.7	0.8 ± 0.1	0.8 ± 0.1	1.2 ± 0.4
SPM [g m^{-3}] ± σ	1.7 ± 0.5	1.4 ± 0.3	3.2 ± 0.7	1.4 ± 0.2	1.5 ± 0.3	1.7 ± 0.5
cDOM [m^{-1}] ± σ	0.4 ± 0.0	0.4 ± 0.1	0.4 ± 0.0	0.4 ± 0.0	0.4 ± 0.0	0.5 ± 0.0

Increasing water depth leads to increasing inaccuracies of the retrieved depth (white foil: overestimation; black foil: underestimation). For the medium (~6 m) and shallow (~3 m) water depths, the inversion above the white foil shows slightly better estimates of the water depth. The derived water constituents show the same values of cDOM absorption with very

low standard deviations for all depths and over both foils. The concentrations of SPM and CHL show different values between the black and the white foil with higher mean value variations and standard deviations above the white foil. This is in good agreement with the results from the simulated data set.

To evaluate the BOMBER inversion result of *in situ* measured reflectances (**Table 5-2**), the retrieved water constituent concentrations were compared to the WASI-derived concentrations from E_d-measurements (**Figure 5-4**). The precision of the WASI inversion results was assessed by plotting the sensor depths (measured with an attached pressure sensor) against the depths estimated by WASI. The result (**Figure 5-3**) shows a very good agreement between derived and measured sensor depths ($R^2 = 0.992$).

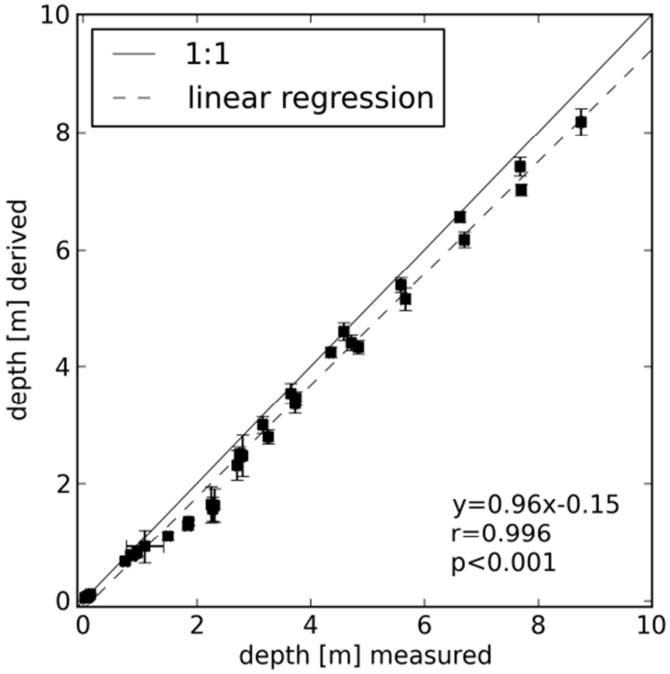

Figure 5-3: Scatterplot of the WASI-derived sensor depth vs. depth of integrated pressure sensor (mean values of 11 iterations).

All E_d-measurements taken under water were processed using WASI. **Figure 5-4** shows the inversion results for the water constituents CHL, SPM and cDOM for the three different water depths. Black squares show the inversion results above the black foil, white squares the results above the white foil.

An increasing concentration can be determined for all IOPs with decreasing sensor depth (please note that always the whole water column above the upward looking sensor is observed). All values have very high standard deviations in the uppermost sensor position (i.e. a water depth of approximately 0.1 m) which can be explained by the very thin water column resulting in large uncertainties of the constituent retrieval. Except for the cDOM concentrations, all depth profiles show the largest value variations at sensor depths between 1 and 2 metres probably due to wave focussing effect at that depth (Gege and Pinnel 2011). In general, the WASI-derived concentrations of CHL (1 mg m^{-3}), SPM (2 g m^{-3}) and cDOM (0.5 m^{-1}) correspond to BOMBER-derived inversion results of r_{rs} above the black foil (**Table 5-2**).

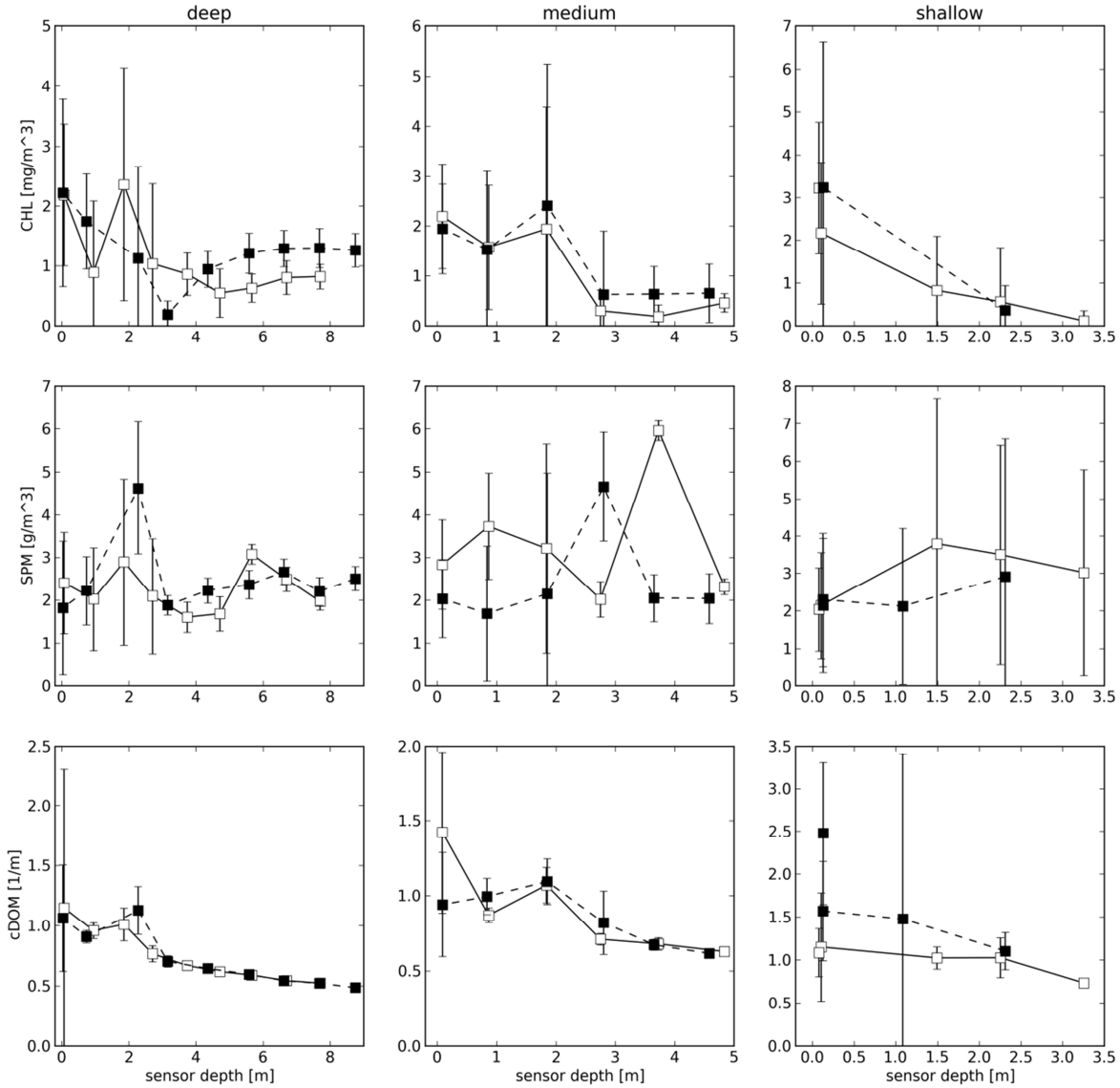

Figure 5-4: Water constituents derived from WASI inversion of E_d-measurements (white squares: above white foil; black square: above black foil), error bars indicate standard deviation of 11 iterated measurements.

5.5.3 BOMBER inversion result of APEX data

The APEX data was delivered atmospherically corrected and additionally corrected for reflection-loss at the water/air interface. The resulting water leaving reflectance (R_w) was further compared to RAMSES measurements above the water surface ($R_{rs}(0+)$). Therefore, pixels representing the foils were manually selected from the APEX image (**Figure 5-5**).

For both foils, the APEX-derived reflectances are lower than the *in situ* measurements. However, the differences between RAMSES and APEX reflectance account only for 3% at maximum above the white foil (in very shallow water) and up to 1.5% above the black foil. This can be explained by neighbouring effects due to the pixel size of 4 metres and a foil width of only 10 metres which leads to mixed pixels.

The same mask to represent the reflectance above the foils (**Figure 5-5**) was used to apply BOMBER to the APEX image only above the foils. **Figure 5-6** shows a map (small subset of the location of the foils) of the BOMBER-derived water constituent

concentrations CHL, SPM and cDOM as well as the result of the bottom coverage unmixing result (for the possible endmembers white foil, black foil and bare sediment).

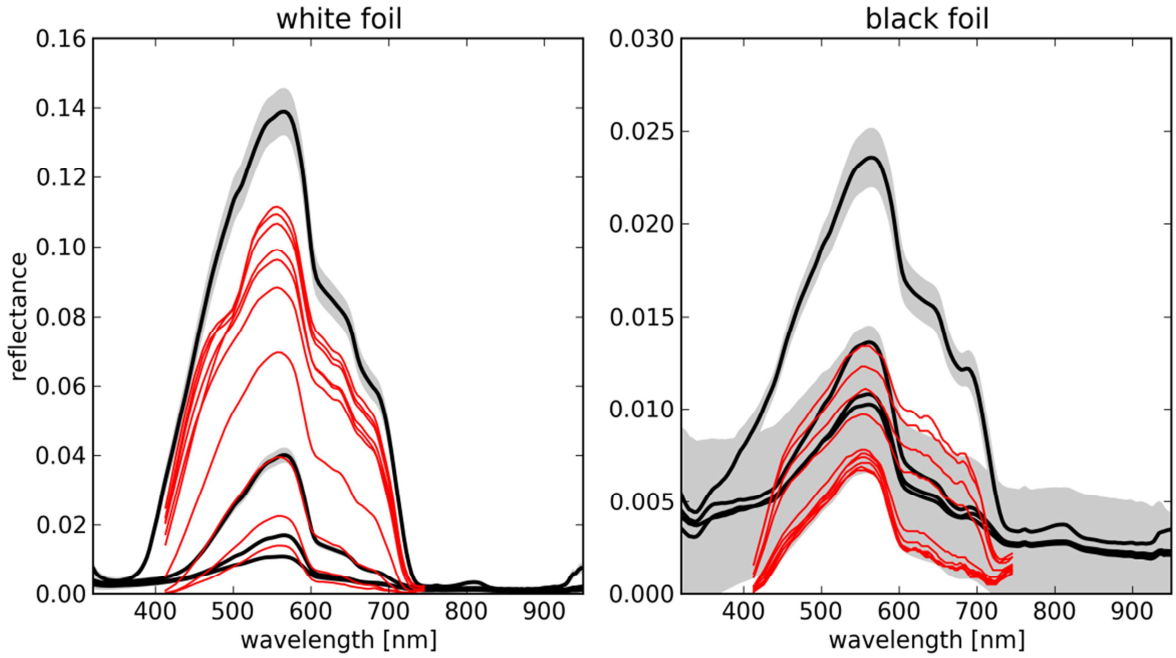

Figure 5-5: Comparison between APEX-derived reflectances (red) and *in situ* measured reflectances (black, grey areas represent the individual standard deviations) above both foils.

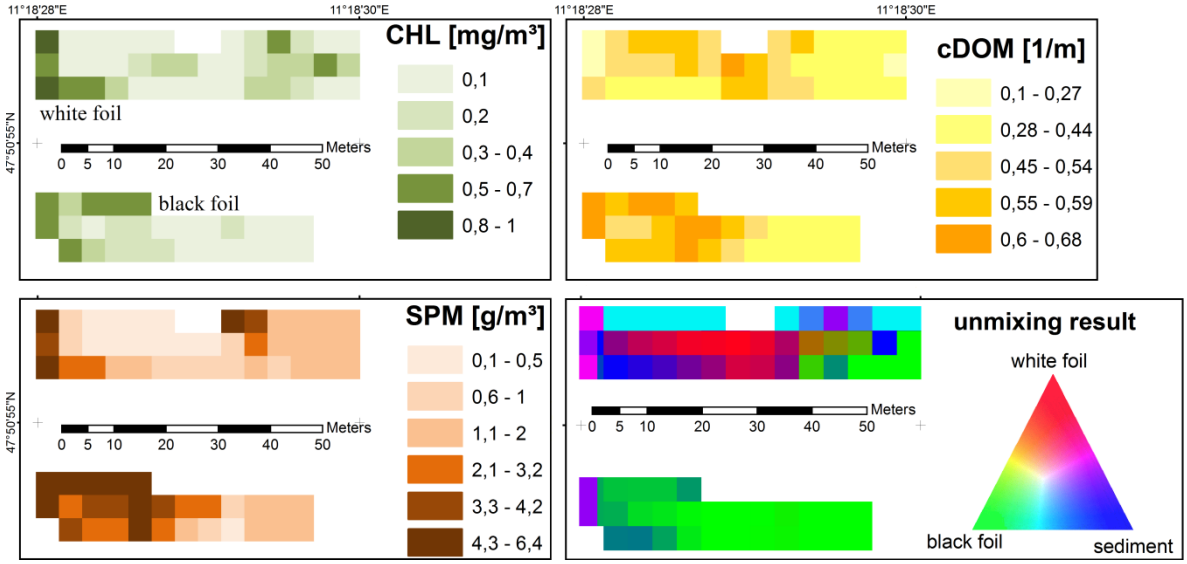

Figure 5-6: Map showing the BOMBER result for the water constituent concentrations CHL, SPM, cDOM and bottom unmixing for a subset of the APEX image (all areas except for the foils are masked).

The resulting concentrations of cDOM and SPM were best estimated above the black foil agreeing well with the concentrations derived from WASI E_d inversion (**Figure 5-4**). CHL was underestimated above both foils. Above the white foil, the water constituent concentrations show larger deviations. This agrees with the inversion results of the simulated data set and the *in situ* reflectance measurements.

In contrast to the simulated data set, the unmixing result of the image data clearly proves that the unnatural bright white foil is not suitable for water constituent retrieval in shallow

water with the BOMBER algorithm due to model restrictions. Only a few pixels were completely assigned to that class. As opposed to this, the black foil was also detected at greater water depths and was assigned correctly.

Finally, BOMBER was applied to the whole scene using the same parameterization as defined by Lee et al. (1999). The results of IOP retrieval and bottom mapping are shown in **Figure 5-7** and **Figure 5-8**.

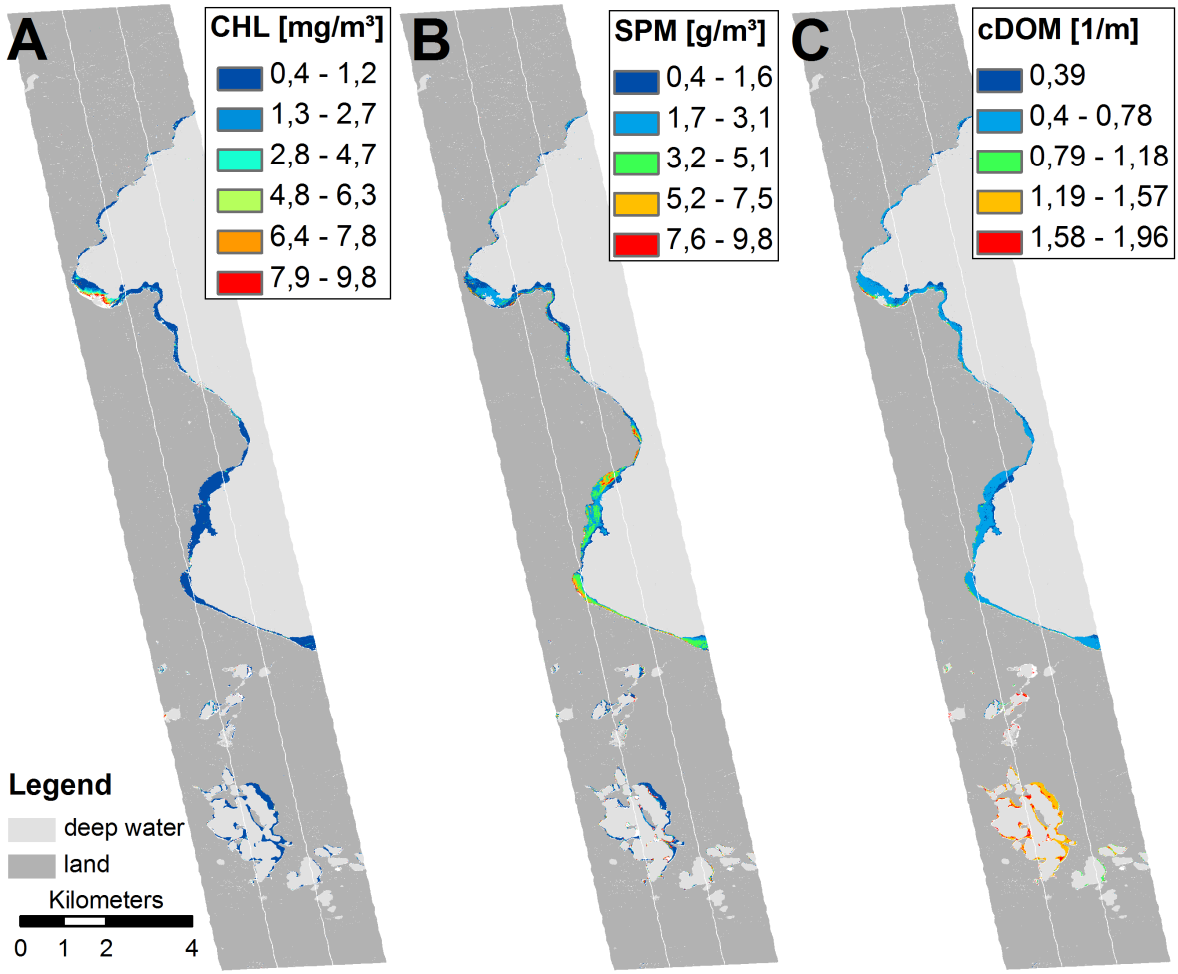

Figure 5-7: BOMBER-derived concentrations of CHL (A), SPM (B) and cDOM (C) for shallow water of the southern APEX strip.

The concentration of CHL was generally low at the shallow areas in Lake Starnberg as well as in the adjacent Osterseen lakes in the south, which drain into Lake Starnberg, confirming previous results (Pinnel 2007). The SPM concentrations had the highest values in the extended littoral terraces at the south-western edge of the lake. This was probably caused by waves resuspending the fine grained silty sediment in this area. In Lake Starnberg, the content of cDOM was constant, while considerable variations at low spatial scales were found in the Osterseen lakes.

The result of spectral unmixing using the endmember *Najas marina*, *Chara* spp. and uncovered sediment are shown in **Figure 5-8**A as well as the estimated water depth (**Figure 5-8**B). The RGB composite was created according to the endmember affiliation.

The result for the test site Bernried shows good recognition of *Najas marina* occurring here at a depth range between 2 and 6 metres. The small bay “Karpfenwinkel” at the

eastern edge of Lake Starnberg is enlarged, because it is known for a dense coverage of *Characea* with interspersed *Najas marina*. Here, the endmember *Najas marina* was overestimated, because *Chara* dominates most of the area. However, the non-vegetated areas were very well detected.

Since the concentrations of water constituents at the whole test site Bernried were comparable to the concentrations obtained above the black foil, they can be regarded as valid. Also, the depth was estimated accurately for this particular area, so we assume a reliable determination of BOMBER for these model outputs for the other regions. The misclassification of the region "Karpfenwinkel" might result from ground reflectances different from our test site.

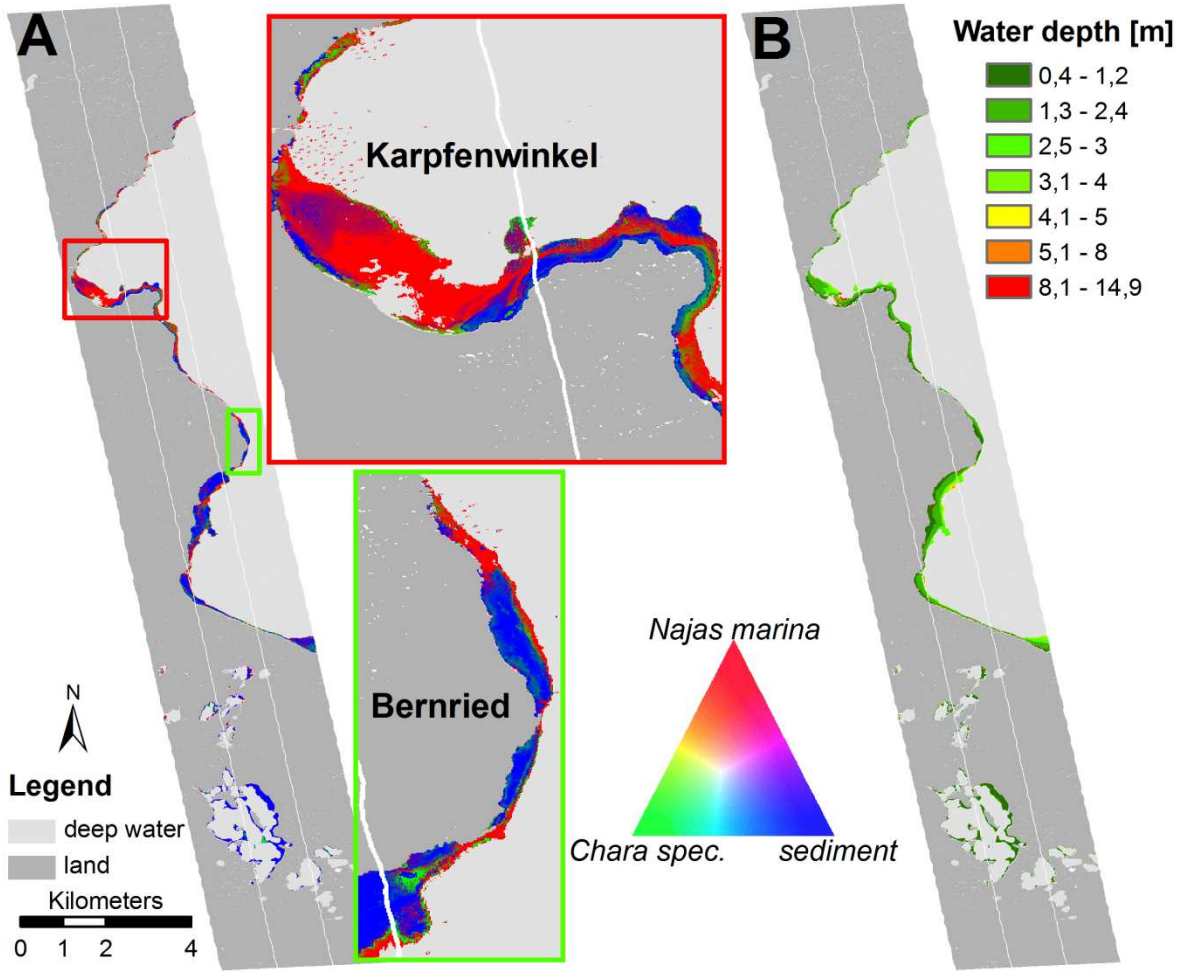

Figure 5-8: Unmixing result for shallow water bottom coverage (A) and bathymetry (B), zoomed areas show the location of the test site "Bernried" and the bay "Karpfenwinkel".

5.6 Conclusions

In this work, we showed how submersed artificial surfaces can be used to validate the image-based retrieval of water constituents and depths using the bio-optical model BOMBER. This validation is especially necessary when no reference measurements of water constituents exist and when the depth is unknown.

Based on the results of the simulated data set we showed that measurements above the black foil are better suited for water constituent retrieval using BOMBER. This finding was confirmed by the application of BOMBER to the *in situ* measured reflectances during the

APEX flight campaign. The results of BOMBER were validated using measurements of the *in situ* downwelling irradiance which were processed using WASI. The resulting water constituents resembled the ones deter-mined above the black foil. Also, the application of BOMBER to the APEX image data showed that the black foil was properly determined even at greater depths. The retrieved water constituents were comparable to the WASI-derived ones. We expect the classification of the whole scene to be relevant as the water constituents of the test site are of the level as above the black foil.

Based on these results, the application of dark artificial surfaces is a powerful tool when no information on water constituents or bathymetry is available. With dark reference surfaces, “deep water” regions can be created containing water constituent concentrations of shallow water (which often differs from the amount of constituents of the adjacent deep water). The retrieved water constituents and bathymetry above these surfaces (e.g. foils) can be used for the validation of bio-optical model inversion results for the adjacent regions with natural bottom coverage (sediment, vegetation) and enhance the result.

5.7 Acknowledgments

This project was funded by the Bavarian State Ministry of the Environment and Public Health under the number ZKL01Abt7_18457. Thanks to VITO and the team of the APEX sensor for providing high quality data, to all colleagues from the Limnological Institute who helped during field work and to Claudia Giardino for providing the software BOMBER. Special thanks to the two anonymous reviewers for their helpful comments and to Katrin Zwirglmaier for improving our English.

6. SYNTHESIS

The aim of this thesis was to find methods suitable to detect invasive aquatic plant species using remote sensing data. The reflectance behaviour of the two invasive plants *Elodea nuttallii* und *Najas marina* as well as other common macrophytes was recorded with a high spectral resolution during two growing seasons. This was accompanied by regular multispectral spaceborne and hyperspectral airborne remote sensing data acquisition. The main idea behind the combination of different remote sensing systems and ground observations was that the loss of spectral information (from hyperspectral to multispectral) can be compensated by increasing temporal resolution (multiseasonal). The chosen study area was Lake Starnberg, which has been subject to earlier studies (Pinnel 2007). According to the objectives of this thesis, three topics will be discussed in the synthesis based on the results of the individual publications (**Chapters 3-5**):

- Since the author created a large dataset for the reflectances of different SAVs and bare substrates and also compiled a database for water constituents, the seasonal variations throughout one year will be discussed.
- Based on the reflection database of SAVs, the separability between different macrophytes (resampled from hyperspectral to multispectral) is evaluated looking at their phenological stages providing best separability with a special focus on the invasive plants *Elodea nuttallii* and *Najas marina*.
- Thirdly, a comparison of the two applied water column correction methods is given.

6.1 Seasonal variations in shallow water

Within the study, a large variability in the reflectance of shallow water regions was observed. In detail, four different sources of variations were noticed: (1) changes in illumination and viewing geometry; (2) changing concentrations of optically active water constituents; (3) changes in submerged aquatic vegetation and (4) changes in the abiotic bottom coverage.

Changes in the illumination and viewing geometry affect the deep water reflectance (r_{rs}^{∞}) and the different attenuation coefficients (K_d, K_{ub}, K_{uw}). Several studies exist relating AOPs to the IOPs total absorption and total backscattering based on changing illumination and viewing geometries (Albert and Mobley 2003; Gordon et al. 1975; Kirk 1984; Morel and Gentili 1993; Sathyendranath and Platt 1997). Above the water surface, unfavourable sun-target-sensor constellations increase sun glint probability (Hedley et al. 2005; Kay et al. 2009; Kutser et al. 2013). For this reason BRDF effects were studied at Lake Starnberg above shallow water using a mobile goniometer system (Wolf et al. 2013b). Such BRDF effects were the subjects of several studies above deep water (Mobley et al. 2003), above sand bottom (Carder et al. 2003; Voss et al. 2003) and above vegetated surfaces (Voss et al. 2003). Latest parameterizations of the reflected skylight at the water surface (Kutser et al. 2013) could be confirmed with reflectance measurements made above optically deep water of the Lakes Osterseen in 2012 (Linnemann 2013).

The IOPs links to the second source of variations: The seasonal changing concentrations of water constituents (Kallio et al. 2001) which is typical for optically complex case-2 waters (Jerlov 1976). Surface water runoff as well as river input increases the content of cDOM, flooding events and strong winds cause turbidity due to resuspension of SPM

(Doxaran et al. 2006) and increasing water temperature as well as increased radiation input leads to stronger phytoplankton (CHL) growth. For 2011, this development had been observed at CHL-concentrations derived as inversion results of E_d-measurements using WASI (Gege 2012)(**Chapter 4.4.1**, **Figure 4-7**).

Phytoplankton growth is influenced by the occurrence of macropyhtes (Søndergaard and Moss 1998), the third source of variations. This variability has been the main subject of the authors study driven by the assumption that a multiseasonal reflectance database can increase classification accuracy. The variation of SAV incorporates the areal coverage (from bare sediment to dense coverage), variations in reflection due to growth and structural changes (intraspecific) and variations in reflectance between different plant species (interspecific). Especially the interspecific differences were investigated searching for times providing best separability (see **Chapter 6.2**).

The fourth variation source concerns especially the application of pixel based bottom unmixing when using bio-optical models. The term "abiotic bottom coverage" is used for areas without any visible coverage by macrophytes. Nevertheless, these areas are covered by algae (Stephens et al. 2003) or biotic microfilms (Decho et al. 2003) as well. The analysis of reflectance spectra of bare ground at 13 locations at Lake Starnberg (4 depths) shows that the spectral shape and intensity of the hyperspectral curves differs significantly even at low spatial scales (**Chapter 2.3**, **Figure 2-9**), their spectral shape and variability is similar to ones of the sediments used by Werdell and Roesler (2003). Therefore, the sediment spectra used for bottom unmixing must be selected carefully in order to obtain reliable results. But not only the locations of different substrates creates variations, also the acquisition time is critical. Some reflectance spectra of bare sediment show a larger coverage by periphyton and the associated absorption features of pigments (Drake et al. 2003).

6.2 Discrimination of macrophytes

The use of interspecific reflectance differences between macrophytes has been subject to earlier studies (Heege et al. 2003; Pinnel 2007) often with a focus on invasive plants like *Codium fragile* subsp. *tomentosoides* (Theriault et al. 2006). The detection of invasive macrophytes at Lake Starnberg was also the opening question of this thesis – especially the identification of *Elodea nuttallii* and *Najas marina*. In general, separability of different SAVs decreases with increasing water depth and with decreasing spectral resolution (O'Neill and Costa 2013; Vahtmäe and Kutser 2007). O'Neill et al. (2011) defined four requirements for the detection of specific macrophytes (*Zostera marina* in their case): (1) their spectral characteristics can be separated from the influence of the atmosphere and the water column; (2) their spectral properties differ from the surrounding benthic coverage; (3) the spectral resolution of the sensor is adequate for resolving these unique spectral characteristics and (4) the spatial resolution of the sensor is adequate for capturing the spatial patterns of the SAV of interest. The first requirement involves the atmospheric correction and water column correction and will be discussed in the next chapter.

For the second requirement, a large database of the reflectance behaviour of different macrophytes (**Chapter 3**) which are common in Lake Starnberg was created to include seasonal variations due to phenology as well. This database was analysed to find

timeframes providing best discriminability using the full hyperspectral resolution of the RAMSES sensors (Wolf et al. 2013a). The author found spatial and temporal changes in macrophyte reflectance during a year which are caused by: (1) the gradual development from non-vegetated areas to fully overgrown patches; (2) changes in pigment composition (Peñuelas et al. 1993); (3) structural changes of the plants (Dierssen et al. 2003) and (4) accumulation of periphyton (Drake et al. 2003). Such multiseasonal databases were already successfully used to differentiate between seagrass species using hyperspectral sensors (Fyfe 2003).

Prior to calculating measures to assess separabilty between the recorded macrophytes, the hyperspectral dataset was resampled to the spectral resolution of the sensor RapidEye using the channel specific spectral response functions (**Chapters 2 and 3**). This conforms with the third requirement defined by O'Neill et al. (2011), since the spectral resolution is reduced to a multispectral system. For both of the applied water column correction methods (see next chapter), two different separability measures were used: For the ln-transformed band ratios the Jeffries-Matusita Index (Richards 1999) was calculated for every band independently as well as for all created 6 artificial bands (**Chapter 3.4.1**, **Table 3-1**). Best discriminability was achieved when all band ratios were used. The M-statistic of Kaufman and Remer (1994) was applied to find timeframes best suited to differentiate between the observed species. It allowed including intraspecific variations in reflectance behaviour (i.e. standard deviation) when calculating separability measures for each spectral band (**Chapter 4.4.1**, **Table 4-1**). The M-statistic has been successfully applied to similar studies (O'Neill et al. 2011) using hyperspectral *in situ* measurements and it revealed generally good separability for first derivatives and ratios, which is in good accordance with previous studies on Lake Starnberg (Pinnel 2007). For above water spectroradiometric measurements, O'Neill et al. (2013) found the spectral slope between 500 and 530 nm and the first derivatives at 566, 580 and 602 nm best suited for detection of eelgrass (*Zostera marina*). For water column corrected measurements, they propose using the ratios 566:600 nm and 566:710 nm for identification. These ratios describe the decreasing reflectance from the local reflection maximum in the Green wavelength region to the Red absorption region and further the strong increase of reflection towards the NIR plateau (Lillesand et al. 2008). Since the centre wavelengths of the green, Red and Red Edge channel of RapidEye (556, 658 and 709 nm) are comparable to the wavelengths proposed by O'Neill et al. (2011), the author expected good discriminability.

This assumption was confirmed for the discrimination of bare sediments, vegetated areas and deep water regions, especially at the end of the growing season (September). The least separability was found in May, where the absence of vegetation causes strong sediment signals with high deviations (**Chapter 4.4.1**). Discrimination was achieved by calculating the M-statistic for each band.

However, the presented separabilities are only valid for the absence of water (the effects of the remaining 20 cm water column above the plant surface were removed with the measured attenuation), a perfect atmospheric correction and no noise in the data. With an overlaying water column, the Green spectral band of multispectral imagery is less affected by absorption of the water body and its constituents (Cho 2007). Thus, being less affected by noise due to general higher transmission, it gives hints that species can be separated even on multispectral images incorporating the Green spectral band.

The fourth requirement was the compensation of the spatial resolution. A main problem in remote sensing of submersed macrophytes is the inadequate spatial resolution of spaceborne hyperspectral imagers like CHRIS/Proba or Hyperion (Vahtmäe and Kutser 2007). The loss of information can be visualized by gradually reducing the spatial resolution of an underwater photography (covering an area of approximately 1 m²) of *E. nuttallii* (above in **Figure 6-1**) and *N. marina* (below in **Figure 6-1**), respectively.

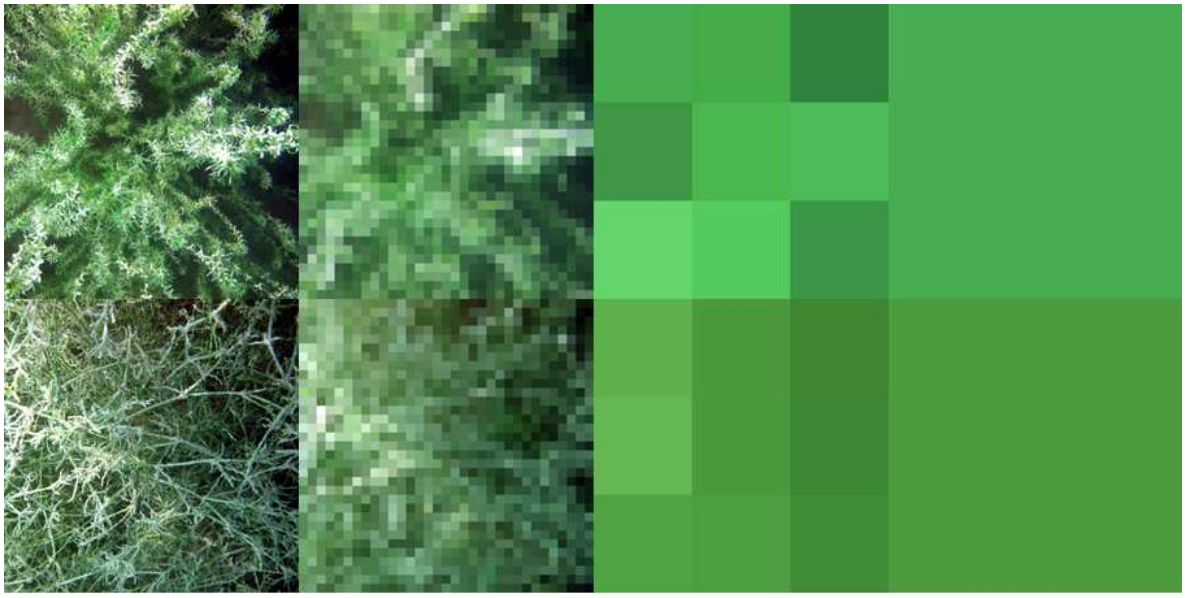

Figure 6-1: effects of changing spatial resolution for a photograph (multispectral image) of an area covered by *Elodea nuttallii* (above) and *Najas marina* (below). The original size was approximately 1 m². Spatial resolution changes from left to right: 125,316 Pixels, 1,089 Pixels, 9 Pixels and 1 Pixel.

Since the spatial resolution of both multispectral and hyperspectral sensors mostly requires spectral unmixing, several studies exist focusing on this subject (Bierwirth et al. 1993; Hedley and Mumby 2003). Within the studies the author decided to use the matched filtering method (Manolakis and Shaw 2002) instead of linear spectral unmixing procedures to prevent a forced assignment of unsuitable endmembers.

One source of inaccuracies occurring when working on littoral benthic habitat mapping is the shape of the underwater relief (Gagnon et al. 2007; Gasperini 2005; Mobley and Sundman 2003; Zanefeld and Boss 2003). At the test site Bernried, a strong inclination at low spatial scales was observed which has to be considered when working with water column correction methods. **Figure 6-2** shows a bathymetric map (original 2 m pixel size) recorded with sonar scanning of the test site Bernried resampled to a pixel size of 5 and 10 metres. As described by Kanno et al. (2011), already the interpolation from point measurements to raster causes inaccuracies. The difference rasters between the two resampled spatial resolutions show that uncertainties due to spatial resampling cause deviations ranging from -1 metre to +3 metres. This effect will have strong influences on the results of water column correction and on bathymetric applications using sensors with a large areal coverage like MODIS (Feng et al. 2011; Hu 2008), or on highly dynamic reliefs like bathymetry of rivers (Legleiter and Roberts 2009; Legleiter et al. 2009; Lejot et al. 2007)

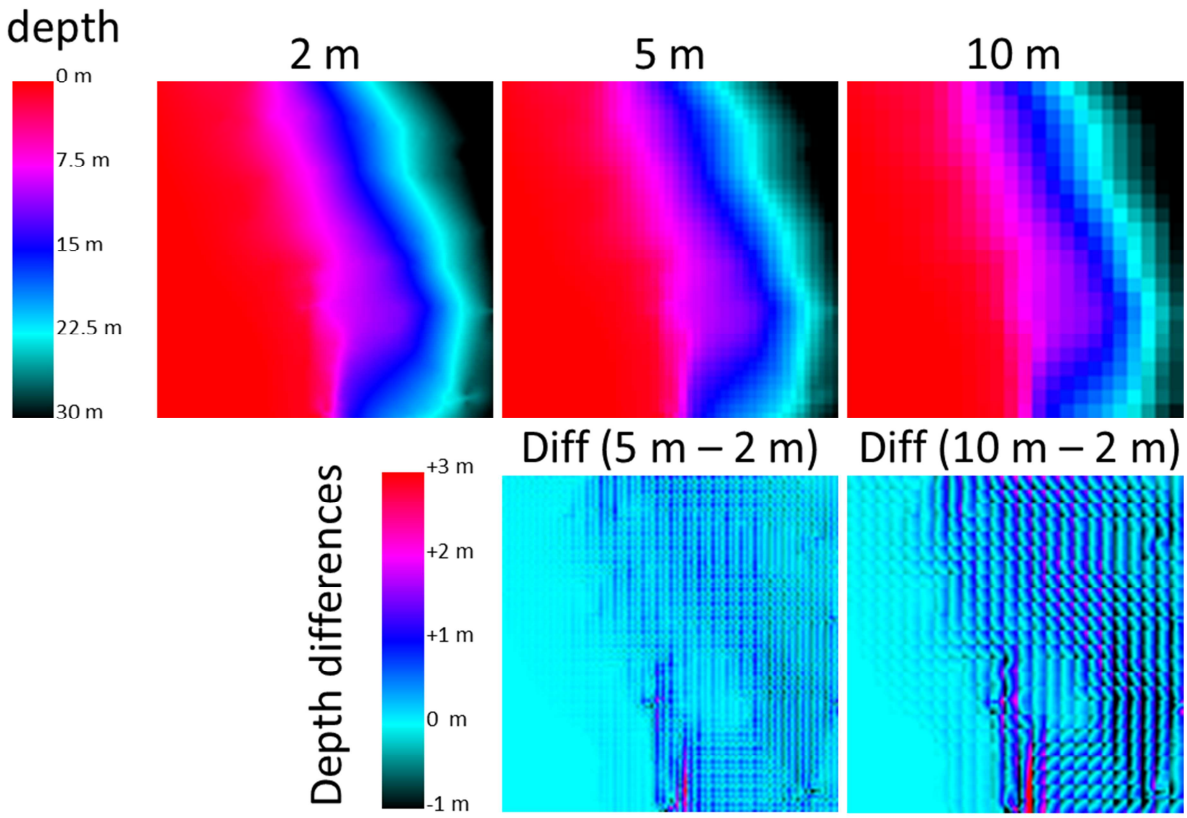

Figure 6-2: bathymetric map of the test site Bernried (resampled from 2 m spatial resolution to 5 m and 10 m) and derived difference raster for the resampled depth maps.

Zanefeld and Boss (2003) showed that ignoring the slope of the littoral bottom can cause errors in reflectance/depth retrieval of up to 30%. They propose a correction of the effective reflectance by using the average cosine of the bottom slope. Mobley and Sundman (2003) developed a backward Monte Carlo 3D (BMC3D) code for relating inhomogeneous and sloping bottoms to commonly used 1D radiative models. However, this problem is ignored in widely used water column correction methods. Besides this topographic error source, also drastic differences in exposure due to spatial averaging may result in misclassification and has not been yet explored.

6.3 Comparison of water column correction methods

This chapter discusses the separability of macrophytes based on their spectral properties – either hyperspectral or with a broadband reduced multispectral resolution. This separability was calculated for the absence of an overlaying water column (i.e. reflectance of the vegetation coverage), since the radiance intensities recorded by any sensor above the water surface are strongly influenced by the water column with its optically active constituents (Kirk 1984). The widely used equation for radiation transfer in shallow water (Maritorena et al. 1994) can be rewritten as:

$$R(0-,z) = R_\infty + (R_b - R_\infty)\exp(-2Kz) \tag{6.1}$$

Since only the right term of Eq. 6.1 contains information of the ground, the useable information for bottom property retrieval is reduced to: $R(0-,z) - R^\infty$. The remaining reflectance value contains information of the bottom if it is higher than the detection

threshold (Dekker et al. 2005). This threshold can be either derived from the signal-to-noise ratio of the sensor (Vahtmäe et al. 2006) or from the standard deviation of the deep-water reflectance (Brando et al. 2009; Wettle et al. 2004). This general problem has different effects on the two methods used in this thesis for eliminating the disturbing effects of the water column.

6.3.1 Transformed band-ratio method

The band ratio method presented in **Chapter 3** according to Lyzenga (1978) has several constraints but also advantages. Limitations are given by the required *a priori* knowledge of attenuation coefficients and by the fact that these coefficients must be vertical and horizontal consistent for the whole lake. If no information on the attenuation coefficients exists, they can be estimated from the multispectral reflectance of deep-water areas using the Quasi-Analytical Algorithm (QAA) of Lee et al. (2002; 2009). This method is not applicable if the shallow water reflectance is lower than the corresponding deep water reflectance, being the case for high loads of suspended particles like in Vahtmäe et al. (2006). Thus, the maximal application depth depends on the highest attenuation coefficient, the bottom reflectance and the deep-water reflectance of this spectral band. Since best separability in case of RapidEye was achieved by using all possible band ratios covering the VIS and Red Edge (**Chapter 3.4.1**, **Table 3-1**), the attenuation values of the Red Edge channel were limiting for application depth. Highly reflective sediment allowed higher application depths than strong absorbing plants. The main advantage is that there is no need for atmospheric correction and thus top-of-atmosphere reflectance can be used for processing. For lakes with consistent water constituent concentrations, or if the seasonal development of these are known, robust indices can be derived since ratios are less affected by systematic errors like sun glint.

Regarding the generally bad separability between different plants using the semi-empirical band ratio technique with *ln*-transformed reflectance spectra (Lyzenga 1978, 1981), another effort was to find a way to differentiate between bare bottom and vegetated areas. By using simple band-ratios of ETM+ (without considering the attenuation), Cho (2007) found that the ratio Blue / Green correlates well with depth and the ratio Green / Red correlates well with the coverage of macrophytes. As presented in **Chapter 3.4.1** all *ln*-transformed band ratios are well suited to differentiate between bare soil and vegetated areas (regarding the Jeffries-Matusita Index). For the differentiation between *Elodea nuttallii* and uncovered sediment, especially the ratio between the Red (b3) and the Red Edge (b4) channel of RapidEye is best suited to differentiate between them (**Table 3-1**). To test if this index can also be used for a larger range of water constituent concentrations, a simulated dataset was created using random percentage of bottom coverage of two bottom types (*Najas marina* and uncovered sediment), a random water depth (0.1 – 5 m), and random water constituent concentrations of phytoplankton (0.1 – 5 µg/l), suspended particulate matter (0.1 – 5 mg/l) and Gelbstoff (0.1 – 2.0 m^{-1}). The result of 1000 randomly created and processed data points is shown in **Figure 6-3**.

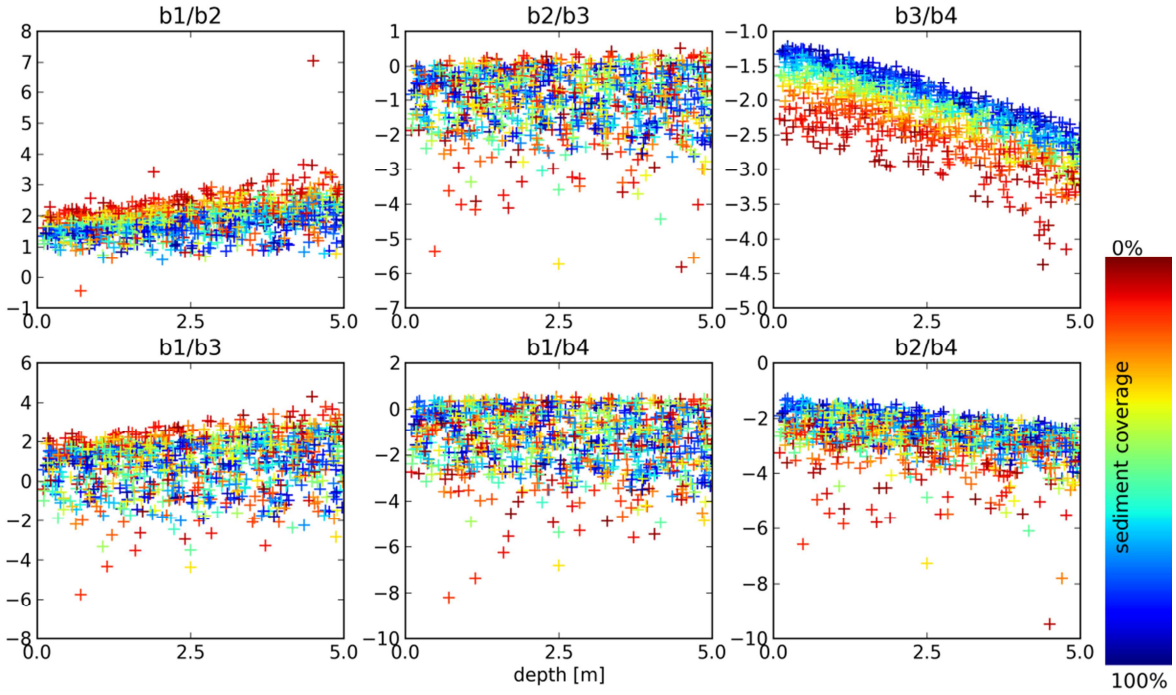

Figure 6-3: depth-invariant indices of the spectral resolution of RapidEye calculated from 1000 random values. Colour coding shows the fraction of sediment coverage.

It is obvious that the depth-invariant index b3/b4 (Red / Red Edge) always allows a good differentiation of sediment coverage – independent of water constituents. Further analysis of the ratio between the individual attenuation coefficients between Red and Red Edge showed, that the attenuation of the Red Edge channel is approximately twice the Red (1.99 ± 0.09) for the given concentration range of water constituents. Thus the equation of Lyzenga (1978) takes the form (Eq. 6.2):

$$Y_{Red/RedEdge} = \frac{2\ln(\rho_{Red} - \rho_{Red}^{\infty}) - \ln(\rho_{RedEdge} - \rho_{RedEdge}^{\infty})}{2.236} \qquad (6.2)$$

This opens new possibilities for the application of the *ln*-transformed ratio method and can even be applied to aerial photos, if the near-infrared region is captured (**Figure 6-4**).

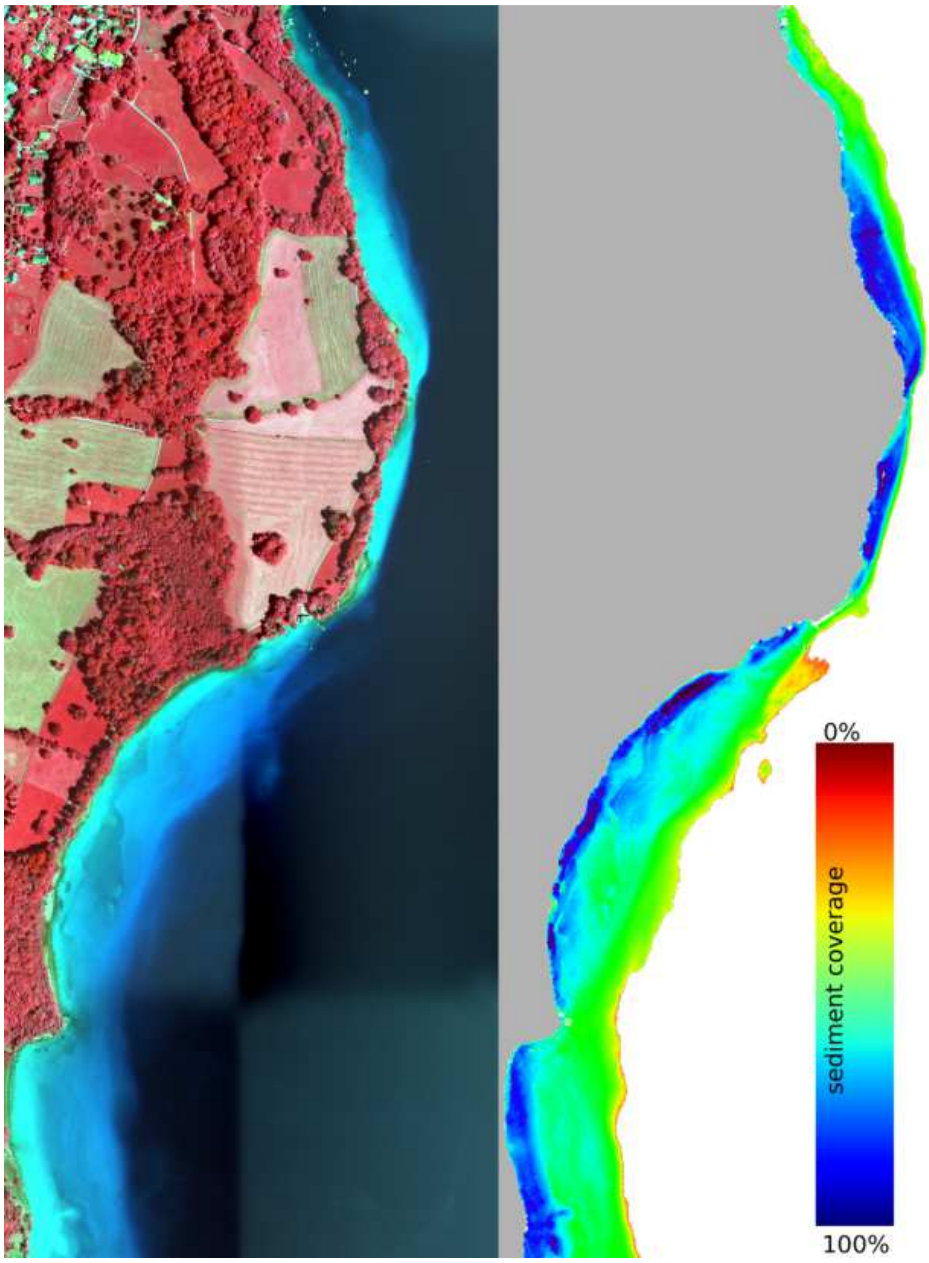

Figure 6-4: Application of the depth-invariant index between the Red and the near-infrared channel on an aerial image of Lake Starnberg (test site Bernried) to differentiate between vegetated (green to red) and non-vegetated areas (blue)

6.3.2 Bio-optical model inversion

The second method used for water column correction only needs bottom reflectance spectra or a group of spectra if spectral unmixing is performed. The application of the bio-optical model BOMBER is described in **Chapter 4** and **Chapter 5**. In contrast to the classification of the *ln*-transformed band ratios, the bottom classification during the application of bio-optical models is part of the optimization. A reliable estimation of water constituents and depths requires a very good knowledge of the expected bottom reflectance (discussed in **Chapter 5**).

The seasonal development has been considered by interpolating the created reflectance database to get reflectance spectra suitable for classification for each day of the year (**Chapter 4.4.1**, **Figure 4-3**). The use of look-up-tables (LUTs) is common when using

physically based models for bottom unmixing (Louchard et al. 2003). LUTs can also be created by simulating the above water reflectance for specific bottom coverages for a large range of water constituent concentration and depths and used for supervised classifications (Vahtmäe and Kutser 2007).

As described by Gordon (1994), a classification is accurate if the classification input property (reflection) and the physical property (depth) forms unique clusters. Several studies exist validating the strong relationship between these two elementary properties (Lee et al. 1998; Maritorena et al. 1994). In **Chapter 5**, the separability of very unique artificial bottom features is evaluated. Although the M-statistics between the white and the black foil and sediment area in-between them indicates a very good separability (exemplary for the sensor AISA) in nearly all spectral bands (in **Figure 6-5**, below), the white foil was misclassified. The great variability of the M-statistics for neighbouring channels greater than 700 nm is due to general low reflectance of shallow water in this spectral region and results from the sensor specific signal-to-noise ratio (theoretically 1:1250 for AISA EAGLE but much lower for low-reflecting surfaces). In shallow water remote sensing application spectral channels with wavelengths greater 700 nm are usually cut (Armstrong 1993; Maeder et al. 2002; Pinnel 2007; Wolter et al. 2005).

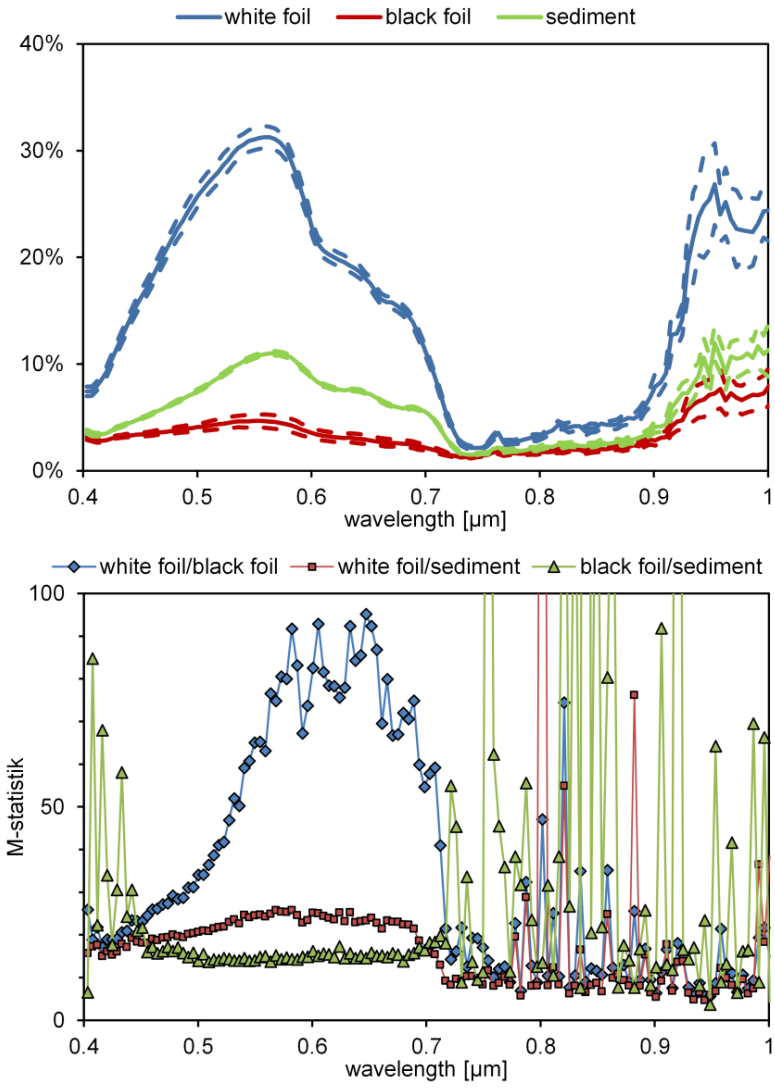

Figure 6-5: AISA-EAGLE reflectance of foils and sediment in 0.5 m water depth (above) and derived M-statistic (below)

Although the requirements of Gordon (1994) are fulfilled, the uniqueness between the above water reflectance spectra is not sufficient. Also the proportion of the bottom reflective part to the overall reflectance plays a major role. The dependency of Q (E_u/L_u) on BRDF effects is analyzed by Foss et al. (2003) for non-nadir viewing sensors and above different bottom coverage. A non-linear dependency between bottom reflectance intensity and Q-factor variability was detected using the submersed foils. **Figure 6-6** shows Q-factors for measurements above both foils at a water depth of 5.5 metres (the sensor was deepening in 1 m steps).

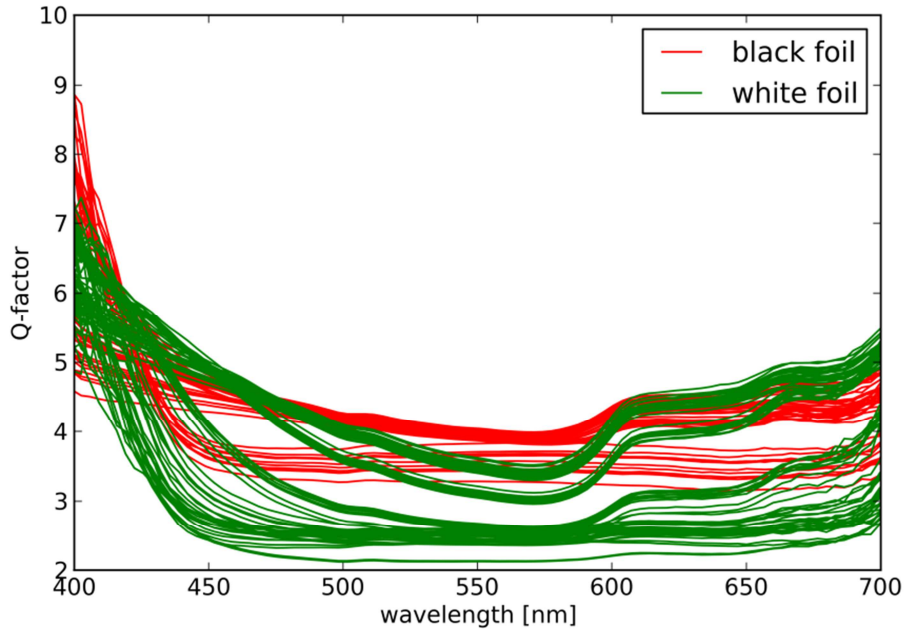

Figure 6-6: *Q*-factors derived from RAMSES measurements (acquired during the AISA EAGLE campaign at 17/08/2011) at different depths measured above the white foil and the black foil at a water depth of 5.5 metres.

By analyzing specific wavelengths and the distance to the bottom, the non-linear relationship can be evaluated using polynomial regression analysis (**Figure 6-7**).

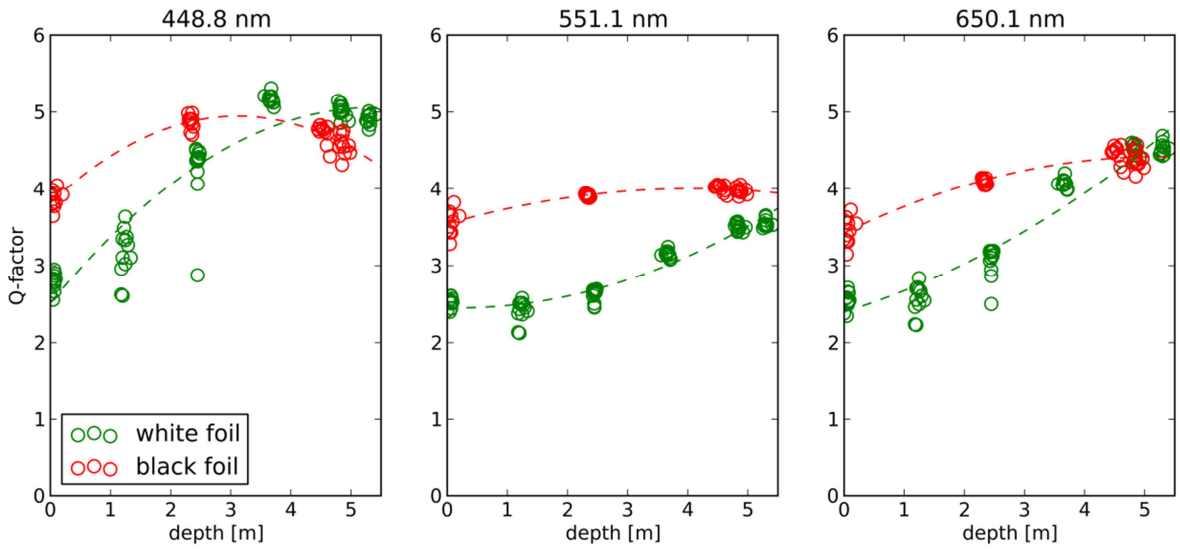

Figure 6-7: relationship between *Q*-factor and sensor depths (distance to the foil) for three selected RAMSES wavelengths

The very low Q-factor at measurements just above the white foil can be an explanation for the bad classification accuracy regarding the white foil (compare **Chapter 5**). In BOMBER, a fixed Q-factor must be set regardless to the bottom albedo. The foil measurements can help to model Q-variability which can be interpolated for natural reflectances since the reflection intensity of natural surfaces will be in between them, comparable to an empirical line correction.

6.4 Conclusion

The study was set out to evaluate the use of multiseasonal *in situ* and remote sensing data to monitor the expansion behaviour of invasive submerged aquatic vegetation. Due to the special demands for an operational use like frequent observations and low costs, the focus within this thesis was set to multispectral spaceborne systems. This lead to issues known from other shallow water remote sensing applications as well as sensor specific ones. The seasonal variations of water constituents, the reflectance of the plants itself and changes in the atmosphere comprises a large potential of errors which have to been solved. Two different correction and classification approaches as well as an experimental setup were presented in the embedded publications and discussed in the synthesis.

The main empirical findings from the three main chapters are that there is a good spectral separability regarding the plants or surface coverages without an overlaying water column. The multiseasonal data acquisition proves that there are certain times during the phenological cycle when the plants are separable even at a multispectral scale. The water column, the sensor specific noise and effects in the atmosphere and the water-air-interface reduces this potential separability significantly. However, a separation between bare ground and vegetated areas was always possible. Concerning the variable content of water constituents, the uncertainty of the results of BOMBER was very large when using multispectral data. But this causes only small errors in the total attenuation and does not affect the classification. In any case, a good atmospheric correction is essential for valuable classification results. In order to solve the uncertainties in classification, additional bathymetric data can be used to enhance classification accuracy. Together with the multiseasonal attempt, rulesets can be created to include only those plants in the classification which are likely to occur at a certain depth and at a certain time.

The two presented methods can be easily adapted for any other lakes to give a first overview of the littoral coverage, even if the species differentiation is difficult. The use of further information like water constituents, bathymetry or *in situ* measured plant- and sediment reflectance enhances the classification result. Together with regular diving observations according to the Water Framework Directive, the presented methods can be used for preliminary classification and help to upscale local observations.

The use of multispectral remote sensing for the classification offers various possibilities for future research. Seasonal databases for other lakes/plants and the improvement of water constituent retrieval using the presented method would be the main aspect. The technical developments towards sensors with lower signal-to-noise ratios offer new possibilities.

Finally, regarding the question if hyperspectral data is better suited to discriminate different species, the answer will still remain “yes”. But, since the investigated SAV were all green macrophytes, their reflectance shows nearly no significant changes in terms of

different pigment absorption curves. So, the main advantage of hyperspectral data is the better estimation of water constituent concentrations and thus a better water column correction. Together with the (mostly) higher spatial resolution, the classification results thus are better. However, taking the costs and the limitations of airborne observations into account, frequent observations must be performed by multispectral satellites.

BIBLIOGRAPHY

Ackleson, S.G., & Klemas, V. (1987). Remote sensing of submerged aquatic vegetation in lower chesapeake bay: A comparison of Landsat MSS to TM imagery. *Remote Sensing of Environment, 22*, 235-248

Albert, A. (2004). Inversion technique for optical remote sensing in shallow water. (p. 188). Oberpfaffenhofen: German Aerospace Center

Albert, A., & Mobley, C. (2003). An analytical model for subsurface irradiance and remote sensing reflectance in deep and shallow case-2 waters. *Optics Express, 11*, 2873-2890

Anderson, R.R. (1969). The Evaluation of Species Composition as a Qualitative Factor in Primary Productivity. *Chesapeake Science, 10*, 307-312

Andréfouët, S., Kramer, P., Torres-Pulliza, D., Joyce, K.E., Hochberg, E.J., Garza-Pérez, R., Mumby, P.J., Riegl, B., Yamano, H., White, W.H., Zubia, M., Brock, J.C., Phinn, S.R., Naseer, A., Hatcher, B.G., & Muller-Karger, F.E. (2003). Multi-site evaluation of IKONOS data for classification of tropical coral reef environments. *Remote Sensing of Environment, 88*, 128-143

Arias-González, J., Acosta-González, G., Membrillo, N., Garza-Pérez, J., & Castro-Pérez, J. (2012). Predicting spatially explicit coral reef fish abundance, richness and Shannon–Weaver index from habitat characteristics. *Biodiversity and Conservation, 21*, 115-130

Armstrong, R.A. (1993). Remote sensing of submerged vegetation canopies for biomass estimation. *International Journal of Remote Sensing, 14*, 621-627

Beer (1852). Bestimmung der Absorption des rothen Lichts in farbigen Flüssigkeiten. In J.C. Poggendorf (Ed.), *Annalen der Physik und Chemie* (pp. 78-88). Leipzig: Verlag von Jahann Ambrosius Barth

Beisl, U. (2001). Correction of bidirectional effects in imaging spectrometer data. In. Zurich: Remote Sensing Laboratories

Bejarano, S., Mumby, P.J., Hedley, J.D., & Sotheran, I. (2010). Combining optical and acoustic data to enhance the detection of Caribbean forereef habitats. *Remote Sensing of Environment, 114*, 2768-2778

Bierwirth, P.N., Lee, T.J., & Burne, R.V. (1993). Shallow sea-floor reflectance and water depth derived by unmixing multispectral imagery. *Photogrammetric Engineering and Remote Sensing, 59*, 331-338

Bostater, J.C.R., Ghir, T., Bassetti, L., Hall, C., Reyeier, E., Lowers, R., Holloway-Adkins, K., & Virnstein, R. (2004). Hyperspectral remote sensing protocol development for submerged aquatic vegetation in shallow waters, 199-215

Botha, E.J., Brando, V.E., Anstee, J.M., Dekker, A.G., & Sagar, S. (2013). Increased spectral resolution enhances coral detection under varying water conditions. *Remote Sensing of Environment, 131*, 247-261

Brando, V.E., Anstee, J.M., Wettle, M., Dekker, A.G., Phinn, S.R., & Roelfsema, C. (2009). A physics based retrieval and quality assessment of bathymetry from suboptimal hyperspectral data. *Remote Sensing of Environment, 113*, 755-770

Carder, K.L., Chen, F.R., Cannizzaro, J.P., Campbell, J.W., & Mitchell, B.G. (2004). Performance of the MODIS semi-analytical ocean color algorithm for chlorophyll-a. *Advances in Space Research, 33*, 1152-1159

Carder, K.L., Liu, C.-C., Lee, Z., English, D.C., Patten, J., Chen, F.R., Ivey, J.E., & Davis, C.O. (2003). Illumination and turbidity effects on observing faceted bottom elements with uniform Lambertian albedos. *Limnology and Oceanography, 48*, 355-363

Carvalho Júnior, O.A., Guimarães, R.F., Santos, N.B.F., Martins, E.S., Gomes, R.A.T., & Shimabukuro, Y.E. (2010). Analysis of channel morphology of São Francisco River using remote sensing data. *International Journal of Remote Sensing, 31*, 1981-1994

Ceyhun, Ö., & Yalçın, A. (2010). Remote sensing of water depths in shallow waters via artificial neural networks. *Estuarine, Coastal and Shelf Science, 89*, 89-96

Cho, H.J. (2007). Depth-variant spectral characteristics of submersed aquatic vegetation detected by Landsat 7 ETM+. *International Journal of Remote Sensing, 28*, 1455-1467

Cho, H.J., & Lu, D. (2010). A water-depth correction algorithm for submerged vegetation spectra. *Remote Sensing Letters, 1*, 29-35

Ciotti, A.M., & Bricaud, A. (2006). Retrievals of a size parameter for phytoplankton and spectral light absorption by colored detrital matter from water-leaving radiances at SeaWiFS channels in a continental shelf region off Brazil. *Limnology and Oceanography: Methods, 4*, 237-253

Conel, J.E., Green, R.O., Vane, G., Bruegge, D.J., Alley, R.E., & Curtiss, B.J. (1987). AIS-2 radiometry and a comparison of methods for the recovery of ground reflectance. In, *Proceedings of the 3rd Airborne Imaging Spectrometer Data Analysis Workshop* (pp. 18-48). Pasadena JPL

de Vel, O.Y., & Bour, W. (1990). The structural and thematic mapping of coral reefs using high Resolution SPOT data: Application to the Tétembia reef (New Caledonia). *Geocarto International, 5*, 27-34

Decho, A.W., Kawaguchi, T., Allison, M.A., Louchard, E.M., Reid, R.P., Stephens, C., Voss, K.J., Wheatcroft, R.A., & Taylor, B.B. (2003). Sediment properties influencing upwelling spectral reflectance signatures: The biofilm gel effect. *Limnology and Oceanography, 48*, 431-443

Dekker, A., Brando, V.E., & Anstee, J.M. (2005). Retrospective seagrass change detection in a shallow coastal tidal Australian lake. *Remote Sensing of Environment, 97*, 415-433

Dekker, A., Brando, V.E., Anstee, J.M., Pinnel, N., Kutser, T., Hoogenboom, E.J., Peters, S., Pasterkamp, R., Vos, R., Olbert, C., & Malthus, T.J.M. (2001). Imaging Spectroscopy of water. In F.D. Van der Meer, & S.M. De Jong (Eds.), *Imaging Spectrometry* (pp. 307-359)

Dierssen, H.M., Zimmerman, R.C., Leathers, R.A., Downer, T.V., & Davis, C.O. (2003). Ocean color remote sensing of seagrass and bathymetry in the Bahamas Banks by high resolution airborne imagery. *Limnology and Oceanography, 48*, 444-455

Doerffer, R. (1992). Imaging spectroscopy for detection of chlorophyll and suspended matter. In F. Toselli, & J. Bodechtel (Eds.), *Imaging Spectroscopy: Fundamentals and Prospective Applications* (pp. 215-257). London: Kluwer Academic Publishers

Dogan, O.K., Akyurek, Z., & Beklioglu, M. (2009). Identification and mapping of submerged plants in a shallow lake using quickbird satellite data. *Journal of Environmental Management, 90*, 2138-2143

Doxaran, D., Castaing, P., & Lavender, S.J. (2006). Monitoring the maximum turbidity zone and detecting fine-scale turbidity features in the Gironde estuary using high spatial resolution satellite sensor (SPOT HRV, Landsat ETM+) data. *International Journal of Remote Sensing, 27*, 2303-2321

Drake, L.A., Dobbs, F.C., & Zimmerman, R.C. (2003). Effects of epiphyte load on optical properties and photosynthetic potential of the seagrasses *Thalassia testudinum* Banks ex König and *Zostera marina* L. *Limnology and Oceanography, 48*, 456-463

Feng, L., Hu, C., Chen, X., Li, R., Tian, L., & Murch, B. (2011). MODIS observations of the bottom topography and its inter-annual variability of Poyang Lake. *Remote Sensing of Environment, 115*, 2729-2741

Fesq-Martin, M., Lang, A., & Peters, M. (2008). *Der Starnberger See - Natur- und Vorgeschichte einer bayerischen Landschaft*. (p. 145). München: Pfeil-Verlag

Fyfe, S.K. (2003). Spatial and temporal variation in spectral reflectance: Are seagrass species spectrally distinct? *Limnology and Oceanography, 48*, 464-479

Gagnon, P., Scheibling, R.E., Jones, W., & Tully, D. (2007). The role of digital bathymetry in mapping shallow marine vegetation from hyperspectral image data. *International Journal of Remote Sensing, 29*, 879-904

Gasperini, L. (2005). Extremely Shallow-water Morphobathymetric Surveys: The Valle Fattibello (Comacchio, Italy) Test Case. *Marine Geophysical Research, 26*, 97-107

Gege, P. (2004). The water color simulator WASI: an integrating software tool for analysis and simulation of optical in situ spectra. *Computers & Geosciences, 30*, 523-532

Gege, P. (2012). Estimation of phytoplankton concentration from downwelling irradiance measurements in water. *Israel Journal of Plant Sciences, 60*, 193-207

Gege, P., & Pinnel, N. (2011). Sources of variance of downwelling irradiance in water. *Applied Optics, 50*, 2192-2203

Giardino, C., Candiani, G., Bresciani, M., Lee, Z., Gagliano, S., & Pepe, M. (2012). BOMBER: A tool for estimating water quality and bottom properties from remote sensing images. *Computers & Geosciences, 45*, 313-318

Giardino, C., & Zilioli, E. (2001). Imaging spectrometry for submerged vegetation mapping in Lake Garda. In, *Geoscience and Remote Sensing Symposium, 2001. IGARSS '01. IEEE 2001 International* (pp. 2749-2751 vol.2746)

Gordon, A.D. (1994). Identifying genuine clusters in a classification. *Computational Statistics and Data Analysis, 18*, 561-581

Gordon, H.R., Brown, O.B., & Jacobs, M.M. (1975). Computed Relationships Between the Inherent and Apparent Optical Properties of a Flat Homogeneous Ocean. *Applied Optics, 14*, 417-427

Gordon, H.R., & Clark, D.K. (1981). Clear water radiances for atmospheric correction of coastal zone color scanner imagery. *Applied Optics, 20*, 4175-4180

Gordon, H.R., Clark, D.K., Brown, J.W., Brown, O.B., Evans, R.H., & Broenkow, W.W. (1983). Phytoplankton pigment concentrations in the Middle Atlantic Bight: comparison of ship determinations and CZCS estimates. *Applied Optics, 22*, 20-36

Gordon, H.R., & Wang, M. (1994). Retrieval of water-leaving radiance and aerosol optical thickness over the oceans with SeaWiFS: a preliminary algorithm. *Applied Optics, 33*, 443-452

Gullström, M., Lundén, B., Bodin, M., Kangwe, J., Öhman, M.C., Mtolera, M.S.P., & Björk, M. (2006). Assessment of changes in the seagrass-dominated submerged vegetation of tropical Chwaka Bay (Zanzibar) using satellite remote sensing. *Estuarine, Coastal and Shelf Science, 67*, 399-408

Hakvoort, H., de Haan, J., Jordans, R., Vos, R., Peters, S., & Rijkeboer, M. (2002). Towards airborne remote sensing of water quality in The Netherlands - validation and error analysis. *ISPRS Journal of Photogrammetry and Remote Sensing, 57*, 171-183

Hansen, J.E., & Travis, L.D. (1974). Light scattering in planetary atmospheres. *Space Science Reviews, 16*, 527-610

Hedley, J.D., Harborne, A.R., & Mumby, P.J. (2005). Simple and robust removal of sun glint for mapping shallow-water benthos. *International Journal of Remote Sensing, 26*, 2107-2112

Hedley, J.D., & Mumby, P.J. (2003). A Remote Sensing Method for Resolving Depth and Subpixel Composition of Aquatic Benthos. *Limnology and Oceanography, 48*, 480-488

Heege, T., Bogner, A., & Pinnel, N. (2003). Mapping of submerged aquatic vegetation with a physically based processing chain. In E. Kramer (Ed.), *SPIE-The International Society for Optical Engineering* (pp. 43-50). Barcelona: SPIE

Herold, M., Metz, J., & Romsos, J.S. (2007). Inferring littoral substrates, fish habitats, and fish dynamics of Lake Tahoe using IKONOS data. *Canadian Journal of Remote Sensing, 33*, 445-456

Hestir, E.L., Khanna, S., Andrew, M.E., Santos, M.J., Viers, J.H., Greenberg, J.A., Rajapakse, S.S., & Ustin, S.L. (2008). Identification of invasive vegetation using

hyperspectral remote sensing in the California Delta ecosystem. *Remote Sensing of Environment, 112,* 4034-4047

Hochberg, E.J., Andrefouet, S., & Tyler, M.R. (2003). Sea surface correction of high spatial resolution Ikonos images to improve bottom mapping in near-shore environments. *Geoscience and Remote Sensing, IEEE Transactions on, 41,* 1724-1729

Holben, B.N., Eck, T.F., Slutsker, I., Tanré, D., Buis, J.P., Setzer, A., Vermote, E., Reagan, J.A., Kaufman, Y.J., Nakajima, T., Lavenu, F., Jankowiak, I., & Smirnov, A. (1998). AERONET—A Federated Instrument Network and Data Archive for Aerosol Characterization. *Remote Sensing of Environment, 66,* 1-16

Hooker, S.B., Zibordi, G., Berthon, J.-F., & Brown, J.W. (2004). Above-Water Radiometry in Shallow Coastal Waters. *Applied Optics, 43,* 4254-4268

Hu, C. (2008). Ocean Color Reveals Sand Ridge Morphology on the West Florida Shelf. *Geoscience and Remote Sensing Letters, IEEE, 5,* 443-447

Huen, W.-K., & Zhang, Y. (2011). Preliminary studies on coral mapping in Tung Ping Chau of the eastern Hong Kong using high-resolution SPOT satellite imagery. *Annals of GIS, 17,* 93-98

Hueni, A., Biesemans, J., Meuleman, K., Dell'Endice, F., Schlapfer, D., Odermatt, D., Kneubuehler, M., Adriaensen, S., Kempenaers, S., Nieke, J., & Itten, K.I. (2009). Structure, Components, and Interfaces of the Airborne Prism Experiment (APEX) Processing and Archiving Facility. *Geoscience and Remote Sensing, IEEE Transactions on, 47,* 29-43

Jerlov, N.G. (1976). *Marine Optics*. (p. 246). New York: Elsevier Science Ltd.

Kallio, K., Kutser, T., Hannonen, T., Koponen, S., Pulliainen, J., Vepsäläinen, J., & Pyhälahti, T. (2001). Retrieval of water quality from airborne imaging spectrometry of various lake types in different seasons. *Science of The Total Environment, 268,* 59-77

Kallio, K., Pulliainen, J., & Ylöstalo, P. (2005). MERIS, MODIS and ETM+ Channel Configurations in the Estimation of Lake Water Quality from Subsurface Using Semi-analytical and Empirical Algorithms. *Geophysica, 41,* 31-55

Kanno, A. (2011). Coral Reef Bathymetry using Satellite Imagery - Validation of Accuracy Improvement with Doubled Bands. *Journal of Japan Society of Civil Engineers, Series B2 (Coastal Engineering), 67,* 1341-1345

Kanno, A., Koibuchi, Y., & Isobe, M. (2011). Statistical Combination of Spatial Interpolation and Multispectral Remote Sensing for Shallow Water Bathymetry. *Geoscience and Remote Sensing Letters, IEEE, 8,* 64-67

Kao, H.-M., Ren, H., Lee, C.-S., Chang, C.-P., Yen, J.-Y., & Lin, T.-H. (2009). Determination of shallow water depth using optical satellite images. *International Journal of Remote Sensing, 30,* 6241-6260

Kaufman, Y.J., & Remer, L.A. (1994). Detection of forests using mid-IR reflectance: an application for aerosol studies. *IEEE Transactions on Geosciences and Remote Sensing, 32*, 672-683

Kay, S., Hedley, J., & Lavender, S. (2009). Sun Glint Correction of High and Low Spatial Resolution Images of Aquatic Scenes: a Review of Methods for Visible and Near-Infrared Wavelengths. *Remote Sensing, 1*, 697-730

Kirk, J.T.O. (1984). Dependence of Relationship Between Inherent and Apparent Optical Properties of Water on Solar Altitude. *Limnology and Oceanography, 29*, 350-356

Knudby, A., LeDrew, E., & Brenning, A. (2010). Predictive mapping of reef fish species richness, diversity and biomass in Zanzibar using IKONOS imagery and machine-learning techniques. *Remote Sensing of Environment, 114*, 1230-1241

Knudby, A., & Nordlund, L. (2011). Remote sensing of seagrasses in a patchy multi-species environment. *International Journal of Remote Sensing, 32*, 2227-2244

Koponen, S., Pulliainen, J., Kallio, K., & Hallikainen, M. (2002). Lake water quality classification with airborne hyperspectral spectrometer and simulated MERIS data. *Remote Sensing of Environment, 79*, 51-59

Kutser, T., Miller, I., & Jupp, D.L.B. (2006). Mapping coral reef benthic substrates using hyperspectral space-borne images and spectral libraries. *Estuarine, Coastal and Shelf Science, 70*, 449-460

Kutser, T., Vahtmäe, E., Paavel, B., & Kauer, T. (2013). Removing glint effects from field radiometry data measured in optically complex coastal and inland waters. *Remote Sensing of Environment, 133*, 85-89

Lacoul, P., & Freedman, B. (2006). Environmental influences on aquatic plants in freshwater ecosystems. *Environmental Reviews, 14*, 89-136

Lafon, V., De Melo Apoluceno, D., Dupuis, H., Michel, D., Howa, H., & Froidefond, J.M. (2004). Morphodynamics of nearshore rhythmic sandbars in a mixed-energy environment (SW France): I. Mapping beach changes using visible satellite imagery. *Estuarine, Coastal and Shelf Science, 61*, 289-299

Lafon, V., Froidefond, J.-M., & Castaing, P. (2000). Méthode d'analyse de l'évolution morphodynamique d'une embouchure tidale par imagerie satellite. Exemple du bassin d'Arcachon (France). *Comptes Rendus de l'Académie des Sciences - Series IIA - Earth and Planetary Science, 331*, 373-378

Lafon, V., Froidefond, J.M., Lahet, F., & Castaing, P. (2002). SPOT shallow water bathymetry of a moderately turbid tidal inlet based on field measurements. *Remote Sensing of Environment, 81*, 136-148

Lee, Z., Carder, K.L., & Arnone, R.A. (2002). Deriving Inherent Optical Properties from Water Color: a Multiband Quasi-Analytical Algorithm for Optically Deep Waters. *Appl. Opt., 41*, 5755-5772

Lee, Z., Carder, K.L., Mobley, C.D., Steward, R.G., & Patch, J.S. (1998). Hyperspectral Remote Sensing for Shallow Waters. I. A Semianalytical Model. *Applied Optics, 37*, 6329-6338

Lee, Z., Carder, K.L., Mobley, C.D., Steward, R.G., & Patch, J.S. (1999). Hyperspectral Remote Sensing for Shallow Waters. 2. Deriving Bottom Depths and Water Properties by Optimization. *Applied Optics, 38*, 3831-3843

Lee, Z., Lubac, J., Werdell, J., & Arnone, R.A. (2009). An update of the quasi-analytical algorithm (QAA_v5). In, *International Ocean Color Group software report*

Legleiter, C.J., & Roberts, D.A. (2009). A forward image model for passive optical remote sensing of river bathymetry. *Remote Sensing of Environment, 113*, 1025-1045

Legleiter, C.J., Roberts, D.A., & Lawrence, R.L. (2009). Spectrally based remote sensing of river bathymetry. *Earth Surface Processes and Landforms, 34*, 1039-1059

Lejot, J., Delacourt, C., Piégay, H., Fournier, T., Trémélo, M.L., & Allemand, P. (2007). Very high spatial resolution imagery for channel bathymetry and topography from an unmanned mapping controlled platform. *Earth Surface Processes and Landforms, 32*, 1705-1725

Lillesand, T.M., Kiefer, R.W., & Chipman, J.W. (2008). *Remote Sensing and Image Interpretation*. (6th Edition ed.). (p. 768). New York: Wiley & Sons

Linnemann, K. (2013). Untersuchung der saisonalen Entwicklung optischer Eigenschaften von Wasserinhaltsstoffen in vier ausgewählten Osterseen. In, *Limnological Station* (p. 87). Weihenstephan: Technische Universität München

Lira, J. (2006). Segmentation and morphology of open water bodies from multispectral images. *International Journal of Remote Sensing, 27*, 4015 - 4038

Louchard, E.M., Reid, R.P., Stephens, F.C., Davis, C.O., Leathers, R.A., & Downes, T.V. (2003). Optical Remote Sensing of Benthic Habitats and Bathymetry in Coastal Environments at Lee Stocking Island, Bahamas: A Comparative Spectral Classification Approach. *Limnology and Oceanography, 48*, 511-521

Lu, D., & Cho, H.J. (2010). An improved water-depth correction algorithm for seagrass mapping using hyperspectral data. *Remote Sensing Letters, 2*, 91-97

Lyzenga, D.R. (1978). Passive remote sensing techniques for mapping water depth and bottom features. *Appl. Opt., 17*, 379-383

Lyzenga, D.R. (1981). Remote sensing of bottom reflectance and water attenuation parameters in shallow water using aircraft and Landsat data. *International Journal of Remote Sensing, 2*, 71 - 82

Lyzenga, D.R. (1985). Shallow-water bathymetry using combined lidar and passive multispectral scanner data. *International Journal of Remote Sensing, 6*, 115-125

Maeder, J., Narumalani, S., Rundquist, D.C., Perk, R.L., Schalles, J., Hutchins, K., & Keck, J. (2002). Classifying and mapping general coral-reef structure using Ikonos data. *Photogrammetric Engineering and Remote Sensing, 68,* 1297-1305

Malthus, T.J., & Karpouzli, E. (2003). Integrating field and high spatial resolution satellite-based methods for monitoring shallow submersed aquatic habitats in the Sound of Eriskay, Scotland, UK. *International Journal of Remote Sensing, 24*, 2585-2593

Manolakis, D., & Shaw, G. (2002). Detection algorithms for hyperspectral imaging applications. *Signal Processing Magazine, IEEE, 19*, 29-43

Maritorena, S. (1996). Remote sensing of the water attenuation in coral reefs: a case study in French Polynesia. *International Journal of Remote Sensing, 17*, 155 - 166

Maritorena, S., Morel, A., & Gentili, B. (1994). Diffuse Reflectance of Oceanic Shallow Waters: Influence of Water Depth and Bottom Albedo. *Limnology and Oceanography, 39*, 1689-1703

McFeeters, S.K. (1996). The use of the Normalized Difference Water Index (NDWI) in the delineation of open water features. *International Journal of Remote Sensing, 17*, 1425 - 1432

McIntyre, M., Naar, D., Carder, K., Donahue, B., & Mallinson, D. (2006). Coastal Bathymetry from Hyperspectral Remote Sensing Data: Comparisons with High Resolution Multibeam Bathymetry. *Marine Geophysical Research, 27*, 129-136

Melzer, A. (1976). Makrophytische Wasserpflanzen als Indikatoren des Gewässerzustandes oberbayerischer Seen. In, *Dissertationes Botanicae; 34; 1-195* (p. 195). Vaduz: J.Cramer

Melzer, A. (1999). Aquatic macrophytes as tools for lake management. *Hydrobiologia, 396*, 181-190

Melzer, A., Grosser, S., & Pohl, W. (1993). Der Rückgang der Röhrichtbestände an vier oberbayerischen Seen - Luftbildauswertung, Biometrie und erste Rückungsursachen. *Münchener Beiträge zur Abwasser-, Fischerei- und Flußbiologie, 48*, 257-279

Mertes, L.A.K., Smith, M.O., & Adams, J.B. (1993). Estimating suspended sediment concentrations in surface waters of the Amazon River wetlands from Landsat images. *Remote Sensing of Environment, 43*, 281-301

Minghelli-Roman, A., & Dupouy, C. (2013). Influence of Water Column Chlorophyll Concentration on Bathymetric Estimations in the Lagoon of New Caledonia, Using Several MERIS Images. *Selected Topics in Applied Earth Observations and Remote Sensing, IEEE Journal of, PP*, 1-7

Minghelli-Roman, A., Goreac, A., Mathieu, S., Spigai, M., & Gouton, P. (2009). Comparison of bathymetric estimation using different satellite images in coastal sea waters. *International Journal of Remote Sensing, 30*, 5737-5750

Mishra, D., Narumalani, S., Lawson, M., & Rundquist, D. (2004). Bathymetric Mapping Using IKONOS Multispectral Data. *GIScience & Remote Sensing, 41*, 301-321

Mishra, D.R., Narumalani, S., Rundquist, D., & Lawson, M. (2005). Characterizing the vertical diffuse attenuation coefficient for downwelling irradiance in coastal waters: Implications for water penetration by high resolution satellite data. *ISPRS Journal of Photogrammetry and Remote Sensing, 60*, 48-64

Mishra, D.R., Narumalani, S., Rundquist, D., & Lawson, M. (2006). Benthic habitat mapping in tropical marine environments using QuickBird multispectral data. *Photogrammetric Engineering and Remote Sensing, 72*, 1037–1048

Mishra, D.R., Narumalani, S., Rundquist, D., Lawson, M., & Perk, R. (2007). Enhancing the detection and classification of coral reef and associated benthic habitats: A hyperspectral remote sensing approach. *J. Geophys. Res., 112*, C08014

Mobley, C.D. (1994). *Light and Water*. (p. 592). San Diego, Kalifornien: Academic Press

Mobley, C.D., & Sundman, L.K. (2003). Effects of optically shallow bottoms on upwelling radiances: Inhomogeneous and sloping bottoms. *Limnology and Oceanography, 48*, 329-336

Mobley, C.D., Zhang, H., & Voss, K.J. (2003). Effects of optically shallow bottoms on upwelling radiances: Bidirectional reflectance distribution function effects. *Limnology and Oceanography, 48*, 337-345

Moran, M.S., Bryant, R., Thome, K., Ni, W., Nouvellon, Y., Gonzalez-Dugo, M.P., Qi, J., & Clarke, T.R. (2001). A refined empirical line approach for reflectance factor retrieval from Landsat-5 TM and Landsat-7 ETM+. *Remote Sensing of Environment, 78*, 71-82

Morel, A. (1980). In-water and remote measurements of ocean color. *Boundary-Layer Meteorology, 18*, 177-201

Morel, A., & Bélanger, S. (2006). Improved detection of turbid waters from ocean color sensors information. *Remote Sensing of Environment, 102*, 237-249

Morel, A., & Gentili, B. (1993). Diffuse reflectance of oceanic waters. II Bidirectional aspects. *Applied Optics, 32*, 6864-6879

Mumby, P.J., Clark, C.D., Green, E.P., & Edwards, A.J. (1998). Benefits of water column correction and contextual editing for mapping coral reefs. *International Journal of Remote Sensing, 19*, 203 - 210

Mumby, P.J., Green, E.P., Edwards, A.J., & Clark, C.D. (1997). Coral reef habitat mapping: how much detail can remote sensing provide? *Marine Biology, 130*, 193-202

O'Neill, J.D., & Costa, M. (2013). Mapping eelgrass (Zostera marina) in the Gulf Islands National Park Reserve of Canada using high spatial resolution satellite and airborne imagery. *Remote Sensing of Environment, 133*, 152-167

O'Neill, J.D., Costa, M., & Sharma, T. (2011). Remote Sensing of Shallow Coastal Benthic Substrates: In situ Spectra and Mapping of Eelgrass (Zostera marina) in the Gulf Islands National Park Reserve of Canada. *Remote Sensing, 3*, 975-1005

Odermatt, D., Gitelson, A., Brando, V.E., & Schaepman, M. (2012). Review of constituent retrieval in optically deep and complex waters from satellite imagery. *Remote Sensing of Environment, 118*, 116-126

Onaindia, M., Bikuña, B.G., & Benito, I. (1996). Aquatic plants in relation to environmental factors in Northern Spain. *Journal of Environmental Management, 47*, 123-137

Peñuelas, J., Gamon, J.A., Griffin, K.L., & Field, C.B. (1993). Assessing community type, plant biomass, pigment composition, and photosynthetic efficiency of aquatic vegetation from spectral reflectance. *Remote Sensing of Environment, 46*, 110-118

Philpot, W.D. (1989). Bathymetric mapping with passive multispectral imagery. *Applied Optics, 28*, 1569-1578

Phinn, S., Roelfsema, C., Dekker, A., Brando, V., & Anstee, J. (2008). Mapping seagrass species, cover and biomass in shallow waters: An assessment of satellite multi-spectral and airborne hyper-spectral imaging systems in Moreton Bay (Australia). *Remote Sensing of Environment, 112*, 3413-3425

Pinnel, N. (2007). A method for mapping submerged macrophytes in lakes using hyperspectral remote sensing. In, *Limnologische Station, WZW, Department für Ökologie* (p. 164). München: Technische Universität München

Rahel, F.J., & Olden, J.D. (2008). Assessing the Effects of Climate Change on Aquatic Invasive Species. *Conservation Biology, 22*, 521-533

RapidEye (2011). Satellite Imagery Product Specifications. (p. 47)

Richards, J.A. (1999). *Remote Sensing Digital Image Analysis*. Berlin: Springer-Verlag

Richter, R. (1996). A spatially adaptive fast atmospheric correction algorithm. *International Journal of Remote Sensing, 17*, 1201 - 1214

Roessler, S., Wolf, P., Schneider, T., & Melzer, A. (2013). Multispectral Remote Sensing of Invasive Aquatic Plants Using RapidEye. In J.M. Krisp, L. Meng, R. Pail, & U. Stilla (Eds.), *Earth Observation of Global Changes (EOGC)* (pp. 109-123): Springer Berlin Heidelberg

Rößler, S., Wolf, P., Schneider, T., & Melzer, A. (2012). Identifizierung und Überwachung invasiver Wasserpflanzen mit RapidEye. In E. Borg, H. Daedelow, & R. Johnson (Eds.), *RapidEye Science Archiven (RESA) - Vom Algorithmus zum Produkt* (pp. 73-91). Berlin: GITO Verlag

Rößler, S., Wolf, P., Schneider, T., & Melzer, A. (2013a). Littoral bottom mapping in lakes using multitemporal RapidEye data. In E. Borg, H. Daedelow, & R. Johnson (Eds.), *RapidEye Science Archiven (RESA) - From the Basics to the Service* (pp. 107-127). Berlin: GITO Verlag

Rößler, S., Wolf, P., Schneider, T., Zimmermann, S., & Melzer, A. (2013b). water constituent retrieval and littoral bottom mapping using hyperspectral APEX imagery and submersed artificial surfaces. *EARSeL eProceedings, 12*, 44-57

Sagawa, T., Boisnier, E., Komatsu, T., Mustapha, K.B., Hattour, A., Kosaka, N., & Miyazaki, S. (2010). Using bottom surface reflectance to map coastal marine areas: a new application method for Lyzenga's model. *International Journal of Remote Sensing, 31*, 3051-3064

Sagawa, T., Mikami, A., Komatsu, T., Kosaka, N., Kosako, A., Miyazaki, S., & Takahashi, M. (2008). Technical Note. Mapping seagrass beds using IKONOS satellite image and side scan sonar measurements: a Japanese case study. *International Journal of Remote Sensing, 29*, 281-291

Sathyendranath, S., & Platt, T. (1997). Analytic model of ocean color. *Appl. Opt., 36*, 2620-2629

Sawaya, K.E., Olmanson, L.G., Heinert, N.J., Brezonik, P.L., & Bauer, M.E. (2003). Extending satellite remote sensing to local scales: land and water resource monitoring using high-resolution imagery. *Remote Sensing of Environment, 88*, 144-156

Silva, T., Costa, M., Melack, J., & Novo, E. (2008). Remote sensing of aquatic vegetation: theory and applications. *Environmental Monitoring and Assessment, 140*, 131-145

Søndergaard, M., & Moss, B. (1998). Impact of Submerged Macrophytes on Phytoplankton in Shallow Freshwater Lakes. In E. Jeppesen, M. Søndergaard, M. Søndergaard, & K. Christoffersen (Eds.), *The Structuring Role of Submerged Macrophytes in Lakes* (pp. 115-132): Springer New York

Spitzer, D., & Dirks, R.W.J. (1987). Bottom influence on the reflectance of the sea. *International Journal of Remote Sensing, 8*, 279-308

Stephens, F.C., Louchard, E.M., Reid, R.P., & Maffione, R.A. (2003). Effects of microalgal communities on reflectance spectra of carbonate sediments in subtidal optically shallow marine environments. *Limnology and Oceanography, 48*, 535-546

Stumpf, R.P., Holderied, K., & Sinclair, M. (2003). Determination of Water Depth with High-Resolution Satellite Imagery over Variable Bottom Types. *Limnology and Oceanography, 48*, 547-556

Tassan, S. (1996). Modified Lyzenga's method for macroalgae detection in water with non-uniform composition. *International Journal of Remote Sensing, 17*, 1601 - 1607

Theriault, C., Scheibling, R., Hatcher, B., & Jones, W. (2006). Mapping the distribution of an invasive marine alga (Codium fragile spp. tomentosoides) in optically shallow coastal waters using the compact airborne spectrographic imager (CASI). *Canadian Journal of Remote Sensing, 32*, 315-329

Thiemann, S., & Kaufmann, H. (2002). Lake water quality monitoring using hyperspectral airborne data - a semiempirical multisensor and multitemporal approach for the Mecklenburg Lake District, Germany. *Remote Sensing of Environment, 81*, 228-237

Tolk, B.L., Han, L., & Rundquist, D.C. (2000). The impact of bottom brightness on spectral reflectance of suspended sediments. *International Journal of Remote Sensing, 21*, 2259-2268

Topliss, B.J., Almos, C.L., & Hill, P.R. (1990). Algorithms for remote sensing of high concentration, inorganic suspended sediment. *International Journal of Remote Sensing, 11*, 947-966

Ustin, S.L., DiPietro, D., Olmstead, K., Underwood, E., & Scheer, G.J. (2002). Hyperspectral remote sensing for invasive species detection and mapping. In, *Geoscience and Remote Sensing Symposium, 2002. IGARSS '02. 2002 IEEE International* (pp. 1658-1660 vol.1653)

Vahtmäe, E., & Kutser, T. (2007). Mapping Bottom Type and Water Depth in Shallow Coastal Waters with Satellite Remote Sensing. *Journal of Coastal Research, SI 50 (Proceedings of the 9th International Coastal Symposium)*, 185-189

Vahtmäe, E., Kutser, T., Martin, G., & Kotta, J. (2006). Feasibility of hyperspectral remote sensing for mapping benthic macroalgal cover in turbid coastal waters—a Baltic Sea case study. *Remote Sensing of Environment, 101*, 342-351

Van Hengel, W., & Spitzer, D. (1991). Multi-temporal water depth mapping by means of Landsat TM. *International Journal of Remote Sensing, 12*, 703-712

Van Stokkom, H.T.C., Stokman, G.N.M., & Hovenier, J.W. (1993). Quantitative use of passive optical remote sensing over coastal and inland water bodies. *International Journal of Remote Sensing, 14*, 541-563

Vanderstraete, T., Goossens, R., & Ghabour, T.K. (2006). The use of multi-temporal Landsat images for the change detection of the coastal zone near Hurghada, Egypt. *International Journal of Remote Sensing, 27*, 3645-3655

Vis, C., Hudon, C., & Carignan, R. (2003). An evaluation of approaches used to determine the distribution and biomass of emergent and submerged aquatic macrophytes over large spatial scales. *Aquatic Botany, 77*, 187-201

Voss, K.J., Mobley, C.D., Sundman, L.K., Ivey, J.E., & Mazel, C.H. (2003). The spectral upwelling radiance distribution in optically shallow waters. *Limnology and Oceanography, 48*, 364-373

Werdell, P.J., & Roesler, C.S. (2003). Remote assessment of benthic substrate composition in shallow waters using multispectral reflectance. *Limnology and Oceanography, 48*, 557-567

Wettle, M., Brando, V.E., & Dekker, A.G. (2004). A methodology for retrieval of environmental noise equivalent spectra applied to four Hyperion scenes of the same tropical coral reef. *Remote Sensing of Environment, 93*, 188-197

Williams, D., Rybicki, N., Lombana, A., O'Brien, T., & Gomez, R. (2003). Preliminary Investigation of Submerged Aquatic Vegetation Mapping using Hyperspectral Remote Sensing. *Environmental Monitoring and Assessment, 81*, 383-392

Wolf, P., Roessler, S., Schneider, T., & Melzer, A. (2013a). Collecting in situ remote sensing reflectances of submersed macrophytes to build up a spectral library for lake monitoring. *European Journal of Remote Sensing, 46*, 401-416

Wolf, P., Rößler, S., Schneider, T., & Melzer, A. (2013b). Evaluation of the anisotropy factor on aquatic test sites caused by RapidEye off-nadir data acquisition with the Mobile Goniometric System (MGS). In E. Borg, H. Daedelow, & R. Johnson (Eds.), *RapidEye Science Archiven (RESA) - From the Basics to the Service* (pp. 221-237). Berlin: GITO Verlag

Wolter, P.T., Johnston, C.A., & Niemi, G.J. (2005). Mapping submergent aquatic vegetation in the US Great Lakes using Quickbird satellite data. *International Journal of Remote Sensing, 26*, 5255-5274

Yuan, L., & Zhang, L.-Q. (2007). The spectral responses of a submerged plant *Vallisneria spiralis* with varying biomass using spectroradiometer. *Hydrobiologia, 579*, 291-299

Zanefeld, J.R.V., & Boss, E. (2003). The influence of bottom morphology on reflectance: Theory and two-dimensional geometry model. *Limnology and Oceanography, 48*, 374-379

Zhang, Y., Gao, J., & Gu, Y. (2011). A simple method for mapping bathymetry over turbid coastal waters from MODIS data: possibilities and limitations. *International Journal of Remote Sensing, 32*, 7575-7590

DANKSAGUNG

Dem Bayerischen Staatsministerum für Umwelt und Gesundheit und ganz besonders Frau Dr. Tanja Gschlössl möchte ich an dieser Stelle meinen besonderen Dank aussprechen für die Förderung des Projekts (unter dem Zeichen ZKL01Abt7_18457). Ebenso gilt mein Dank dem RapidEye Science Archive für die kostenlose Bereitstellung eines immensen Datensatzes, hierbei möchte ich vor allem Herrn Dr. Erik Borg und Dr. Holger Daedelow danken für die freundliche Unterstützung und der spannenden jährlichen Workshops in Neustrelitz.

Ein großer Teil dieser Arbeit ist aber erst möglich geworden durch die herausragenden Arbeitsbedingungen die man in der Limnologischen Station der TU München in Iffeldorf vorfindet. Es herrscht eine Hilfsbereitschaft die einmalig ist und dies ist vor allem Prof. Dr. Arnulf Melzer und Dr. Uta Raeder zu verdanken. Hierfür möchte ich meinen größten Dank aussprechen. Für all die Unterstützung, die guten hilfreichen Gespräche und einfach die Arbeitsatmosphäre die hier geschaffen wurde kann ich euch gar nicht genug danken. Im gleichen Atemzug möchte ich mich bei allen Kollegen und Freunden bedanken. Hierbei möchte ich vor allem meinen Betreuer Dr. Thomas Schneider nennen, der in all den Jahren viel mehr als ein Betreuer war und immer für einen da war. Tomi, danke einfach für alles! Bei meinem „Doktorbruder“ Patrick Wolf möchte ich mich natürlich auch bedanken, mit dem mich schon seit unserer Zeit an der Uni Augsburg eine sehr gute Freundschaft verbindet. Und natürlich allen Doktoranden, Diplomanden, Masteranden, Bacheloranten und Praktikanten wovon einige zu guten Freunden wurden. Vielen Dank an Stefan Zimmermann, einem großartigen Menschen vor allem wenn es um die Verwirklichung von Unterwasserprojekten geht. Ein großer Dank geht an Kathrin Linnemann für ihre hervorragende Masterarbeit und natürlich für ihre Freundschaft.

Ein großes Dankeschön geht an Dr. Peter Gege vom Deutschen Zentrum für Luft- und Raumfahrt für zahlreiche „Nachhilfestunden“ im Bereich der Gewässerfernerkundung und schöne Stunden am Starnberger See. Der gleiche Dank gilt Dr. Nicole Pinnel, die mich überhaupt erst auf die Idee gebracht hat meine Promotion an der Limnologischen Station zu machen.

Ich möchte natürlich auch meiner Familie danken, meinen Schwestern, meiner Mutter und natürlich Willi. Vor allem meiner Mutter für ihre liebevolle Unterstützung über alle schwierigen Zeiten hinweg. Der letzte, aber natürlich auch größte Dank gilt meiner Freundin Tanja Soukup. Ohne meine Zeit in Iffeldorf hätte ich sie nie kennengelernt und ich möchte dir hiermit danke sagen für all die Unterstützung, Aufmunterung, Antrieb und Liebe in den letzten Jahren.

APPENDIX

- Curriculum vitae
- List of publications
- Letter of authorization from the publishers

Curriculum Vitae

Sebastian Rößler

Date of birth 19.12.1983, Munich, Germany

education

1990-1994	Primary school in Esting
1994-2003	Abitur (High school entrance qualification), Gymnasium Olching
2004-2010	Study in physical Geography, Regional Planning and resource Geography at the University of Augsburg Thesis: “Charakterisierung von Oberflächen und Thermokarstformen auf eisreichen Permafrostablagerungen im Lena Delta (Russland)“ (in German)
2010	Scientific diver certification
2009-2013	PhD thesis at the Limnological Institute of the Technical University of Munich

job experience

2005	Practical training at the Bavarian State Office for Environmental (Augsburg)
2006	Practical training at the Government of Swabia (Augsburg)
2006	Practical training at the Bavarian State Ministry of Economy, Infrastructure, Transport and Technology; Department: Regional Development
2008	Practical training at the Alfred Wegener Institute, Helmholtz Centre for Polar and Marine Research – Research Unit Potsdam
2008	Participation at the expedition LENA 2008 to the Lena Delta (Jakutia, East Siberia, Russia)
2009	Practical training at the German Aerospace Center (DLR), German Remote Sensing Data Center (DFD)
2009	Field assistance at a soil spectroscopy campaign of the DLR in South Africa (Port Elizabeth)
2012	Research stay at the german-russian Otto-Schmidt-Laboratory for Polar and Marine Research in St-Petersburg (Russia)
2013	Participation at the Polarstern cruise ANT-XXIX/7 (Punta Arenas – Cape Town)
since 2013	Scientific employee at FIELAX GmbH (Bremerhaven)

peer-reviewed

Roessler, S., Wolf, P., Schneider, T., & Melzer, A. (2013). Multispectral Remote Sensing of Invasive Aquatic Plants Using RapidEye. In J.M. Krisp, L. Meng, R. Pail, & U. Stilla (Eds.), Earth Observation of Global Changes (EOGC) (pp. 109-123): Springer Berlin Heidelberg

Rößler, S., Wolf, P., Schneider, T., & Melzer, A. (2012). Identifizierung und Überwachung invasiver Wasserpflanzen mit RapidEye. In E. Borg, H. Daedelow, & R. Johnson (Eds.), RapidEye Science Archiven (RESA) - Vom Algorithmus zum Produkt (pp. 73-91). Berlin: GITO Verlag

Rößler, S., Wolf, P., Schneider, T., & Melzer, A. (2013). Littoral bottom mapping in lakes using multitemporal RapidEye data. In E. Borg, H. Daedelow, & R. Johnson (Eds.), RapidEye Science Archiven (RESA) - From the Basics to the Service (pp. 107-127). Berlin: GITO Verlag

Rößler, S., Wolf, P., Schneider, T., Zimmermann, S., & Melzer, A. (2013). water constituent retrieval and litoral bottom mapping using hyperspectral APEX imagery and submersed artificial surfaces. EARSeL eProceedings, 12, 44-57

Wolf, P., Roessler, S., Schneider, T., & Melzer, A. (2013). Collecting in situ remote sensing reflectances of submersed macrophytes to build up a spectral library for lake monitoring. European Journal of Remote Sensing, 46, 401-416

Wolf, P., Rößler, S., Schneider, T., & Melzer, A. (2013). Evaluation of the anisotropy factor on aquatic test sites caused by RapidEye off-nadir data acquisition with the Mobile Goniometric System (MGS). In E. Borg, H. Daedelow, & R. Johnson (Eds.), RapidEye Science Archiven (RESA) - From the Basics to the Service (pp. 221-237). Berlin: GITO Verlag

Conference paper

Rößler, S., Wolf, P., Schneider, T., & Melzer A. (2011). Die Option eines Multisaisonalen Monitorings invasiver Wasserpflanzen mit RapidEye. In E. Borg, H. Daedelow (Eds.), RapidEye Science Archive (RESA) - Erste Ergebnisse (pp. 28-42). Berlin: GITO Verlag

Rößler, S., Wolf, P., Schneider, T., & Melzer, A. (2011). Hyperspectral remote sensing of invasive aquatic plants. 7th EARSeL SIG Imaging Spectroscopy Workshop, Edinburg (Schottland), 11.-13. April 2011.

Rößler, S., Wolf, P., Schneider, T., & Melzer, A. (2011). Monitoring of invasive aquatic plants by multispectral remote sensing. 5th EARSeL Workshop on Remote Sensing of the Coastal Zone, Prag (Tschechien), 1.-3. Juni 2011.

Rößler, S., Wolf, P., Schneider, T., & Melzer, A. (2011). Multispektrale Fernerkundung invasiver Makrophyten - Jahrestagung 2011, Freising-Weihenstephan 12.09.-16.09.2011. Ed.: Deutsche Gesellschaft für Limnologie e.V.: (in print)

Rößler, S., Wolf, P., Schneider, T., & Melzer, A. (2012). Monitoring of invasive aquatic plants using multitemporal RapidEye data. 1st EARSeL Workshop on Temporal Analysis of Satellite Images, Mykonos (Griechenland), 23.-25. Mai 2012.

Rößler, S., Wolf, P., Schneider, T., Zimmermann, S., Raeder, U., & Melzer, A. (2011). Fernerkundung zur Bestimmung von Wasserinhaltsstoffen. – Jahrestagung 2010, Bayreuth 27.09.-01.10.2010. Ed.: Deutsche Gesellschaft für Limnologie e.V.: 422-427.

Schneider, T., Rößler, S., Wolf, P., Melzer, A., Gege, P., & Pinnel, N. (2010). Water column characterization on base of HyMap airborne and RAMSES underwater spectroradiometer data of an artificial surface in Lake Starnberg. ISPRS 1910-2010 Centenary Celebration Vienna, 1.-7. Juli 2010, Wien, Österreich.

Wolf, P., Rößler, S., Schneider, T., & Melzer, A. (2011). Abschätzen der Pigment-Zusammensetzung von submersen Makrophyten durch UW-Spektroskopie – Jahrestagung 2011, Freising-Weihenstephan 12.09.-16.09.2011. Ed.: Deutsche Gesellschaft für Limnologie e.V.: (in print)

Wolf, P., Rößler, S., Schneider, T., & Melzer, A. (2011). Assessing the pigment composition of submerse macrophytes by remote sensing reflectance. 7th EARSeL SIG Imaging Spectroscopy Workshop, Edinburg (Schottland), 11.-13. April 2011.

Wolf, P., Rößler, S., Schneider, T., & Melzer, A. (2011). Remote sensing reflectance of submerse macrophytes – searching for true spectra. 5th EARSeL Workshop on Remote Sensing of the Coastal Zone, Prag (Tschechien), 1.-3. Juni 2011.

Wolf, P., Rößler, S., Schneider, T., & Melzer, A. (2012). Using multispectral Sentinel-2 data to monitore submerse macrophytes. First Sentinel-2 Preparatory Symposium, Frascati (Italien), 23.-27. April 2012, ESA SP-707, July 2012.

Wolf, P., Rößler, S., Schneider, T., & Melzer, A. (2013). Spectral library of submersed macrophytes – how distinct is their reflectance? 8th EARSeL SIG Imaging Spectroscopy Workshop, Nantes (Frankreich), 8.-10. April 2013. (in print)

Springer

July 26, 2013

Springer reference

Lecture Notes in Geoinformation and Cartography 2013
Earth Observation of Global Changes (EOGC)
Editors: Jukka M. Krisp, Liqiu Meng, Roland Pail, Uwe Stilla
ISBN: 978-3-642-32713-1
Chapter: "Multispectral Remote Sensing of Invasive Aquatic Plants Using RapidEye" by Sebastian Roessler, Patrick Wolf, Thomas Schneider, Arnulf Melzer pp 109-123

Your project

University: TU München
Title: Dissertation/Thesis – Sebastian Rößler

With reference to your request to reuse material in which Springer Science+Business Media controls the copyright, our permission is granted free of charge under the following conditions:

Springer material

- represents original material which does not carry references to other sources (if material in question refers with a credit to another source, authorization from that source is required as well);
- requires full credit (journal title, volume, year of publication, page, article title, name(s) of author(s), original copyright notice) is given to the publication in which the material was originally published by adding: "With kind permission of Springer Science+Business Media";
- you may not use the publisher's PDF version of the article.
- figures and illustrations may be altered minimally to serve your work.

This permission

- is non-exclusive;
- is valid for one-time use only for the purpose of defending your thesis, and with a maximum of 100 extra copies in paper.
- includes use in an electronic form, provided it is an author-created version of the thesis on his/her own website and his/her university's repository, including UMI (according to the definition on the Sherpa website: http://www.sherpa.ac.uk/romeo/);
- is subject to courtesy information to the co-author or corresponding author;
- is personal to you and may not be sublicensed, assigned, or transferred by you to any other person without Springer's written permission;
- is valid only when the conditions noted above are met.

Permission free of charge does not prejudice any rights we might have to charge for reproduction of our copyrighted material in the future.

Best regards,

Rights and Permissions
Springer-Verlag GmbH
Tiergartenstr. 17
69121 Heidelberg
Germany
E-mail: permissions.heidelberg@springer.com

GITO Verlag
Detmolder Str. 62
10715 Berlin

Abdruckgenehmigung

Geplante Publikation:

Wolf, Patrick: In situ measurements as a basis for reflection-/growth-models of submerse macrophytes. Selbstverlag. Herausgeber: Universitätsbibliothek der Technischen Universität München

Rößler, Sebastian: Methods for multitemporal mapping of submerged aquatic macrophytes using multi- and hyperspectral remote sensing. Selbstverlag. Herausgeber: Universitätsbibliothek der Technischen Universität München

Quellen:

Rößler, S., Wolf, P., Schneider, T. & A. Melzer (2013): Litoral bottom mapping in lakes using multitemporal RapidEye data. In: Borg, E., Daedelow, H., Johnson, R. (Hrsg.): RapidEye Science Archive (RESA) – From the Basics to the Service. 5. RESA Workshop. GITO Verlag, Berlin, S. 107-127.

Wolf, P., Rößler, S., Schneider, T. & A. Melzer (2013): Evaluation of the anisotropy factors on aquatic test sites caused by RapidEye off-nadir data acquisition with the Mobile Goniometric System (MGS). In: Borg, E., Daedelow, H., Johnson, R. (Hrsg.): RapidEye Science Archive (RESA) – From the Basics to the Service. 5. RESA Workshop. GITO Verlag, Berlin, S. 221-237.

Rößler, S., Wolf, P., Schneider, T. & A. Melzer (2011): Die Option eines Multisaisonalen Monitorings invasiver Wasserpflanzen mit RapidEye. In: Borg, E., Daedelow, H. (Hrsg.): RapidEye Science Archive (RESA) - Erste Ergebnisse. 3. RESA Workshop. GITO Verlag, Berlin, S. 28-42.

Es wird um Genehmigung zur Verwendung der o.g. Abbildung(en) für die Print-und Online Version der o.g. Dissertationen der **Technischen Universität München** gebeten.

Die Abdruckgenehmigung umfasst ein einfaches, räumlich und zeitlich unbeschränktes Recht der Speicherung, Vervielfältigung, Verbreitung, Weitergabe sowie öffentliche Wiedergabe und Zugänglichmachung der o.g. Abbildung(en) für die **Technische Universität München.** Dieses ist jedoch beschränkt auf die Nutzung in den o.g. Dissertationen in gedruckter oder elektronischer Form (z.B. online, innerhalb von Online-Paketen mit anderen Zeitschriften und Büchern, offline, mobil). Selbstverständlich ist ein korrekter Quellenhinweis gewährleistet.

Beantragt von:

Patrick Wolf - Doktorand -
Lehrstuhl für Aquatische Systembiologie
Technische Universität München
Wissenschaftszentrum Weihenstephan
Limnologische Station Iffeldorf
Hofmark 1 –3, 82393 Iffeldorf

Ort, Datum Unterschrift

Iffeldorf, 29.07.2013 Patrick Wolf

Genehmigt von:

Ort, Datum Unterschrift

Berlin, 26.07.13 M. Braun

GITO mbH Verlag
Detmolder Straße 62
10715 Berlin
Tel.: 030 / 41 93 83 64
Fax: 030 / 41 93 83 67
service@gito.de
www.gito.de

ABDRUCKGENEHMIGUNG

Geplante Dissertation:

Rößler, S. (2013). Methods for multitemporal mapping of submerged aquatic macrophytes using multi- and hyperspectral remote sensing. Selbstverlag. Herausgeber: Universitätsbibliothek der Technischen Universität München

Publikation:

Rößler, S., Wolf, P., Schneider, T., Zimmermann, S., & Melzer, A. (2013). Water constituent retrieval and litoral bottom mapping using hyperspectral APEX imagery and submersed artificial surfaces. *EARSeL eProceedings, 12*, 44-57

Es wird um Genehmigung zur Verwendung der o.g. Publikation für die Print- und Online Version der o.g. Dissertation der Technischen Universität München gebeten.

Die Abdruckgenehmigung umfasst ein einfaches, räumlich und zeitlich unbeschränktes Recht der Speicherung, Vervielfätigung, Verbreitung, Weitergabe sowie öffentliche Wiedergabe und Zugänglichmachung der o.g. Publikation für die Techniche Universität München. Dieses ist jedoch beschränkt auf die Nutzung in der o.g. Dissertation in gedruckter und elektronischer Form (z.B. online, innerhalb von Online-Paketen mit anderen Zeitschriften und Büchern, offline, mobil). Selbstverständlich ist ein korrekter Quellenhinweis gewährleistet.

Beantragt von:

Sebastian Rößler – Doktorand –
Lehrstuhl für Aquatische Systembiologie
Technische Universität München
Wissenschaftszentrum Weihenstephan
Limnologische Station Iffeldorf
Hormark 1-3, 82393 Iffeldorf

RV "Polarstern", 05.10.13 [signature]

Ort, Datum Unterschrift

Genehmigt von:

Dr. Rainer Reuter
University of Oldenburg
Institute of Physics
26111 Oldenburg

Oldenburg, 8.10.2013 [signature]

Ort, Datum Unterschrift